Development of cellulose-based material from wheat straw using a combination of pressurized water and ethanol and high-intensity ultrasound treatments

by

Ana Xochitl Vidrio Sahagun

A thesis submitted in partial fulfillment of the requirements for the degree of

Master of Science

in
Food Science and Technology

Department of Agricultural, Food and Nutritional Science
University of Alberta

ABSTRACT

The increasing demand for food containers, along with growing petroplastics concerns and Canada's single-use plastic ban, led to an interest in replacing petroplastics with renewable, biodegradable materials like cellulose. Wheat is one of the main cereal crops produced in Canada, and thus, large amounts of wheat straw, which is mainly composed of cellulose, is produced annually. Recently, cellulose and cellulose-based materials have been demonstrated to have potential as packaging materials. To isolate cellulose, conventional treatments that involve corrosive and toxic solvents have been used. The objectives of this thesis were to study cellulose isolation processes from wheat straw, including pressurized water + ethanol mixtures and alkaline hydrogen peroxide, with further fibrillation using high-intensity ultrasound (HIUS) to develop sustainable materials for potential food packaging applications. Furthermore, the effect of the incorporation of calcium carbonate and glycerol on the materials chemical properties was also studied. The samples treated with subcritical water and pressurized 20% aqueous ethanol (20% EtOH) showed the highest and the lowest contents of cellulose and hemicellulose, respectively. However, the pressurized 20% EtOH treatment removed more lignin. Therefore, the combination of pressurized 20% EtOH and alkaline hydrogen peroxide for 2.5 h resulted in a cellulose-rich solid residue with a cellulose content of 85.48±0.65%. Then, the bleached solid residue was dispersed and subjected to HIUS treatments up to 1200 W for 6, 13, and 20 min, resulting in a wide range of micro/nanofibers. The addition of calcium carbonate in the cellulosic micro/nanopapers produced a significant change in the water interactions with the cellulosic matrix. This research contributed to the understanding of cellulose isolation from wheat straw utilising

pressurised water + ethanol mixtures hydrolysis, along with the generation of valuable co-products such as phenolics, carbohydrates, and minerals, hence fostering a circular economy in the wheat production and processing industry.

Keywords: wheat straw, SCW, pressurized fluid, cellulose, food-packaging, sustainability.

Acknowledgments

I am really grateful for all the amazing people I met during my M.Sc. program. I am deeply thankful to my supervisor Dr. Marleny D.A. Saldaña for all her valuable help, guidance, and support throughout my MSc. program. I thank Dr. Feral Temelli and Dr. Thava Vasanthan for their time and help as my supervisory committee member and examining committee member, respectively. I am also thankful to Dr. Michael Gänzle for allowing me to use the autoclave equipment in his lab.

I am forever grateful to my family, especially my parents Ana Rosa and Eleuterio, siblings Cuauhtémoc and Liliana, and sister-in-law Katia, for their endless support, love, and help during my master's studies.

I am also thankful to my colleagues, and friends for their help and guidance in the lab and all the important life lessons you all showed me. As well, I am also grateful for the staff of the AFNS department for their support and help.

I am thankful to the University of Guadalajara (UDG), Mitacs, Scotiabank, and the Natural Sciences and Engineering Research Council of Canada (NSERC) for my program's funding and financial support.

Table of contents

List of tables

List of figures

Chapter 1. Introduction and thesis hypothesis and objectives

1.1 Introduction

Food packaging is an essential aspect of the food supply chain, and the increase in the demand for convenience foods (i.e., food products prepared and packed for easy consumption) is forecasted according to changes in modern society, such as the fastened lifestyle in developing countries, the increase in job opportunities for women, etc. (Marketsandmarkets, 2014; Marketsandmarkets, 2018). Some characteristics related to convenient food packaging are easy opening, easy to transport, and single-use (Marketsandmarkets, 2014). The increase in the popularity of convenience foods, in combination with the growth in the world population, give rise to the demand for food packaging production and innovation (Marketsandmarkets, 2018).

Different materials have been used for the production of food containers, including paper-based, plastics, glass, and metals. Plastics have held the largest market revenue in 2022, followed by paper and board, metals and glass (Grandviewresearch, 2021). Most of the plastic materials currently used in food container production are petroleum derivatives, such as low- and high-density polyethylene, polypropylene, and polyethylene terephthalate (Jamshidian et al., 2010). These materials have been used because they are inexpensive, versatile, stable, have excellent mechanical and barrier properties, and have good heat sealability (Marketsandmarkets, 2018; Jamshidian et al., 2010).

Nevertheless, the use of petroplastics is linked to socioeconomic and environmental problems. The United Nations states, “Plastic pollution can alter habitats and natural processes, reducing ecosystems’ ability to adapt to climate change, directly affecting millions

of people's livelihoods, food production capabilities, and social well-being" (UN environment program, 2023). Low degradability rate, high waste production, and the challenges related to recycling are some of the reasons for the issues regarding petroplastics. Incineration has been implemented as an attempt to reduce plastics wastes; however, such practices contribute negatively to climate change (Marketsandmarkets, 2020; Jamshidian et al., 2010). Additionally, there is the concern about the migration of their toxic monomers and/or oligomers to the foodstuffs, representing a risk to the consumer's health (Jamshidian et al., 2010). Another challenge faced by the food packaging industry is the strengthening of government regulations for consumers and environmental protection. For instance, since December 2022, the Government of Canada has established a prohibition on single-use plastics manufacturing and importation for sale. The banned single-use plastics include everyday items, such as checkout bags, cutlery, food service ware, stir sticks, and straight straws (Government of Canada, 2023).

Therefore, the implementation of degradable biomaterials in the food packaging industry may represent an opportunity to replace petroplastics, and thus, reduce the aforementioned problems. Cellulose and nanocellulose components, like cellulose nanofibers (CNF), are promising materials to replace petroplastics in food container production. Cellulose is the most abundant polymer in the world and can be obtained from biological resources, principally plants (Montoya Sánchez, et al., 2022). Trees, an example of a plant resource, have been the most exploited source of cellulose for the production of paper and board (Montoya Sánchez, et al., 2022). Paper and board have been used for packaging production, such as Tetra Pak containers for milk and juices. They have also been proposed

as the prime candidates for petroplastics replacement (Montoya Sánchez, et al., 2022; Garrido-Romero, et al., 2022).

Another example of a plant source for cellulose isolation are agricultural by-products such as wheat straw, canola straw, barley straw, lupin hull, corn stover, cassava peel, rose stems, and grasses (Ciftci et al., 2017; Xu et al., 2018; Bian et al., 2019; Ventura-Cruz et al., 2019; Baruah et al., 2020; Czaikoski et al., 2020; Huerta et al., 2020b; Kang et al., 2020)

Wheat straw, with a cellulose content of ~ 33–38%, is one of the most abundant by-products around the world (Kuan et al., 2011). In 2019, wheat was the fourth most produced crop in the world (FAO, 2021), and according to FAOSTAT (2022), Canada was the fifth largest producer of wheat in 2020 (35.2 million tonnes). Furthermore, Alberta was the second province in terms of wheat production in Canada between 2017 and 2019 (USDA, 2022). In 2018, Alberta produced 8,114,950 kg of wheat straw, more than any other grain in that year. The quantity of straw that can be removed for bailing is around 0.7 kg per kg of grain, and the estimation of bales price range from CAD 0.064 to 0.11 per kg of bale (Budynski, 2020; Saskatchewan Agriculture Knowledge Centre, 2022). To sum up, wheat straw represents an abundant, renewable, and low-cost by-product to produce cellulose and cellulose derived value-added compounds (Cocero et al., 2018; Lou et al., 2022).

To isolate cellulose, hydrolysis treatments are required. Acid/base treatments are commonly used. Other treatments such as ammonia fiber explosion, organosolv, and ionic liquids have also been used at lab scale (Huerta et al., 2018). Such treatments involve the use of corrosive and toxic solvents, neutralization steps, and consequently, the production of waste streams, among other drawbacks. Pressurized hot liquid mixtures of water and ethanol

treatment represent an sustainable alternative to conventional biomass treatment as the involved solvents are safe for the environment and human welfare (Huerta et al., 2018).

CNF are derivatives produced from chemical, mechanical, and/or enzymatic treatments. Such components have shown the potential for the reinforcement and formation of materials for environmentally friendly food packaging development (Garrido-Romero, et al., 2022; Montoya Sánchez, et al., 2022). For instance, CNF had been used to reinforce starch, protein, hemicellulose/chitosan mixtures, chitosan and polyvinyl alcohol (Xu et al. 2019; Okahisaet al., 2020; Mujtaba et al., 2021; Xu et al., 2021; Zhang et al., 2021; Quin et al., 2022; Thongmeepech et al., 2022). CNF has also been mixed with chemically modified starch and reduced graphene oxide for mechanical properties and electric conductivity improvement (Soni et al., 2019; Liu et al., 2021). Film composites for potential food packaging development made purely of cellulosic components were also reported (Moradi et al., 2019; Abral et al., 2020; Balasubramaniam et al., 2020; Hossain et al., 2021; Roy et al., 2021). In the literature, CNF based films formed by solvent casting and vacuum filtration are also regarded as nanopapers (Mokhenaet al., 2021). Previously, the isolation of CNF from wheat straw had been reported (Alemdar et al., 2008; Espinosa et al., 2016; Liu et al., 2017; Shahbazi et al., 2017; Barbash et al., 2017; Bian et al., 2018; Espinosa et al., 2019). However, the development of nanopapers with CNF sourced from wheat straw is limited.

Some additives used in cellulose-containing films include calcium carbonate and glycerol. Nowadays, calcium carbonate is the most popular filler in the pulp and paper industry, (Sáenz et al., 2023; Hu et al., 2022). Fillers used in this industry are employed to reduce supply costs and improve optical, physical, and visual features (Gill et al., 1995). It should also be noted that glycerol is one of the most popular plasticizers in the production of

film composites, improving their flexibility, workability, and distensibility (Vieira et al., 2011).

To the best of my knowledge, there is limited information about the effect of pressurized mixtures of water + ethanol and subcritical water on hydrolysis of wheat straw, and there are no studies on CNF sourced from wheat straw hydrolyzed with pressurized water + ethanol. Furthermore, there are few studies that focus on films formed entirely from CNF sourced from wheat straw. However, the addition of glycerol and calcium carbonate in those nanopapers were not studied. This study therefore contributes to the understanding of isolating cellulose from wheat straw using pressurized water + ethanol mixtures, high power intensity ultrasound fibrillation of the bleached solid residue, and the effect of the addition of calcium carbonate and glycerol on the resulting fibrillated cellulosic material.

1.2 Hypothesis

- Cellulose recovery from wheat straw hydrolysis will be enhanced by the addition of ethanol in the reaction media during the pressurized fluid treatment.
- High power ultrasound (HIUS) will be able to form micro-/nanofibers using cellulose-rich solid residue obtained after wheat straw hydrolysis.
- Mixtures of fibrillated cellulose + glycerol + calcium carbonate will achieve better characteristics than materials composed of only fibrillated cellulose.

1.3 Objectives

1.3.1 Main objective

The main objective of this thesis was to study and generate sustainable materials like micro/nanopapers for food packaging development using fibrillated cellulose-rich residue from wheat straw.

1.3.2 Specific objectives

To achieve the main objective, two specific objectives were proposed.

1) Isolation of cellulose from wheat straw using pressurized water + ethanol mixtures:

- Study the cellulose-rich residue production by evaluating the effect of hydrolysis using pressurized water + ethanol mixtures at different concentrations and optimum conditions of temperature and pressure on the proximal and carbohydrate composition of wheat straw.
- Characterize valuable by-products such as sugars and phenols in the liquid phase (hydrolysates) obtained from the wheat straw hydrolysis. Other characteristics such as hydrolysate pH and brown color were also analyzed.

2) Formation of micro/nanopapers:

- Generate micro/nanopapers employing pressurized water + ethanol hydrolysis, bleaching with alkaline hydrogen peroxide, and mechanical fibrillation with HIUS. Evaluate material properties, including: i) morphological analysis of the fibrillated cellulose dispersions with scanning electron microscope (SEM) and transmission electron microscopy (TEM); ii) water retention value of wet solid residue (WRV_w) and fibrillation degree of the HIUS fibrillated cellulose dispersions; and iii) water

retention value of dry solid residue (WRV_d) of the dry fibrillated cellulose dispersions to analyze the water absorbance property of the materials.

- Study the effect of glycerol and calcium carbonate at different concentrations on the micro/nanopapers. Evaluate materials' chemical interactions with FT-IR, and water sorption isotherms.

Chapter 1 of this thesis contains the thesis introduction, which includes a description on current research on CNF added film composites and nanopapers research gaps in the production of CNF and nanopapers from wheat straw cellulose and states the main and specific objectives of this thesis.

Chapter 2 consists of the literature review and includes the chemical and anatomical description of wheat straw. This chapter also describes research advances on wheat straw hydrolysis using subcritical water and pressurized aqueous alcohol, bleaching treatment using alkaline hydrogen peroxide and acidified sodium chlorite, CNF production with cellulose obtained from different plant sources using HIUS, and CNF production from wheat straw cellulose. Additionally, Chapter 2 includes recent advances of CNF implementation in the development of potential packaging materials, as well as the use of glycerol and calcium carbonate as additives.

In Chapter 3, the effect of pressurized fluid treatment (water + ethanol at various concentrations) on wheat straw was studied. After being treated with pressurized fluids, solid residue and liquid hydrolysates from wheat straw were recovered. These samples were analyzed to study the behavior of wheat straw chemical compounds (mainly cellulose, hemicellulose, and lignin) after the hydrolysis treatment to select the best conditions for cellulose recovery.

Chapter 4 focuses on the formation of micro/nanopapers with the potential for food packaging development. Such material was made with cellulose isolated from the wheat straw solid residue obtained from Chapter 3 at the best conditions. After hydrolysis using pressurized water + ethanol mixtures, the solid residue was bleached using alkaline hydrogen peroxide and acidified sodium chlorite, and fibrillated using high-intensity ultrasound (HIUS). The effects of the addition of glycerol and calcium carbonate were also analyzed.

Finally, Chapter 5 contains the conclusions for the findings obtained on chapters three and four, as well as the recommendations of this thesis.

Chapter 2. Literature review

2.1 Wheat straw conformation

2.1.1 Anatomical components of wheat straw

Wheat straw is composed of leaves and stem of the wheat plant. The steam is mainly formed by the internode, which is the main part of the wheat straw (Zhang et al., 2022). The internode can be described as a hollow cylinder whose main constituents are parenchymatous ground tissue, vascular bundles, and epidermis (Zhang et al., 2022). Each anatomical component of the plant is composed of eukaryotic cells, which contain strong cell walls. The chemical composition of the plant cell walls can vary based on factors such as the plant's source, developmental stage, tissue type, and cell wall layer (Ruel et al., 2012; Dumitriu et al., 2004). However, they are mainly composed of cellulose, hemicellulose, and lignin (Zhang et al., 2022).

The cell wall of plants is comprised of three layers, namely: i) the middle lamella, ii) the primary wall, and iii) the secondary wall (Zhang et al., 2022). The middle lamella is a thin layer that is formed after cell division, attached to neighboring cells, and is mainly composed of pectic material. The primary wall is after the middle lamella and consists mostly of cellulose, hemicellulose, proteins, and pectin (Zhang et al., 2022; Dumitriu et al., 2004). Even though the presence of pectin in wheat straw was suggested, pectin concentration in wheat straw was not reported. As plants age, the middle lamella and the primary wall differentiate from each other, and the secondary wall is developed. The secondary wall is a combination of the first layer constituents and other plant-segregated compounds produced while the plant is aging (e.g., lignin). The type of segregated compounds are dependent on

the plant tissue of which the cell belongs to (i.e. parenchymatous ground tissue, vascular bundles, or epidermis) and the cell type (Zhang et al., 2022; Dumitriu et al., 2004).

2.1.2 Chemical composition of wheat straw

2.1.2.1 Cellulose

In plant tissues, cellulose is present in primary and secondary walls, representing 20-30% (dw) of the cell wall and confers plants with resistance to tensile forces. The orientation and direction of cellulose microfibrils influence the mechanical properties of the wall, and the direction of the plant deformation. In aged plants, the cellulose percentage increases up to 40-90% (dw) (Dumitriu, 2004).

Cellulose, which is the main compound of wheat straw, is a polar molecule composed of glucose units (specifically β-D-glucopyranose) linked by β (1-4) glycosidic bonds (Brunner, 2014). Glucose units contain hydroxyl groups, which establish additional hydrogen bonds (H-bonds) among the cellulose structure. Some hydroxyl groups may interact with the oxygen in the main structure of the adjacent glucose unit, resulting in the linear configuration of cellulose (cellulose chain). The hydroxyl groups of a single cellulose chain may also interact with other glucose units from another cellulose chain, leading to the formation of a sheet-like structure (Alle et al., 2020; Caballero et al., 2015). These two types of interactions are called intra- and inter-molecular interactions, respectively. Intra- and inter-molecular H-bonds play an important role in the formation of the cellulose crystalline arrangements, and thus, in the strong and stable cellulose structure, which is insoluble in water. In addition, cellulose chains are characterized by having a start and an end, and their orientation in the cellulose structure also plays an important role in cellulose fibers properties (Alle et al., 2020; Caballero et al., 2015). Cellulose sheets are linked to each other by van der

Waals forces into structures known as fibrils, which form microfibers when assembled (Caballero et al., 2015).

In plant tissues, cellulose microfibrils encompass crystalline and amorphous regions, being the earlier more stable than the latter (Alle et al., 2020; Dumitriu, 2004). The literature suggests that amorphous regions represent only 1% of native cellulose (Ruel et al., 2012).

Cellulose crystalline structures are characterized by different allomorphs depending on the chemical treatment cellulose is subjected to. For instance, the untreated cellulose found in nature is called native cellulose or cellulose I, which is the most abundant form of cellulose. Cellulose II is generated when cellulose I is subjected to regeneration and mercerization processes. These processes, which induce irreversible changes in the cellulose I structure, are involved in the production of rayon fibers and the improvement of the properties of natural yarns and fabrics, respectively (Dumitriu, 2004). Cellulose III is obtained by treating cellulose I or cellulose II with liquid ammonia or certain amines like ethylene diamine (EDA). Products are called cellulose III_I or III_{II} depending on the type of cellulose used. Finally, cellulose IV is produced when cellulose II is treated with glycerol. Cellulose IV, which is considered a disordered version of cellulose I, can also be produced from III_I or III_{II} and is named accordingly (i.e., cellulose IV_I or IV_{II}, respectively) (Dumitriu, 2004).

Cellulose I is divided into two subgroups, namely cellulose Iα and cellulose Iβ. Cellulose Iα is the predominant type in bacterial and algal cellulose while cellulose Iβ is the main type in higher plants. The difference between these two subgroups is that cellulose Iα crystals have a triclinic unit cell, whereas Iß crystals have a monoclinic unit cell according to X-ray diffraction assays (Dumitriu, 2004).

Liu et al. (2005) characterized the cellulose crystallinity morphology of wheat straw according to their location in the straw structure, where only cellulose Iβ existed in wheat straw tissues. It was found that the orientation of the cellulose in the straw's epidermis went along its growth direction whereas cellulose found in the parenchyma did not have well-defined orientation. In addition, wheat straw surfaces had two kinds of cellulose morphologies. One had a microfiber structure with fibrils diameter of 5 μm, and the other had microfibrils of 10 μm diameter and was characterized by having a serration morphology, which served as a connector among this kind of fiber. They also observed that the vascular bundles consisted of circular rings and cellulose backbones with a spiral structure covered with thin cellulose films (Liu et al., 2005).

2.1.2.2 Hemicellulose

Hemicellulose is an amorphous polysaccharide constructed by different sugar units linked in a linear (backbone) and branched (side chains) display (Fan et al., 2016; Brunner et al., 2014). Sugars include hexoses such as d-glucose, d-mannose, d-galactose, and pentoses such as d-xylose, l-arabinose, and l-rhamnose. However, the types of sugars and other compounds in the hemicellulose fraction depend on the plant source (Fan et al., 2016). Other compounds, like acids (like acetic, uronic and lactic acids) can be found attached to this polymer (Cocero et al, 2018; Ciftci et al., 2015). The backbone in wheat straw hemicellulose is composed of -1,4-linked xylose units, and its side chains may contain arabinose, uronic acids, acetic acid, ferulic acid, and coumaric acid (Rodríguez-Sanz et al., 2022).

In lignocellulosic biomass, hemicellulose is found surrounding the cellulose fibers. The surface associations between hemicellulose and cellulose involve H-bonds and van der Waals forces. Some biological functions attributed to hemicellulose include cell signaling, the precursor of signaling molecules, and/or reserve substances (Fan et al., 2016; Dumitriu

et al., 2004). In addition, hemicellulose helps to stabilize the cell wall structure as it helps to stabilize the cellulose fibers and lignin in the cell wall, thus, hemicellulose is also referred to as “cementing material”. Hemicellulose can be classified according to the main sugar in the backbone, which usually are xylans, mannans, or glucans (Brunner et al., 2014).

2.1.2.3 Lignin

Lignin is a highly complex and stable molecule, mainly constructed by tree enzyme-derived phenyl propane units, namely guaiacyl (G), syringyl (S), and p-hydroxyphenyl (H), which are linked by ether and carbon-carbon bonds (Fan et al., 2016; Brunner et al., 2014). The presence and composition of the phenyl propane units in lignin differ among plant sources and tissues. For instance, straw contains the three phenyl propane units (G, S, and H) with different ratios while hardwoods (G and S) and softwoods (G) contain less units than straw. The main chemical functional groups in lignin are methoxy, carbonyl, carboxylic, and hydroxyl (phenolic and alcoholic hydroxyl). The origin of lignin and the isolation technique determine the relative proportions of these groups on lignin sources (Zhang et al., 2022; Caballero et al., 2015; Fan et al., 2016). Additionally, lignin shows different levels of cross-linking and structural rigidity that vary with the type and substitution degree (Fan et al., 2016).

In lignocellulosic material, lignin is synthesized at the latest phases of plant development, a process referred to as lignification. The resulting lignin polymer lacks regularly repeating motifs. Some biological functions attributed to lignin include the contribution of mechanical strength of the plant and protection against pathogens, as well as water resistance and water content control, and thus, solute transport due to its hydrophobicity (Caballero et al., 2015; Dumitriu et al., 2004).

Lignin in wheat straw contains the three units. Nevertheless, it is reported that the H is present in small amounts, and there are higher amounts of G and S in the ratio of 1: ~1. Even though such lignin structure is close to harwood lignin (1:1 in G/S units), wheat straw lignin is reported to be more complex due to the presence of H (Zhang et al., 2022). Wheat straw lignin is partially acylated, and the flavone tricin (5,7,4′ -trihydroxy-3′,5′-dimethoxy-flavone) is integrated into the lignin, acting as a chain end via -O-4 coupling and improving lignin's antibacterial properties. Additionally, hydroxycinnamic acids such as p-coumaric acid and ferulic acid and their derived esters can be found in the wheat straw lignin structure (Zhang et al., 2022).

Lignin is linked to hemicellulose via covalent bonds, generally between the hemicellulose α-carbon site and the lignin C-4 in the benzene ring. The four main types of covalent connections are benzyl ether, benzyl esters, phenyl glycoside bonds, and acetal linkages. Such associations are called “lignin-carbohydrate complexes”. Covalent bonding between lignin and cellulose is still under debate (Zhang et al., 2022). In wheat straw, hydroxycinnamic acids (mainly ferulic acid) act as bridges in the connections between lignin and hemicellulose. Ferulic acid forms ester-ether bridges in the lignin fragments as it is ether-linked to lignin (52–68%) and ester-linked to hemicellulose side chains (32-48%). The p-coumaric acid in wheat straw is primarily ester-linked to lignin and weakly linked to hemicelluloses (Zhang et al., 2022).

2.1.2.4 Other compounds in plant material

Additional compounds in plant material include VOCs (volatile organic compounds), proteins, and inorganic compounds (minerals). Terpenes, waxes, acids, and alcohols (or VOCs) are responsible for the characteristic fragrances of wood and plant species (Fan et al., 2016). Proteins serve as essential building blocks for the plant cells and are present

in small quantities in wood and biomass straw, and have no significant effect on lignocellulosic material's mechanical properties. (Fan et al., 2016; Brunner et al., 2014). Inorganic compounds are mainly represented by silica, and other minerals (e.g., calcium and potassium) depending on the soil conditions in which the plant was grown (Fan et al., 2016).

2.2 Wheat straw hydrolysis using subcritical water and pressurized water + ethanol mixtures

Due to their potential as sustainable and renewable sources of valuable chemicals for human use, there has been an increasing interest in cellulose, hemicellulose, and lignin. Cellulose is a promising candidate for the production of valuable compounds, like CNF. To produce CNF, cellulose is isolated, and thus, the separation of cellulose from hemicellulose, and lignin, among other structural compounds, is needed. The isolation of cellulose involves hydrolysis and delignification treatments. The hydrolysis treatments typically employ strong acids and bases, which are corrosive and toxic in nature, require neutralization steps, and generate waste streams, among other disadvantages (Huerta et al., 2018).

Subcritical water (SCW) and pressurized water + ethanol offer a sustainable alternative to traditional hydrolysis treatments. Such hydrolysis treatment consists of using water at high temperatures below the critical point (100 to 374°C) and pressures enough to maintain water in its liquid state at such temperatures. Water is a non-toxic and safe solvent whose properties such as density, viscosity, dielectric constant, ionic product, diffusivity, and electric conductance under high pressure and temperature can be adjusted and optimized for the hydrolysis treatment (Lachos-Perez et al., 2016). In the literature, the subcritical water treatment is also regarded as pressurized hot water, pressurized hot liquid water, and hydrothermal treatment. The main benefits of subcritical water treatment are that it needs

minimal biomass pretreatment (e.g., milling, drying, etc.), shorter reaction times, has fewer corrosion issues compared to acid and alkali hydrolysis treatments, does not require toxic or costly solvents, neutralization steps, and reduces the degradation of the main compounds compared to conventional hydrolysis treatments (Lachos-Perez et al., 2016; Huerta et al., 2018; de Oliveira et al., 2022). Alcohols like ethanol, with a critical point of 239°C and 80.9 bar also have been used for pressurized fluid treatment of biomass (Yamazaki et al., 2006). The combination of ethanol with water for pressurized fluid for hydrolysis further improves the removal of compounds, such as phenolics, from biomass (Huerta et al., 2018).

Table 2.1 shows a summary of the studies of pressurized water and pressurized water + ethanol on wheat straw. The treatment pressures are often not discussed as it was concluded that pressure does not provide a significant effect on straw biomass hydrolysis other than maintain the reaction media in liquid state. Hydrolysis of wheat straw using subcritical and supercritical water (water at conditions above the critical point) has been done in batch and continuous reactors, mainly to produce biofuels like bioethanol and biogas (Petersen et al., 2009; Zhao et al., 2009; Abdelmoez et al., 2014; Reynolds et al., 2015; Nanda et al., 2018; Rajput et al., 2018; Chen et al., 2021). To the best of my knowledge, there is only one study on the use of pressurized aqueous alcohol (ethanol and isopropanol) for treating wheat straw to produce bio-oils, which mostly focuses on the impact of this treatment on the oil production and does not provide information on the cellulose contents in the feed before and after the hydrolysis treatment (Patil et al., 2014).

Wheat bran has also been hydrolyzed using subcritical and supercritical water with(out) catalyst and in combination with other treatments for phenolics and sugar alcohol production. Sánchez-Bastardo et al. (2017) investigated the extraction-hydrolysis process of

arabinoxylans from wheat bran utilizing pressurized hot water treatment in combination with a ruthenium-based catalyst and mesoporous silica support (Al-MCM-48). The optimum conditions were obtained at 180ºC and 10 min using 500 mg of Ru/Al-MCM-48, achieving a total arabinoxylan yield of 79% with a purity of 54%. Additionally, Martín-Diana et al. (2021) studied the impact of a sequential process involving hydrothermal treatment (at 115°C, 1.2 bar for 15 and 30 min) and high hydrostatic pressure. After that, enzymatic hydrolysis in the presence of various organic acids, and the stabilization of hydrolysates rich in ferulic acid with spray drying, and microencapsulation in pea protein isolate with a purity of 86% was performed. Organic acids included citric, malic, acetic, and lactic acids. As for the hydrothermal treatment, it was found to increase the contents of ferulic acid and total phenolics in the hydrolysates despite the treatment duration. The antioxidant capacity of such extracts also increased. However, samples treated with the hydrothermal treatment for 30 min showed a decrease in anti-inflammatory activity (Martín-Diana et al., 2021).

Table 2.1. Wheat straw biomass hydrolysis using pressurized water and/or alcohol.

Feed	Hydrolysis intention	Experimental Conditions	Results and remarks	Reference
Wheat straw	Bioethanol production with hydrolyzed carbohydrates	Batch reactor (7.54 cm^3); mildly washed straw; 0.5 g feed reaction media acidified with HCl and H_2SO_4 (pH 1,3,5); 130–270°C; Time: <100 min; Water to straw ratio: 1:1–7:1. The pressure was not mentioned.	Optimum conditions: 190°C/30 min; 6:1 water to straw ratio/ 180–355 μm particle size/ no addition of HCl or H_2SO_4. The maximum yield of reducing sugars (RS) was 51.5% (RS/ structural carbohydrates).	Abdelmoez et al. (2014)
Wheat straw (*Triticum aestivum L.*)	Bioethanol production with solid residue (rich in cellulose)	Straw continuously fed at 50 kg/h to a soaking reactor at 80°C for 5–10 min. The excess water was removed before pretreatment at 185–205°C for 6–12 min. The speed was not mentioned but depended on the reaction time. The reactor dimensions were not mentioned. The pressure was not mentioned.	Untreated sample contained 35 % cellulose, 22.3 % hemicellulose, 15.6 % Klason lignin, and 6.5 % ash. Optimum conditions: 195°C for 6–12 min; 70 % of the hemicellulose was recovered in the liquid phase, 93–94 % of cellulose, and at least 90% of the lignin were recovered in the fibers.	Petersen et al. (2009)
Wheat straw and corn stalks	Fermentable hexose production from lignocellulosic feedstocks using combined supercritical and subcritical hydrothermal treatment	The batch system consisted of two salt baths for the supercritical and subcritical treatments. A reactor (5 cm^3) with the feeds was first placed in the bath for the supercritical (380–392°C, 20–40 mg feed per 2.5 mL water, 16 to 24 s) treatment, then placed in an ice bath. The replicates were mixed, and an aliquot of 2.5 mL was taken for the subcritical treatment (280°C reaction time	Untreated corn stover composed of 16.4 % cellulose, 28.4% hemicellulose, and 7.9% lignin while the untreated wheat straw was 16.4 % cellulose, 28.4% hemicellulose, and 7.9% lignin. Optimum supercritical conditions were 20 mg/2.5 mL water, 384°C, 17 s for corn stalks, and 20 mg/2.5 mL water, 384°C, 19 s for wheat straw. The optimum conditions for the subsequent subcritical treatment were 280°C, 27 s for corn stover and 280°C, 54 s for wheat straw, achieving yields	Zhao et al. (2009)

Table 2.1. Continue.

Feed	Hydrolysis intention	Experimental Conditions	Results and remarks	Reference
		25–40 s and 42–60 s for corn stalks and wheat straw, respectively). The pressure was not mentioned.	of 27.4% and 6.7% (based on raw material) for corn stover and wheat straw, respectively.	Zhao et al. (2009)
Milled and pelletized wheat straw	Fermentation of produced sugars into bioethanol Investigation of fixed-bed properties and axial dispersion	Semi-continuous reactor (3 L) loaded with 1 kg feed; reaction at 200°C and 50 bar for 10, 15, 20, and 30 min with a water mass flow of 0.25 kg/min.	The feed composition was 35.8 wt % cellulose, 23.9 wt % hemicellulose, and 23.9 wt % Klason lignin. Between 0 and 10 min, the hemicellulose content was minimally affected by the hydrothermal treatment, after 15 min the hemicellulose content was reduced to 15.4 wt %. After 30 min, the hemicellulose content was 4.1 wt %. The axial dispersion coefficient and the effective porosity were constant after 15 min of pretreatment. In addition, there was a linear relationship between the axial dispersion coefficient and the interstitial fluid velocity.	Reynolds et al. (2015)
Wheat straw	Study the effect of thermal pretr eatment on the anaerobic digestion of wheat straw to produce biogas	Laboratory scale batch reactor (250 mL) loaded with 80 g feed at 120, 140, 160, and 180°C for 60 min with a feed: water ratio of 8:2 (w/w). The treated wheat straw was dried and stored in a vacuum plastic bag. The pressure was not mentioned.	The lignocellulosic fraction of raw wheat straw was 83.2%. Initial cellulose content was 34.5 % and increased to 47% after thermal pretreatment at 180°C. Additionally, initial hemicellulose and lignin contents were approximately 28.2 % and 19.8 % and decreased to 23.2 % and 17 %, respectively, at the aforementioned condition.	Rajput et al. (2018)

Table 2.1. Continue.

Feed	Hydrolysis intention	Experimental Conditions	Results and remarks	Reference
Wheat straw	Hydrothermal liquefaction of lignocellulosic biomass (wheat straw) into bio-oil	Continuously operated tubular reactor (10 mL) loaded with 3–5 g feed at temperatures up to 350°C, pressures up to 200 bar, and times up to 6 h. Solvents were water and water + alcohol (ethanol and isopropanol) mixtures at the flow rate 0.5–1 mL/min and with(out) catalyst (5 wt% Ru/H-Beta, 0.5–1 g of solid) to facilitate the oxygen removal in presence of hydrogen at a liquid hourly space velocity of 60 h^{-1}.	Optimum conditions were 300°C, 100 bar, water + ethanol mixture (50:50 (v/v) for 2 h. The bio-oil yield and higher heating value were 30.4% and 27.8 MJ/kg, respectively. The addition of Ru/H-Beta catalyst increased higher heating value (HHV) values above 30 MJ/kg.	Patil et al. (2014)
Wheat straw	Bioethanol production	Batch reactor at 176–230°C, 3–37 min, and solid loading (w/v) of 0.80-9.20 %. Dimensions of reactor and feed load are not mentioned. To produce the bioethanol, further enzymatic treatment with cellulases fermentation with *Saccharomyces cerevisiae* NX11424 was applied.	The optimum conditions for subcritical treatment hydrolysis were 220.51°C for 22.01 min with a substrate loading of 2.50% (w/v). The pretreatment reduced the hemicellulose content by 18.37% while increasing the cellulose and lignin by 25.92 and 8.81%, respectively.	Chen et al. (2021)

Table 2.1. Continue.

Feed	Hydrolysis intention	Experimental Conditions	Results and remarks	Reference
Wheat straw	Production of hydrogen fuel through hydrothermal gasification	Hydrolysis consisted of subcritical (300 and 370°C) and supercritical (450 and 550°C) treatments at pressures of 210-230 MPa, different feed concentrations (20-35 wt%) and times (40-70 min) in a batch reactor. The effect of the addition of 5 wt% of Ru/Al_2O_3 or $Ni/Si\text{-}Al_2O_3$ as catalysts was analyzed.	Gasification yields were higher in supercritical conditions than in subcritical. The optimal conditions for wheat straw gasification without catalyst were 550°C, 23 MPa, feed concentration 20 wt%, and 60 min. Such conditions achieved H_2 and total gases yields of 2.98 mmol/g and 10.7 mmol/g, respectively, and a lower heating value (LHV) of 1301 kJ/Nm^3. After the addition of the catalyst, $Ni/Si\text{-}Al_2O_3$ and Ru/Al_2O_3 achieved the yields of H_2 of 5.1 mmol/g and 4.18 mmol/g, respectively. Such catalysts also had total gas yields of 15 and 18.2 mmol/g, respectively. The LHV of the gases obtained from the optimized supercritical water treatment with $Ni/Si\text{-}Al_2O_3$ was 2544 kJ/Nm^3.	Nanda et al. (2018)

Liquid hourly space velocity = liquid volume flow per hour/catalyst volume

2.3 Bleaching

Lignocellulosic bleaching can be defined as the chemical treatment aimed to improve the brightness and whiteness of lignocellulosic material. This is achieved by the removal of lignin; therefore, the bleaching process can also be referred to as a delignification process. Conventionally, chemical delignification is carried out with oxidant and/or chlorinated compounds such as sodium chlorite ($NaClO_2$) and hydrogen peroxide (H_2O_2).

Bleaching with $NaClO_2$ is carried out at acidic conditions (pH values <5), and this process is performed under acidified sodium chlorite (ASC) bleaching (Clark et al. 2011). It is well accepted that $NaClO_2$ is unstable under acidic conditions generating ClO_2 which breaks ether, carbon–carbon bonds between lignin and the carbohydrate portion. Another compound resulting from $NaClO_2$ dissociation is the chloride anion (Cl^-), which is also responsible for lignin removal from lignocellulosic material (Nan et al., 2018). The ASC treatment has been reported to degrade the carbohydrate portion by either acidic cleavage of the glycosidic bonds or oxidative degradation of the polysaccharides (Nan et al., 2018). Anyhow, ASC is also recognized for having minimal effect on the carbohydrate portion (Wang et al., 2021). Additionally, ASC involves chlorinated compounds that have negative impacts on the environment such as the emission of toxic and carcinogenic chlorinated compounds (Zhao et al., 2018).

Bleaching with H_2O_2 is considered more environmentally friendly than ASC and is carried out at alkali conditions; thus, this is called the alkaline hydrogen peroxide treatment. At high pH (11.5–11.6), hydrogen peroxide reversibly dissociates into water (H_2O) and hydroperoxy anion (HOO^-). In addition, HOO^- can also react with the H_2O_2 molecules to generate hydroxyl ($OH^\bullet$) and superoxide ($O^{\bullet -2}$) radicals, and water (Fang et al., 1999; Sun et

al. 2000). HOO^- is the active specie responsible for lignocellulosic material bleaching by the elimination of chromophore groups from lignin. This is achieved by the reaction of HOO^- with lignin carbonyl structures such as quinones and non-conjugated carbonyl groups and double bonds, resulting in carboxyl fragments (Sun et al., 2000). On the other hand, $OH^{\bullet}$ and $O^{\bullet -2}$ are responsible for lignocellulosic material delignification by lignin oxidation (Fang et al., 1999; Sun et al. 2000). The bleaching treatment is improved by the increase of the alkali (maintaining the optimum pH of 11.5–11.6) and H_2O_2 dosages. However, the concentration of these compounds should be controlled, mainly to reduce process costs (Sun et al., 2000). Additionally, the hemicellulose is also affected by these radicals because it is naturally bonded to lignin as lignin-carbohydrate complexes (LCC); and thus, hemicellulose is solubilized and partially degraded aligned with lignin (Fang et al., 1999; Sun et al. 2000). It is also mentioned that cellulose may swell at certain conditions, reducing its crystallinity and increasing its hydration (Fang et al., 1999; Sun et al. 2000).

Table 2.3 shows studies that involve the use of AHP and ASC treatments for lignocellulosic fractionation to obtain value-added components such as microcrystalline cellulose, cellulose nanocrystals, xylooligosaccharides, methane, and bio-oils (Sun et al., 2000; Liu et al.,2011; Nan et al., 2018; Xu et al., 2018; Zhao et al., 2018; Bian et al., 2019; Ventura-Cruz et al., 2019; Baruah et al., 2020; Kang et al., 2020; Ventura-Cruz et al., 2020; Wang et al., 2021). Overall, conditions such as time, pH, H_2O_2, and $NaClO_2$ concentrations in the bleaching media, and solvent-to-feed ratio are important for maximum lignin removal, while also minimizing side effects to the cellulose structure and content, and reducing process costs and waste streams.

Table 2.2. AHP and ASC treatments for lignocellulosic fractionation.

Source	Purpose	Pretreatment	Bleach	Reference
***Saccharum spontaneum* (s Kans grass)** Cellulose: 48.23±1.9%; hemicellulose: 32.01±1.35%; lignin: 17.09±0.60%; ash: 2.67±0.42%; moisture 1.43±0.76%	Microcrystalline cellulose production and characterization	Alkali treatment and steam explosion Cellulose: 61.14±1.10% Hemicellulose 8.4±0.80% lignin 12.64±0.78%; ash 1.01 ± 0.33% moisture 0.76±0.50%	H_2O_2 + NaOH solution. Cellulose was washed by ethanol (95%, v/v) and distilled water until neutral pH was reached. Cellulose: 75±0.54%; hemicellulose: 1.42±0.48%; lignin 0.27±0.57%; ash: 0.77±0.21%; moisture: 0.44±0.35%	Baruah et al. (2020)
Oolong tea waste Cellulose: 17.50% Hemicellulose: 16.40%; lignin: 19.50%; protein 22.70%	Microcrystalline cellulose production and characterization	With 10 mol/L NaOH at 75°C, for 4 h followed by 5% (w/v) $NaClO_2$ at 75°C for 2 h.	Addition of H_2O_2 (0.45% v/v) in the suspension at ratio of 1:20. The pretreatment and bleaching treatments together yielded cellulose 12.1% with purity of 85.5%.	Zhao et al. (2018)
Corn stover Cellulose: 44.4±0.4%; hemicellulose: 27.8±0.3% Lignin: 19.6±0.2	Cellulose nanofibril and characterization	20 g corn stover washed and sieved with a 75 µm sieve. Pretreated with 500 ml of 4 wt.% NaOH at 80 °C for 2 h under stirring conditions at 150 rpm. Pretreatment was repeated twice. Cellulose: 76.20±0.80 Hemicellulose: 3.80±0.04 Lignin: 13.20±0.10	50 g of sodium chlorite + 500 ml nano-pure water + 50 ml glacial acetic acid + pretreated corn stover. The mixture was mechanically stirred at 30 °C for 24 h. 30% of the original corn stover was recovered. Cellulose: 93.10±0.90%; hemicellulose: 2.5±0.03%; lignin: 3.00±0.03%	Xu et al. (2018)
Wheat straw Cellulose: ~35.21%; hemicellulose: ~26.29%; lignin: ~21.56%; Ash: ~6.57%; By-product from the wheat straw pulping industry Cellulose: ~24.04% hemicellulose: 14.62% lignin: ~18.54%; ash: ~35.21%	Cellulose nanofibril and characterization	80 wt% p-Toluenesulfuric acid was added to 10 g db in a mass ratio of 10:1 (g/g). The mixture was agitated at 300 rpm for 20 min. Pretreated samples were consequently mechanically fibrillated with a stone disk grinder. Wheat straw Cellulose: ~69.48% hemicellulose: ~8.45%; lignin: ~5.63%; ash: ~1.88% By-product from the wheat straw pulping industry	The fibrillated samples suspensions (at 1% wt.) were added into 2% H_2O_2 solution and stirred for 12 h at 60°C. Then, the pH of the suspension was adjusted to 11.5 with 4 M NaOH. Wheat straw Cellulose: ~85.45%; hemicellulose: ~8.5%; lignin: ~0.00%; ash: ~0.47%. By-product from the wheat straw pulping industry Cellulose: ~81.69%; hemicellulose: 9.4%; lignin: ~2.11%; ash: ~2.35	Bian et al. (2019)

Table 2.2. Continue.

Source	Purpose	Pretreatment	Bleach	Reference
		Cellulose: ~45.07%; hemicellulose: 10.80%;lignin: ~15.26; ash: ~7.51		Baruah et al. (2020)
Rose stems (Rosa spp.) Holocellulose:71.08%; α-cellulose: 46.96%; lignin: 16.36% ash: 1.53%	Cellulose nanofibril and characterization	0.70 kg of dried Rose stems were mixed with 14 L of NaOH solution (15 g/L) and 0.17 L solution of H_2O_2 (300 g/L). The reaction was carried for 3 h, at 50 °C under continuous agitation.	5 g of solid was mixed with 0.1 L of NaOH solution (50 g/L), and 0.1 L of H_2O_2 solution (160 g/L). The reaction was carried for 90 min at 55 °C.	Ventura-Cruz et al. (2019)
Wheat straw Cellulose 40.1%; hemicelluloses 32.8%; lignin 14.1%, ash 7.6%; extractives 1.9%; protein 1.8%; and water-soluble polysaccharides 1.9%	Study of lignin removal for wheat straw using alkaline hydrogen peroxide.	Dewaxing	5 g Wheat straw in 150 mL of 2% H_2O_2 (w/v) solution. The suspension was adjusted to pH 11.5 with 4 M NaOH and stirred at 50°C for 4, 8.5, 12, 16, 20 and 30 h. The treatment for 4, 8.5, 12, 16, 20 and 30 h resulted in 79, 81, 82, 82, 84 and 86% of the original lignin and 77, 83, 90, 91, 90 and 89% of the original hemicelluloses removal, respectively. There was only 7% lignin solubilized at pH 11.5 in the absence of H_2O_2. Addition of 0.05% to the alkaline peroxide solution did not significantly affect the of delignification effect.	Sun et al. (2000)
Corn stalks Cellulose 45.2%; hemicellulose 28.2%; lignin 21.1 %	Developing a pretreatment process for bio-oil production	n/a	Deionized water (6 mL/g biomass) + $NaClO_2$ (0.2 mg/g biomass) + glacial acetic acid (0.2 mL/g biomass) at 75°C. Reaction media was changed each 0.5 h; the treatment was carried out for 1,1.5 and 3 h 1h Cellulose ~ 47.2%; hemicellulose 22.9%; lignin 24.2% 1.5h Cellulose ~ 54.0%; hemicellulose 17.7%; lignin 22.7% 3h	Liu et al. (2011)

Table 2.2. Continue.

Source	Purpose	Pretreatment	Bleach	Reference
			Cellulose ~ 57.5 %; hemicellulose ~ 20.7%; lignin ~ 16% 1h acid-chlorite treatment partly removed hemicelluloses and minimally affected the lignin content attributed to the acid content in the treatment media, resulting in hemicellulose degradation due to acid hydrolysis.	Liu et al. (2011)
Corn stalks Cellulose ~ 29.5%; hemicellulose ~ 25.2%; lignin ~ 16.6 %; ash ~ 9.8%	Xylo-oligosaccharides extraction	Consecutive water and ethanol pretreatment: Water: Solid-liquid ratio of 1:8 (g/mL) at 80°C for 2 h Ethanol: Solid-liquid ratio of 1:5 (g/mL) at 60°C for 2 h Cellulose ~ 37.5%; hemicellulose ~ 35.3%; lignin ~ 21.0%; ash ~ 3.6%	1-8% (w/v) $NaClO_2$ acid solution at pH values of 3.6-3.8, 75°C, for 2 h. As the dosage of $NaClO_2$ increases, lignin is further removed, minimally affecting the yield of hemicellulose after bleaching. The delignification degree gradually decreases when the $NaClO_2$ concentration is over 4 %. The yield of hemicellulose after bleaching for all $NaClO_2$ concentrations (79.7%-83.3%) was significantly lower than in the pretreatment (~ 100 %). 8% sodium chlorite at 75°C for 2 h had the highest delignification (92.6%). After further enzymatic hydrolysis of hemicellulose, isolated hemicellulose with a purity of 86.1% was achieved.	Wang et al. (2021)
Hybrid *Pennisetum* (tropical grass) Cellulose 36.89%; hemicellulose 23.56%; lignin 18.42 %	Methane production	n/a	3.0 g (dw) of grass was mixed with 0.3 g/g grass of $NaClO_2$ (0.93% w/v), 0.1 mL/g grass of anhydrous CH_3COOH (0.31% v/v), and 32 mL/g grass of deionized water at 80°C. After each 40 min, the bleaching solution was changed and replaced with the same concentrations. The total treatment time was 200 min. Cellulose 48.20 %; hemicellulose 25.66%; lignin 6.67%	Kang et al. (2020)

Table 2.2. Continue.

Source	Purpose	Pretreatment	Bleach	Reference
			After the treatment, 74.9% of lignin was removed; hemicellulose removal was 24.5 %; 90 % of the cellulose was retained, solid recovery was 69.3%. Lignin was mostly removed from secondary cell walls and cell middle lamella. Lignin in the cell corner was resistant to the treatment. Lignin removal increased the biodegradability of the sample (59.6% to 86.4%) and increased methane production (38.3%).	Kang et al. (2020)
Silvergrass Glucan, 33.9%; hemicellulose 18.0%; lignin and 22.9%	Comparison of Acidified sodium chlorite and simplified sodium chlorite treatments on lignocellulosic materials	n/a	Acidified sodium chlorite: 6 wt% of $NaClO_2$ adjusted pH 3.6–3.8 with acetic acid for 2 h Simplified sodium chlorite: 6 wt% of $NaClO_2$ for 0.5–24 h w Both treatments were done using a solid-liquid ratio of 1:10 at 80 °C Xylan loss: Acidified sodium chlorite 18.1%, simplified sodium chlorite 7.8%; glucose yield after 2 h treatment: simplified sodium chlorite for 2 h 70.5%, acidified sodium chlorite 58.7%. The significant loss of carbohydrates observed after acidified sodium chlorite could be due to the acid hydrolysis of biomass caused by acetic acid.	Nan et al. (2018)

2.4 High-intensity ultrasound fibrillation of cellulose

Ultrasound is defined as sound waves at frequencies equal to or higher than 20 kHz. These waves can be classified as low-intensity ultrasound and high-intensity ultrasound (HIUS), depending on their frequency and intensity. HIUS (intensities of 10–1000 W/cm^2 and frequencies of 20–100 kHz), is differentiated from low-intensity ultrasound by its high energy load, capable of forming cavitation in water media (Low et al., 2022). Cavitation is a physical phenomenon in which water vapour bubbles are formed and collapsed due to drastic changes in the media pressure (Redlinger-Pohn et al., 2022¸ Mekala et al., 2022). In the water media, HIUS propagation consists of a series of high-pressure and low-pressure cycles, namely compression and rarefaction cycles. During the rarefaction cycle, cavitation bubbles or nucleation occur due to a phase change from liquid to gas as pressure drops. The subsequent compression cycle may cause bubble size reduction. The bubbles may also collapse if the pressure increase exceeds the vapor pressure (Low et al., 2022; Redlinger-Pohn et al., 2022).

A bubble collapse results in a high energy release, and consequently, there is a generation of a high increment of temperature (above 1000 K) and pressure (up to 1013 bar) at the molecular level, creating shock waves and high-velocity microjets (Low et al., 2022; Redlinger-Pohn et al., 2022; Mekala et al., 2022). The induced temperature increase causes water dissociation and the formation of hydroxyl radicals. Water movement due to the nucleation and changes in bubble size leads to microstreaming (Low et al., 2022; Redlinger-Pohn et al., 2022). Additionally, the oscillation of the size of cavitation bubbles results in the shear stress of nearby molecules and the incorporation of air in the water media, generating

a mixing effect due to the movement of the air bubble in the water phase (Low et al., 2022; Redlinger-Pohn et al., 2022).

The effect of HIUS on the water media promotes physical and chemical reactions and improves heat and mass transfer (Low et al., 2022). Thus, the interest in HIUS applications in the industry has been increasing. For CNF production, HIUS has been used to assist cellulose isolation, surface modification, and fibrillation, among other applications, such as the production of colloidal and gel systems (Low et al., 2022; Huerta et al., 2020a). HIUS has been proven to fibrillate cellulose bundles sourced from lupin hull, canola straw, wood pulp, okara, bamboo, wheat straw, and flax seed, as shown in Table 2.3 (Ciftci et al., 2017; Huerta et al., 2020b; Wu et al., 2021; Chen et al., 2011; Redlinger-Pohn et al., 2022). HIUS fibrillation was also applied on chemically treated cellulose isolated from wood pulp and cassava peel (Yang et al., 2022; Czaikoski et al., 2020; Redlinger-Pohn et al., 2022). There are also studies of cellulose fibrillation using HIUS and other technologies, such as high-pressure homogenization, and hydrodynamic cavitation (Soto-Salcido et al., 2022; Pinjari et al., 2010).

Overall, HIUS fibrillation treatments have been carried out at working powers of 100 to 1200 W for treatment times of 5–110 min, achieving fibers with a diameter from 5 to 301 nm, depending on cellulose source, content, and chemical modification. Fibrillation conditions such as power, time, cellulose concentration in the dispersion, and dispersion quantity also significantly impacted the fibrillation treatment. In addition to studying the effect of HIUS on cellulose fibrillation, some studies also used the developed nanocellulose to generate hydrogels (Pinjari et al., 2010; Chen et al., 2011; Ciftci et al., 2017; Czaikoski et al., 2020; Huerta et al., 2020b; Wu et al., 2021; Redlinger-Pohn et al., 2022; Soto-Salcido et

al., 2022; Yang et al., 2022), scaffolds (Ciftci et al.,2017; Huerta et al., 2020b), anti-reflection and anti-fingerprint coatings (Yang et al., 2022), and ultrafiltration membranes for textile industries (Soto-Salcido et al., 2022), showing the potential of HIUS-produced nanocellulose in multiple industries.

2.5 CNF isolated from wheat straw

In the literature, the CNF isolation from wheat straw has already been reported. Liu et al. (2017) isolated high-purity cellulose from wheat straw (500 g) using steam explosion at 100°C and 30 bar for 2 min, and then, acid-hydrolyzed with 1 M HCl with a solid to liquid ratio of 1:20 w/v, at 80±1°C for 2 h. After that, it underwent microwave-assisted alkali hydrolysis where a 1.5 g sample was suspended in 30 mL of 2% NaOH aqueous solution under stirring conditions. This treatment was carried on for 20 min. The temperature was increased to 140 ± 2°C within 3 min and maintained for 20 min. Further operational conditions of the microwave-assisted alkali hydrolysis were not mentioned. Fibrillation was performed with a high-pressure microfluidizer at the cellulose concentration of 0.1% under pressures of 1,500 bar to 1,590 bar with a total of five passes. The cellulose content of the samples increased from 44.81 % to 94.23 %. The isolated cellulosic fibers had an average individual diameter of 5.42 nm. The authors also observed a partial crystalline transformation of cellulose I to cellulose II after microwave-assisted alkali hydrolysis. The authors concluded that the obtained CNFs may have potential applications in the auto industry, chemical industry, agriculture, environmental protection, and medical biocomposites production.

Moreover, Espinosa et al. (2016) studied the production of lignocellulosic nanofibers from wheat straw treated with soda pulping, passed through a pulp disintegrator

(1200 rpm/30 min) and mechanically pretreated with a beater. High-pressure homogenization was the mechanical fibrillation treatment. The high-pressure homogenization was carried out with 1.5 % aqueous suspension at 60–70°C, passed through the equipment 4 times at 300 bar, 3 times at 600 bar, and 3 times at 900 bar to avoid clogging. The cellulose content increased from 39.7% to 73.0%. The calculated fibrillation yield was 55.6% and the morphology analysis revealed a wide distribution of widths with an average diameter of 28 nm. The application of lignocellulosic nanofibers as an additive in papermaking was also studied by Espinosa et al. (2016). Papers added with 4 wt% lignocellulosic nanofibers presented the highest density and reduced porosity as a consequence of an increase in the paper's compactness. The addition of lignocellulosic nanofibers on papers also improved the breaking length and burst index compared to unreinforced paper, while minimally affecting the tear index.

Table 2.3. Fibrillation of cellulose isolated from different plant sources using HIUS.

Sample and composition	Purpose	HIUS conditions	Results and remarks	Reference
Lupin hull treated with subcritical water at 180°C, 50 bar, pH 6.2, and 5 mL/min, bleached with 1.7 % acidified sodium chlorite.	Nanocellulose production Aerogel preparation	Cellulose concentrations of 1, 1.5, and 2 wt% Probe with the maximum output power of 700 W and frequency of 50/60 Hz working at an amplitude of 80%. Time: 40 min.	Nanofiber filaments with diameters of 5–100 nm, and lengths of several microns. Cellulose concentration >1 wt% increased the aggregation of nanofibers and impeded their flow ability due to a hydrogel viscosity increase. No fibrillation yield or WRV reported.	Ciftci et al. (2017)
Canola straw hydrolyzed with pressurized 20 % ethanol, bleached with 1.7% acidified sodium chlorite. High lignin (HL) sample: 70.73% cellulose; 4.90 % hemicellulose; 18.22% lignin Low lignin (LL) sample: 81.92% cellulose 3.68% hemicellulose; 7.98% lignin	Nanocellulose production Scaffolds production	Dispersion with 1 % cellulose. 20-mm diameter probe at 20 kHz in a continuous mode. Nominal powers of 240, 720, and 1200 W. Time: 8 min.	At a nominal power of 1200 W, LL and HL had maximum fibrillation yields of 46 and 40 wt.%, respectively. The WRV were 82 and 34 g/g for HL and LL, respectively. The HL had nanofibers with an average diameter size of 18 nm. Fibers with diameters of 20-30 nm had a relative frequency of 23%; fibers with diameter size >50 nm had a relative frequency of 3%. The LL had an average diameter size of 14 nm. Fibers with a diameter of <10 nm had a high relative frequency (43%).	Huerta et al. (2020b)
Flocculent wood pulp board ≥91.0% cellulose; ≤0.10% ash ≤3.0% pentosan; ≤0.30% resin ≤15 ppm iron The sample was first modified via semi-dry esterification with maleic anhydride. The esterification reaction consisted of mixing 1.0 g ground pulp and 5.0 g maleic anhydride, then purified	Nanocellulose production study. Anti-reflection and anti-fingerprint coatings without any other compound addition.	10 mm diameter probe at 22 kHz with 1 s/2 s on/off cycles. 30 g sample in 50 mL, water/pulp mass ratio of 2.5. Powers: 300 W and 600 W. Time: 30 min.	The HIUS treatment at 300 W for 30 min led to CNFs with about 200–400 nm in length and 20–25 nm in width. No fibrillation yield or WRV reported.	Yang et al. (2022)

Table 2.3. Continue.

Sample and composition	Purpose	HIUS conditions	Results and remarks	Reference
water was added at the water/pulp mass ratio of 0.0, 2.5, 5.0, 7.5 and 10.0. The mixtures were stirred, dried in an oven at 120°C for 4 h, and washed until neutral pH was reached.				Yang et al. (2022)
Okara (a by-product of soybean milk and tofu production) Sample treatment before HIUS included degreasing, decolorizing, delignification (10% sodium hydroxide solution), and bleaching (~ 9% alkaline hydrogen peroxide). Final solid residue had lignin and hemicellulose contents of 2.1 and 3.4%, respectively.	Nanocellulose production	Cellulose dispersion (4%) was homogenized at 24°C at 10,000 rpm for 5 min. High-intensity ultrasound compared to high-pressure homogenization treatments. HIUS conditions: 400 W for 15 min and 30 min; 600 W for 15 min; 30 min. High-pressure homogenization conditions: 100, 120, and 140 MPa with 3 repetitions each.	The average diameter of non-fibrillated okara cellulose was 2.43 μm. Samples treated with HIUS at 600 W for 15 min had the smallest average diameter (0.22 μm) polydispersity index (0.21) and highest swelling ratio (7.6 g/g). No fibrillation yield or WRV reported.	Wu et al. (2021)
Cassava peel were pretreated with alkaline (KOH), then bleached (H_2O_2 + NaOH + diethylenetriaminepentaacetic acid +$MgSO_4$) Pretreated and bleached peels were previously treated with acid	Nanocellulose production	HIUS treatment for 20 min with a power of 300 W.	The nanocellulose dispersions presented a gel-like behavior when prepared at concentrations of 1.0–1.8 % w/w. Acid-hydrolyzed and TEMPO-mediated oxidated samples had average diameters of 8 and 16 nm, respectively. After HIUS, the average diameters of treated samples were 5 and 8 nm, respectively. HIUS application increased the viscoelastic properties of	Czaikoski et al. (2020)

Table 2.3. Continue.

Sample and composition	Purpose	HIUS conditions	Results and remarks	Reference
hydrolysis or TEMPO-mediated oxidation.			acid-hydrolyzed and TEMPO-mediated oxidated samples. No fibrillation yield or WRV reported.	Czaikoski et al. (2020)
Spruce wood pulp was pretreated with deep eutectic solvents (choline chloride + lactic acid in a molar ratio of 1:20).	Nanocellulose production Coating of ultrafiltration membranes to remove methylene blue from water.	A solution of 400 mL at a concentration of 0.1% (w/v) was homogenized for 1 h at 24,000 rpm at room temperature. Then treated with ultrasound (probe working at 100 W, 20 kHz) at 100% amplitude and pulse of 6 s for 1 h.	Deep eutectic solvents weakened the cellulose structure, improving the fibrillation. The diameters of the fibers were ~50-100 nm. No fibrillation yield or WRV reported. At coating concentrations of 6.5 g/m^2 (g of cellulose/m^2 membrane), membranes showed dye retention of 2.5 higher than uncoated membranes; the pure water permeability was unaffected. At coating concentrations of 19.5 g/m2, the dye retention was 4 times higher, but the pure water permeability decreased by about 30%.	Soto-Salcido et al. (2022)
Cellulose isolated from: Wood (80.2% cellulose, 17.7% hemicellulose, 1.1% lignin). bamboo (84.4% cellulose, 14.6% hemicellulose, 0.9% lignin). wheat straw (84% cellulose, 13.9% hemicellulose, 1.9% lignin). flax fibers (88.8% cellulose, 9.1% hemicellulose, 0.4% lignin).	Nanocellulose production	Cellulose samples dispersed in 1% w/w. HIUS for at 20–25 kHz and power of 1000 W. Time: 30 min.	The diameter of nanofibers from wood was 10–20 nm, for bamboo was 10–40 nm, and for wheat straw 15–35 nm. Flax cellulose was not uniformly nano-fibrillated, attributed to stronger H-bonding between the nanofiber bundles. Most of the flax nanofibers were still in the nano-range (15–100 nm). No fibrillation yield or WRV reported.	Chen et al. (2011)

Table 2.3. Continue.

Sample and composition	Purpose	HIUS conditions	Results and remarks	Reference
Delignification with acidified sodium chlorite (concentration not mentioned); pretreated with 2 wt% KOH further purified acidified sodium chlorite solution.				Chen et al. (2011)
4 types of cellulose fiber pulp samples were individually fibrillated: Untreated Enzymatic pretreated with Endoglucanase Carboxymethylated TEMPO-mediated oxidized	Nanocellulose production study.	Hydrodynamic cavitation and acoustic cavitation were compared. 0.40% w/w for all samples, and 2% for carboxymethylated and TEMPO-oxidized cellulose. The ultrasonic horn with a diameter of 12.7 mm worked at the frequency of 20 kHz and maximum output power of 750 W. 40% and 100% of the maximum horn power were used. 5, 15, 30 min	Sonication was more efficient for cellulosic fibrillation. After the ultrasound treatment at 40 and 100% probe power, the fibers with a size of 100 μm and smaller fibrils with a size of <100 μm were obtained. The nanocellulose fraction was insignificant for untreated and enzymatically treated after ultrasound treatments of 40% for 12.5 min and 100% for 5 min. However, chemically modified cellulosic, particularly in the Carboxymethylated fibers had higher nanocellulose fraction. No WRV reported. The sonication power, time, and relative size of the zone below the sonication horn influenced the fibrillation of the carboxymethylated cellulose fibers.	Redlinger-Pohn et al. (2022)
Cellulose (Natural Cellulose) Details of cellulose purity, and source are not provided in the study.	Nanocellulose production	Used hydrodynamic as well as acoustic cavitation. The aqueous solution of 1% (0.5 kg solids in 50 x 10^3 m^3 water).	The cellulose particle had an initial size of 63 μm. The average particle size obtained after hydrodynamic treatment was 1.36 μm. The average size of HIUS-treated particles was 301 nm.	Pinjari et al. (2010)

Table 2.3. Continue.

Sample and composition	Purpose	HIUS conditions	Results and remarks	Reference
		Probe with a diameter of 35 mm working at a frequency of 22 kHz, working at a maximum power of 750 W at 80% amplitude (600 W), calorimetric efficiency of 10%, and Intensity: 3.4 x10^5 W/m. Time: 110 min	The crystallinity of the untreated sample was 86.56%. The crystallinity of the sample was reduced to 37.76% due to the effect of cavitation. No fibrillation yield or WRV reported.	Pinjari et al. (2010)

WRV = water retention value; HIUS = high intensity ultrasound; TEMPO = 2,2,6,6-Tetramethylpiperidine-1-oxyl radical Huerta, R. (2020c).

Later, Espinosa et al. (2019) compared the high-pressure homogenizer with two other mechanical treatments with twin-screw extruder, and ultra-fine grinder to evaluate various methods of nanocellulose production. Conditions for the fibrillation treatments were: i) ultra-fine grinder (cellulose fiber suspension at 2 wt%, 2500 rpm for 2.5 h, where pulp passed for 1 s 60 times per h through the nip zone); ii) twin-screw extruder (cellulose fiber suspension at 18–20 wt%, L/D ratio = 4, 10°C, 400 rpm) with(out) enzymatic pretreatment feed with endoglucanase, and; iii) high-pressure homogenizer (same conditions as the aforementioned paragraph). The twin-screw extruder technology required 5 times less energy than the high-pressure homogenization and ultrafine grinder to produce nanocellulose when assisted with the enzymatical pretreatment, and the energy consumption was reduced to half when compared with the non-enzymatically assisted twin-screw extruder technology. Also, the lignocellulosic nanofibers were added to cardboard as a reinforcement agent. It was found that the addition of 1.5% to 4.5% doubled Young's modulus and burst index of recycled cardboard pulp.

Nanofiber production from waste wheat straw has also been reported. Waste wheat straw is a byproduct of the wheat straw pulping industry. It is generally obtained from crude wheat straw by screening, and is mainly composed of leaves, straw scraps, soil, and a large amount of ash (Bian et al., 2018; Huan et al., 2017). Bian et al. (2018) studied the lignocellulosic nanofibrils production from waste wheat straw. First, the waste wheat straw was prewashed with deionized water to remove the free ash at different solid-to-liquid ratios, equal to 1:50, 1:200, and 1:500. The water + feed mixture was mixed at 600 rpm for 15 min, and then, the mixture was pressed with a cloth bag to remove the liquid phase. Then, the washed feed was hydrolyzed with 80% (w/w) p-toluenesulfonic acid solution at 80 °C for

20 min at a liquor to solid mass ratio of 10:1. Hydrolyzed samples were then fibrillated with a stone disk grinder SuperMassCollodier. Finally, fibrillated samples were post-treated using endoglucanase. The increase in the water dosage in the prewashing step from 50 to 500 times the feed weight decreased the ash content. The maximum ash removal was reached at the feed-to-water ratio of 1:500, reducing the ash content from ~35% to ~10%, enhancing the non-cellulosic compounds removal. The p-toluenesulfonic acid hydrolysis + prewashing at the feed-to-water ratio of 1:500 increased the cellulose content from 24.28 ± 0.01 to 49.19 ± 1.46 %. The prewashed (with the 1:500 ratio) and acid hydrolyzed feed was fibrillated into lignocellulosic nanofibrils with an average diameter of 57.0 nm. The endoglucanase post-treatment produced less entangled lignocellulosic nanofibrils with diameters around 47 nm.

Furthermore, the characteristics of wheat straw sourced CNF were compared to those sourced from other feeds. Alemdar et al. (2008) isolated CNF from wheat straw and soy hulls. Cut feeds were soaked into the sodium hydroxide solution (17.5% w/w) for 2 h. Then, they were hydrolyzed by 1 M HCl at 80 ± 5°C for 2 h (to hydrolyze the hemicelluloses and pectin). Then, treated again with 2% w/w of NaOH solution (time not mentioned). For nanofibril production, samples were cryocrushed, soaked in 2 L water, and mechanically fibrillated using a Cramer disintegrator, at 2000 rpm. Samples were also homogenized by 20 passes through a laboratory fibrillator with pressure < 300 bar. Chemical characterization of the wheat straw nanofibers confirmed that the cellulose content was increased from 43% to 84%. The wheat straw nanofibers were determined to have diameters in the range of 10–80 nm and lengths of a few thousand nanometers. They concluded that the obtained CNF had potential for aerospace, automotive and medical biocomposites production.

Additionally, Shahbazi et al. (2017) extracted CNF from wheat straw and poplar wood. The feed was swelled with NaOH 17.5 wt% for 2 h at 25°C to remove extractives and other soluble components. The effect of the swelling treatment on the cellulose, hemicellulose, and lignin contents was not further reported in that study. Then, the obtained pulps were bleached by H_2O_2 at optimized conditions (46°C for 90 min for wheat straw). After that, fibers were hydrolyzed with HCl solution (0.5 M) at 121 ± 1°C and 1 bar for 0.5 h in an autoclave. Afterward, they were washed with distilled water until a neutral pH was obtained and then dried at 25°C for 24 h. Hydrolyzed samples were alkali treated again with 2 wt% NaOH at 80 ± 5°C for 2 h. A secondary bleaching process was applied again. Pulp slurry was acidified to pH 2.3 with 10 wt% H_2SO_4, and then, 0.15 g $NaClO_2$ per 1 g sample was added. The bleaching process was carried out at 55°C for 1 h (after 30 min bleaching, another 0.12 g $NaClO_2$ was added). The isolated cellulose was fibrillated at a concentration of ~1% using an ultrafine grinder. Untreated wheat straw had a cellulose content of 47.6 %, which was increased to 84.67 % after swelling, hydrolysis and bleaching treatments. The average diameters of CNF were 43 nm for the wheat straw.

2.6 Calcium carbonate

Calcium carbonate ($CaCO_3$) is a common chemical found in rocks all over the world, mainly as limestone. It is also the main component of the shells of many marine species, including snails, coal balls, pearls, and eggshells (Al Omari et al., 2016). Calcium carbonate had been implemented in many industries for different applications, including i) food additives in the food industry; ii) nutritional supplements, cosmetics ingredients, excipient, and active ingredients of antacids in the pharmaceutical industry; iii) fire extinguisher foam filler, and; iv) filler in paper, paint, adhesives and sealants, and polymers

(Al Omari et al., 2016). Additionally, the Food and Drug Administration (FDA) of US considers calcium carbonate as a generally recognized as safe (GRAS) substance, under certain specifications (FDA, 2023a).

In the pulp and paper industry, calcium carbonate is currently the most popular filler (Sáenz et al., 2023; Hu et al., 2022). The term "filler" often refers to inorganic compounds employed at concentrations of between 10-20 % to reduce supply costs and improve paper properties, such as its optical, physical, and visual attributes (Gill et al., 1995). Fillers have been in use for a long time, and their use could lead to enhanced paper quality as well as cost-effectiveness at optimum concentrations and paper matrix integration techniques (Gill et al., 1995).

Global calcium carbonate consumption increased with the transition from acid to alkaline papermaking processes in the 1950s. The interest in neutral/alkaline papermaking systems increased at that time due to the need for long-life book papers from large libraries and the development of alkaline sizing agents, which provided papermaking systems with environmental, financial, and quality advantages in comparison with the traditional acid papermaking processes at those times (Gill et al., 1995).

Calcium carbonate fillers can be classified as: i) natural products obtained by physically grinding limestone, and; ii) precipitated calcium carbonate, produced by chemical reactions. Compared to precipitated materials, natural products often contain bigger particles and wider size distributions. On the other hand, different particle morphologies of precipitated calcium carbonate can be obtained by regulating the precipitation conditions during manufacture (Gill et al., 1995). Customized precipitated carbonate can be manufactured 'on-site' by constructing a small factory within the paper mill site. The host

mill supplies the water and CO_2 required for the precipitation process, and the precipitated calcium carbonate dispersed in water is sent directly to the paper mill through a short-length pipeline. In comparison to natural ground products, precipitated carbonates have higher chemical purity, more uniform particle size, and distinct morphologies. As a result, precipitated carbonate fillers typically offer superior opacity, bulk, and lower internal sheet abrasion (Gill et al., 1995).

Calcium carbonate filler has a long history as a valuable papermaking additive, substantially contributing to the improvement of paper properties such as brightness, smoothness, and dimensional stability while lowering overall production costs (Hafez et al., 2020). Through its application, wet web dryness was improved, drying operations use less steam, and paper bulk was increased (Song et al. 2022). Additionally, calcium carbonate filler considerably improves the final paper product's opacity, whiteness, and ink absorption (Hu et al., 2022). However, the addition of calcium carbonate is usually restricted to a maximum level because it may result in the hindering of cellulosic fiber bonding (Song et al. 2022; Sáenz et al., 2023).

Recently, research has been carried out aiming to increase the calcium carbonate filler content while reducing its negative effect on fiber bonding by their combination with cellulose nanofibers. Some examples are further detailed in Table 2.4. Precipitated calcium carbonate was used predominantly as the mineral filler, and the effect of the mineral filler content in the paper samples was studied at concentrations of 20% to 50% based on the dry paperweight. The combination of the compounds was achieved with the addition of cationic starch (He et al., 2016), mixing cellulose nanofiber suspension with already developed commercial cellulose nanofiber + calcium carbonate press cake (Hafez et al., 2020),

implementation of co-refining processing of cellulose nanofiber and calcium carbonate (Song et al. 2022), and precipitation of calcium carbonate in the presence of cellulose nanofibers (Kim et al. 2022). Then, the filler mixture was added to the pulp under stirring conditions and dried to form paper samples. Overall, it was found that combining the calcium carbonate filler with CNF can improve the mechanical properties of paper using high mineral filler content, as CNF acts as a bridge material that improves the connection between pulp fibers and the mineral filler due to CNF high surface area.

2.7 Glycerol

Glycerol (or glycerin) is a triol with a propane structure substituted at positions 1, 2, and 3 by hydroxyl groups recognized as GRAS (FDA, 2023b). It is a viscous, hydrophilic, colorless, and odorless liquid that readily dissolves in water due to the H-bonds formed between its hydroxyl groups and water. Glycerol is widely used in a variety of industrial applications, including as a humectant in the food, cosmetics, personal care, and pharmaceutical sectors (Kruelák et al., 2023). Glycerol is also one of the most widely utilized plasticizers for the production of film composites (Vieira et al., 2011). Plasticizers are chemicals that are added to plastics or elastomers to improve flexibility, workability, and distensibility. They reduce the tension, hardness, density, viscosity, and electrostatic charge of polymers while increasing chain flexibility, fracture resistance, and dielectric constant (Vieira et al., 2011). Additionally, plasticizers impact other properties like crystallinity, optical clarity, electric conductivity, fire behavior, and resistance to biological degradation (Vieira et al., 2011).

Table 2.4. Glycerol and calcium carbonate addition on cellulose-containing composites for food packaging development.

Materials	Function	Making procedure	Result	Reference
Bleached softwood kraft Pulp Precipitated calcium carbonate (2.2 μmaverage size) Cationic starch (degree of substitution of 0.04) Cellulose nanofibrils (CNF)	Paper filler and additive development for paper sheets	The feed was beaten to 150 mL CSF (Canadian standard freeness) in a laboratory Valley beater. Pulp with a consistency of 1% was fibrillated with a wet disk-milling at 1800 rpm with a gap clearance of −150 μm and 35 passes. A 2 g/L starch solution was boiled at 95°C for 25 min before use. PCC-CNF filler formation: CNF diluted to 0.1%, mixed with 2% precipitated calcium carbonate suspensions and stirred for 5 min/600 rpm. Then, cationic starch solution was added and stirred for 5 min/600 rpm. CNF and cationic starch dosages were 2% (based on pulp weight) and 2.5 % (based on calcium carbonate weight). The dosages of precipitate calcium carbonate were 20%, 30%, and 40% on pulp weight for the paper formation. The components were mixed at 1000 rpm for ~1 min, The hand sheets (80 g/m^2) were formed in a conventional hand-sheet former. Poly-aluminum chloride, anionic polyacrylamide, and micro-polymer were added for filler retention.	The PCC-CNF fillers had retention of ~ 90% filler; the filler containing just CNF had a retention of around 85%. The SEM analysis showed that the starch and the CNF were lying on the outer surface of the PCC–CNF filler during formation, embedding the calcium carbonate and facilitating the H-bonding with the hydroxyl groups of cellulosic molecules in the pulp. The starch functioned as a wet-end additive, facilitating the flocculation and adsorption of CNFs and calcium carbonate onto the cellulose fiber surface. Also, starch could anchor itself on the calcium carbonate surface, enhancing the bonding between the pulp fibers and fillers. The tensile index and burst index decreased as the calcium carbonate content increased, hindering the formation of H-bonds between the fibers. In PCC–CNF added composites, the highest tensile index and burst index were observed at calcium carbonate contents of 20 %, ascribed to the higher bonding ability within cellulose fibers and filler. The handsheet with PCC-CNF fillers had superior light scattering compared to the handsheet loaded with conventional PCC, attributed to the formation of complexes between the fillers and CNF, resulting in a densified network with a higher number of small-sized optically active pores.	He et al. (2016)
Cellulose nanofibrils (CNF) Microfibrillated cellulose/calcium carbonate (50:50)	Bio-based composite films development	Composites made of CNF and FLC were analyzed pure and mixed at the ratio of 1:1 with a final dry weight of 1g. The three tested composites had calcium carbonate contents of 0, 25, and 50 wt%.	The tensile strength of composites prepared with a mixture of CNFs and FLC did not show a significant difference when compared to pure CNF films. However, the tensile strength of FLC films was significantly lower compared to the other two samples. The strain at maximum stress, decreased with the calcium carbonate increased in the composite.	Hafez et al. (2020)

Table 2.4 Continue

Materials	Function	Making procedure	Result	Reference
produced by FiberLean Technologies UK (FLC)		Feeds were suspended at 0.5 wt%. Composites were produced by the vacuum filtration technique. The wet composites were placed between two WhatmanTM Grade 5 filtering papers, and then, between two stainless steel disks (load of 2 kg) and dried at 75°C for 24 h.	The XRD analysis suggested that all samples were cellulose I (peak at 22.9°). The crystallinity indices of the three composites were 88.2, 91.4 and 87.9% for CNF, FLC-CNFs, and FLC, respectively. The morphological analysis revealed the uniform distribution of calcium carbonate on all the composite's surfaces.	Hafez et al. (2020)
Precipitated calcium carbonate (PCC) TEMPO-oxidized cellulose nanofibrils (CNF)	PCC/CNF filler development Generation of special paper materials requiring high mineral content	The CNF (1.45 wt%) and precipitated calcium carbonate mixture were blended and placed into a PFI refiner for 7 min. The resulting CNF/calcium carbonate composite was formed by gelation, and the total dry weight consisted of 3 g dw CNF + 40 g dw calcium carbonate. For the PCC/CNF composite filler generation, the composite was diluted to a concentration of 10 wt% and uniformly dispersed using hydraulic shear at 600 rpm. The PCC/CNF filler was mixed with refined pulp diluted at 0.25%, which consisted in a mixture of softwood fiber + hardwood fiber at the ratio of 1:3 g. cationic polyacrylamide (CPAM) was added as a retention aid at the concentration of 0.03% dw based on the slurry. The filler contents on the paper samples were 18%, 25%, and 32.	PCC/CNF filler at the concentration of 32% increased 44.3% in the tensile index compared to conventional PCC-filled paper. The strength enhancement of fiber and PCC/CNF filler was more pronounced at a higher filler content. Morphological analysis showed that CNF acted as a bridge to increase the connection area of the cellulosic fiber and calcium carbonate particles, improving the tensile strength. The XRD analysis confirmed that the CNF had cellulose I crystalline structure, which remained unaffected by the refining process. The crystallinity index decreased from 88.50% to 76.66% as the refining revolutions increased. The FT-IR analysis showed that the peak at 3458 cm^{-1} shifted and broadened, suggesting interactions between OH- groups and calcium ions between CNF and PCC. The process implemented in this study, disassociated calcium ions on the surface of precipitated calcium carbonate particles, improving the interactions with CNF. The hydration of calcium ions on the PCC surface generated hydroxyl groups that interacted with cellulose via H-bonding.	Song et al. (2022)

Table 2.4 Continue

Materials	Function	Making procedure	Result	Reference
Cellulose nanofiber (CNF) Flexible Calcium Carbonate (FCC; CNF + precipitated calcium carbonate) Ground calcium carbonate (GCC)	Paper (handsheets) production	FCC: 44.9 g carbon dioxide was injected to 1 L of 0.2% CNF suspension constantly stirred at 350 rpm for 30 min at 30°C; the temperature was increased to 33-34°C as the reaction progressed. The reaction was terminated after reaching a pH of 7.0. The fibers for the paper development were mixed with FCC and GCC to make handsheets of 80 g/m^2 with 20, 30, and 40 wt% ash content.	The addition of FCC resulted in higher bulk, stiffness, breaking length, and better smoothness compared to GCC. The FCC added paper required less calendaring pressure to achieve the same smoothness as GCC-added paper. Using FCC as a filler allowed a reduction of ~10% in wood fiber usage for printing paper manufacturing. From the SEM analysis, it was concluded that the FCC fillers in the papers may form clusters between wood fibers and could undergo deformation during wet pressing and calendering. FCC-containing paper showed clean surface fibers that could form H-bonds. In contrast, GCC fillers in GCC-containing papers were randomly located with no clean surface fibers.	Kim et al. (2022)
Tapioca starch Thermo-mechanical modified tapioca starch Glycerol TEMPO-oxidized cellulose nanofiber (CNF)	Development of potential material for food packaging applications	The modified starch was produced with a shear-and-heat milling machining. Glycerol and CNF were used as plasticizer and reinforcement agents, respectively. Raw or modified starch was blended with glycerol and CNF gel. The final concentration of those components in the films were 65, 35, and 0-10 wt%, respectively. The mixtures (60 g total) underwent melt-compounding in a torque rheometer at 120°C and 60 rpm for 6 min. Then, pelletized and vacuum dried at 50°C for 24 h. The films were produced through compression at 120°C and 15 MPa for 15 min.	The addition of 10 wt% CNF increased the elastic modulus from 60 to 95 MPa for the unmodified starch film, and from 23.7 to 286.4 MPa for the modified starch film. CNF addition reduced the elongation at break from 211.91% for modified starch + glycerol to 23.14% for modified starch + glycerol + CNF, and from 177.66% for the raw starch + glycerol film to 102.84% for raw starch + glycerol + CNF film. The shear-and-heat milling machining process increased particle roughness and enhanced active H-bonds, improving interactions among starch, glycerol, and CNFs. A band that corresponded to O-H bonds slightly shifted to a lower wavenumber after the addition of glycerol and CNF, indicating an alteration in the energy of H-bonds in the film due to the formation of intramolecular H-bonds. With the addition of CNF, peaks that represent C-O-H and C-O-C stretching, respectively, shifted to lower wavenumbers, suggesting a molecular-scale interaction between starch and CNF.	Thongmeepech et al. (2022)

Table 2.4 Continue

Materials	Function	Making procedure	Result	Reference
Capsicum leaf protein Cellulose nanofiber (CNF)	Biodegradable plastic development	0.25 g capsicum leaf protein was dissolved in 5 mL water, and then, 1 mL of 1 mol/L urea solution was added. The protein solution was stirred for 4 h, 70°C at the speed of 150 rpm. After that, CNF was added at concentrations of 0%, 20%, 40%, 60%, 80%, and 100% based on the protein mass. After 30 min stirring, glycerin at the concentration of 3% (based on the protein weight) was added. The mixture underwent an additional 30 min stirring and 1 min homogenization at 10,000 rpm. The resultant solution was degassed in a vacuum drying oven at 0.09 MPa for 20 min, and finally, cast and dried for 6 h at 60°C.	CNF increased the tensile strength and young's modulus of the protein films from 0.5763 to 3.0732 MPa, and 1.3003 to 16.1925 MPa, respectively. The elongation at the break also increased, until the maximum value reached 16.22 % (CNF content of 60%) but then decreased. The addition of glycerol reduced the density of protein-protein interactions and increased the mobility of polymer chains. The crosslinking of CNF with the amino groups of the protein resulted in longer polymer chains, contributing to the elongation at the break of the films. SEM images showed high surface roughness of the protein films; which significantly impacted the films mechanical properties and hydrophobicity. The addition of CNF at contents of 20%, 40%, and 60% lead to more smooth and compact films due to CNF's high specific surface area. The CNF contents above 60% resulted in poor dispersion of the CNF within the protein matrix due to excessive agglomeration and an uneven surface of the films. The water contact angle increased by increasing CNF content. The maximum angle of 66.50° was achieved at the CNF concentration of 60%. As the CNF content increased the strength of the amide I and amide III bands was less prominent. Hydroxyl groups in glycerol and CNF interacted with the principal polypeptide chains of proteins, predominantly forming H-bonding with the amino and carboxyl groups of the proteins, altering the protein's conformation and hydrophobicity.	Quin et al., (2022)
Hemicelluloses Chitosan Cellulose nanofiber (CNF)	Development of edible plasticized film reinforced by cellulose nanofibers	A 2% (w/v) chitosan solution was formed in 1% (v/v) acetic acid under stirring at 40 °C for 1 h. Also, a 2% (w/v) hemicelluloses solution was formed in 2% (v/v) acetic acid under magnetic stirring at 60 °C for 24 h. The chitosan and hemicellulose solution were mixed, and the	By adding 5% CNF, the film tensile strength increased from 16.24 to 53.75 MPa. Those with glycerol showed the highest tensile strain at break (7.80–18.53%), while sorbitol-plasticized films had the highest tensile strength (23.14–48.96 MPa). Films with 20–30% glycerol showed high tensile strength (31.02–38.56 MPa) and tensile strain at break (10.07–15.98%).	Xu et al. (2019)

Table 2.4 Continue

Materials	Function	Making procedure	Result	Reference
Plasticizers (glycerol, sorbitol, or xylitol)	Biodegradable plastic development	chitosan:hemicelluloses on the dry film ratios were 1:1. CNF added at concentrations of 5, 10, 15, and 20 % (based on dry chitosan + hemicelluloses). Plasticizers (glycerol, sorbitol, or xylitol) at concentrations of 10, 20, 30, and 40% (based on the dry weight of chitosan + hemicelluloses) were added. The film-formed solution was stirred at 25 °C for 30 min, then centrifuged and ultrasonic degassing (conditions not specified), 7 mL of the solution was cast into a 5.5 cm petri dish and vacuum-dried at 60 °C for 6 h.	The C–O–C stretching vibration broadened and shifted due to the overlap of the ether bond in hemicelluloses and chitosan, indicating their miscibility through strong H-bonds between the molecular chains. Plasticized films showed a decrease in the intensity of the O–H peak, suggesting a weakening of H-bonds between the polymers. Additionally, a new peak related to the vibration of the $–NH_3^+$ group in chitosan emerged in the film spectra, indicating possible interaction with CNF through electrostatic attraction. The SEM images showed that plasticizers reduced the compatibility of the films, attributed to the disruption of H-bonds and electrostatic interactions between the polymer chains. The contact angle of the films containing 5% CNF and 0% plasticizer was 101.1°, attributed to the hydrophobic nature of chitosan. The contact angles of the plasticized composite films decreased with increasing plasticizer contents. Films with 20–30% glycerol displayed slightly higher contact angles.	Xu et al. (2019)

In the literature, most film composites containing cellulose nanofibers and glycerol are found to be mainly composed of another polymer, and cellulose nanofibers and glycerol would be used in minor concentrations as reinforcement and plasticizer agents, respectively. Some examples of the aforementioned are composites made of starch, protein, and hemicellulose/chitosan mixture (Xu et al., 2019; Xu et al., 2021; Quin et al., 2022; Thongmeepech et al., 2022). Studies of cellulose-based composites plasticized with glycerol are also mentioned in the literature (Hassan et al., 2016; Ezati et al., 2020). Ezati et al. (2020) developed a colorimetric pH indicator made of carboxymethylcellulose (CMC) or CNF and alizarin while Hassan et al. (2016) generated nanocomposites based on nano fibrillated cellulose + chitosan nanoparticles intended for paper coating.

Studied glycerol contents in the composites ranged from 3 to 40%. The lowest concentration was applied to the protein composite while concentrations above 9% were used in starch and cellulose-based composites. Overall, an increase in the elongation at break and a decrease in tensile strength in composites based on starch were observed. As for cellulose, Hassan et al. (2016) reported a reduction of the tensile strength, Young's modulus, and strain at break in the TEMPO-oxidized cellulose nanofiber composite after the addition of 25% glycerol. The neat cellulose nanofiber composite values for tensile strength, Young's modulus, and strain at break were 47.8 MPa, 2.07 GPa, and 6.2%, respectively, and after the addition of glycerol, the values were reduced to 12.86 MPa, 0.56 GPa, and 11.1%, respectively. It was concluded that the plasticized cellulose nanofiber composite was less brittle and more flexible than the neat cellulose nanofiber composite.

2.8 Cellulose nanofibers (CNF) films/composites

As mentioned before, the use of biomass lignocellulosic material such as wheat straw to produce value-added compounds has been gaining attention due to biomass abundance, low cost, and availability. CNF are an example of value-added compounds derived from biomass lignocellulosic material, and can be defined as cellulose-composed fibrils that typically are <100 nm in diameter and a few micrometers in length (Huerta et al., 2018a; Huerta et al., 2020b). Some properties that make CNF an interesting biomaterial include high aspect ratio, surface area (150–600 m^2/g), excellent mechanical properties (elastic modulus of 79–220 GPa and tensile strength of 1.7–7.7 GPa), low coefficient of thermal expansion, low density, non-toxicity, and biodegradability properties, as well as easy functionalization (Huerta et al., 2018a; Huerta et al., 2020; Mokhenaet al., 2021). CNF sourced from plants are usually produced using multiple treatments to separate the three main components of lignocellulosic material (i.e., cellulose, lignocellulose, and lignin) and isolate cellulose, followed by a mechanical process, which disintegrates the big cellulose fibers into smaller cellulose fibrils of nano-scale dimensions (Patil et al., 2022).

Several films/composites containing cellulose-based materials have been generated and studied since the start of this century. The studies presented in this section were published in recent years from 2019 to 2021 and are further discussed in Table 2.5. This section also focused on CNF. The CNF-containing films/composites were reported to have potential applications for packaging development, intelligent or active packaging, and conductive nanocomposite development. In those studies, CNF was used both as a matrix component and as a reinforcement agent. When CNF was used as reinforcement, other polymers such as chitosan and polyvinyl alcohol were used as matrix compounds (Okahisaet al., 2020; Mujtaba

et al., 2021; Zhang et al., 2021). Other examples of matrix compounds such as starch, protein, and hemicellulose/chitosan mixtures were already mentioned in section 2.7 of this chapter. Those film composites were mainly prepared using the solvent casting method, where the impregnation and pelletization + compression methods were also mentioned.

There were other studies that mixed CNF with other compounds to form improved film composite matrices. For example, CNF was mixed with chemically modified starch and reduced graphene oxide to produce composites with improved mechanical properties before and after soaking the film composite in water and providing electric conductivity in the composite, respectively (Soni et al., 2019; Liu et al., 2021). These composites were fabricated using the solvent casting and vacuum filtration methods, respectively. During the fabricationof these composites, the ratios of CNF and the second matrix compounds were from 1:0 to 0:1 w/w and 2:1 to 1:2 w/w, respectively.

Films/composites made purely of cellulosic compounds were also reported. Recently, Hossain et al. (2021) produced an oil-resistant container with CNF and lignocellulosic nanofibers using the layer-by-layer method. Additionally, Abral et al. (2020) generated a film with CNF sourced from ginger tubers using the solvent casting method, which was also called nanopaper. Furthermore, studies about film composites based on CNF added with black carrot-sourced anthocyanins and gromwell roots-sourced shikonin to generate pH indicators were also reported (Moradi et al., 2019; Roy et al., 2021). The pH indicators with anthocyanins were prepared by immersing purchased bacterial cellulose sheets in an anthocyanin-rich solution, and the shikonin added indicator was made by integrating shikonin on the film-forming solution before casting. Finally, the modification of CNF composite in the surface and bulk with saturated fatty acids to provide a hydrophobic characteristic was studied by Balasubramaniam et al. (2020). For those hydrophobic

composites, CNF films were first produced with the solvent casting method. The modification was then performed by soaking the CNF films in pyridine and fatty acid chlorides (lauroyl chloride, stearoyl chloride, and palmitoyl chloride) for the bulk modification, and presoaking the CNF films in pyridine solution and applying the fatty acid chlorides with a brush.

In the literature, CNF-based films are often called CNF papers or nanopapers. Mokhenaet al. (2021) defined nanopapers as thin films composed of strong hydrogen-bonded fibrous nanocellulose. These papers are made from CNF suspensions in which the liquid is removed to allow for fibril interactions. Solvent casting is the most frequently used process to create nanopapers. It involves the formation of a homogeneous nanofibril suspension in which the nanofibrils accumulate as the liquid evaporates, improving H-bonding interactions. Nevertheless, this procedure may lead to a prolonged evaporation process and wrinkle formation. Vacuum filtration is an alternative method that speeds up preparation by creating a dense network of fibrils on the filter. However, moisture concentration gradients might result in wrinkles. To prevent this, mild pressure is frequently used while drying to reduce wrinkling (Mokhenaet al., 2021).

To the best of my knowledge, there is just one study that formed nanopapers made with CNF isolated from wheat straw without any further addition of compounds. Earlier, Barbash et al. (2017) isolated CNF from organosolv-treated wheat straw with a combination of acid treatment with sulfuric acid and sonication. Then, they formed nanopapers using the solvent-casting method. Wheat straw was initially treated in an organosolv system comprised of isobutyl alcohol–H_2O–KOH–hydrazine. Next, the organosolv-treated sample was thermochemically treated with acetic acid and hydrogen peroxide in a volume ratio of 70:30% with 15% catalyst–sulfuric acid (organosolv-treated sample-based weight) at

95 ± 2°C for 180 min. An acid hydrolysis treatment with 43% sulfuric acid, at the liquid-to-solid ratio of 10:1 v/w for 30 and 60 min at 20 and 60°C were also performed. To fibrillate the treated feed, sonication was applied at 22 kHz for 30 min. The nominal power and the dispersion concentration were not mentioned in the study. Finally, nanocellulose films (nanopapers) were produced by pouring the sonicated dispersions into Petri dishes and dried at room temperature. The initial cellulose content was 44.2%, however, the final cellulose content was not mentioned. The combination of hydrolysis treatment and sonification improved the nanofibril formation, producing fibrils with diameters ranging from 10 to 40 nm. Furthermore, nanopapers had a tensile strength of up to 42.3 MPa and Young's modulus of 11.45 GPa.

Table 2.5. Films/composites containing CNF.

Materials	Function	Making procedure	Results	Reference
Bacterial nanocellulose Black carrot anthocyanins	pH-sensing indicator	The bacterial cellulose material (purity ≤ 99%) produced by *Komagataeibacter xylinus.* The indicator was generated by dip-coating a piece of bacterial cellulose material (400 mm^2) into the Black carrot anthocyanins solution with a total anthocyanin content of 6 mg/ml for 30 min.	FT-IR: Typical cellulose spectra patern. X-ray: There was a peak assigned to cellulose Iα (14.5°). The crystallite size and crystallinity index were 1.87 nm and 66.39% The pH-sensing indicator displayed discernible color variations depending on the freshness of the fish fillets. In addition, the total color differential values of the indicator had a correlation with the bacterial count and total volatile basic nitrogen.	Moradi et al. (2019)
TEMPO-oxidized cellulose nanofiber (TCNF) mixed with three types of modified starch: hydroxypropyl starch, acetyl starch, and acetyl oxidized starch with a degree of substitution of 0.11, 0.08, and 0.04, respectively.	Single-use plastic replacement	TCNF (0.8%, W/V) and starch (5%, W/V) solutions were blended together in different weight ratios and stirred until the dispersion was homogeneous. TCNF:starch weight ratio were: 1:0, 1:0.2, 1:06, 1:1, 1:1.5, 1:6, 0:1. The cellulosic/starch dispersion was casted and dried in an oven at 45°C/6 h.	The mixture of hydroxypropyl starch with the TCNF achieved the best results for the mechanical properties. The TCNF films had a tensile modulus of 6.4 GPa. The dried membrane of TCNF + hydroxypropyl starch 1:0.2 had the highest tensile modulus of 7.6 GPa in these experimental conditions. The ratio of 1:0.6 had 7.3 GPa. It was concluded that the addition of a certain amount of starch acts as a binder of cellulose nanofibers. The swelling ratio and the mechanical properties of wet films were investigated by immersing the samples in water. The TCNF film had the highest swelling of ~6500% and the lowest tensile modulus (0.05 MPa). The lowest swelling ratio (~600%) and the highest wet tensile modulus of 7 MPa were achieved in the ratio of TCNF + hydroxypropyl starch 1:0.6.	Soni et al. (2019)

Table 2.5. Continue.

Materials	Function	Making procedure	Results	Reference
Polyvinyl alcohol Cellulose nanofibers (CNF) derived from oil palm	Development of ductile nanocomposites. Comparison of two techniques for nanocomposite development (impregnation vs casting)	Cellulose was isolated from dry powder prepared from oil palm trunk (*Elaeis guineensis*) using toluene + methanol, bleaching with ASC, and alkaline extraction. The CNF suspension was achieved after grinding the purified cellulose. **Impregnation:** Wet CNF sheets were prepared by filtering 0.5 % CNF suspension. Then, CNF sheets with different low void ratio and a density were prepared (0.2, 0.8, and 1.1 g/cm^3) from the wet CNF sheets using different drying techniques. CNF sheets were impregnated with 10 wt% PVA solution and drying at 30°C, achieving nanocomposites with 30, 50, and 70 wt% CNF, according to their different low void ratio and a density. **Casting:** CNF suspension and PVA solution were mixed, casted, and dried at 30°C, achieving nanocomposites 30, 50, and 70 wt% CNFs.	XRD: A decrease in the intensity of the peak at 2θ = 19.4◦ and the increase at 2θ = 22.5◦ was associated with addition of CNF. The average diameter of the cellulosic fibrils was 40 nm. Tensile strength and young modulus of PVA were 118.5 and 11.1. CNF tensile strength and young's modulus were 219.2 and 18.1. The tensile strength and young modulus of PVA films were increased with the addition of CNF. The purely made CNF sheet was negatively affected by environment moisture, which decreased tensile strength and Young's modulus. It was proposed to include cross-linking, grafting, and /or coating with hydrophobic substances to overcome this problem. An intensification of CO− stretching vibration indicated interaction of hydroxyl groups in PVA and CNF Nanocomposites prepared by impregnation had higher thermal melting temperature and tensile toughness.	Okahisa et al. (2020)
Cellulose nanofiber (CNF, 90% fine content) Lignocellulosic nanofibrils (LCNF; 90, 70% fines)	Development of oil-resistant food serving containers	The composite was generated by adding a layer of LCNF-OCC or CNF mixed with wood particles onto a paper substrate, with a top layer of LCNF or CNF. The core layer was created with 2 wt% LCNF-OCC or CNF suspensions sonicated at 80%	At 90% fines content, CNF had the largest volume of smaller particles. CNF and LCNF had more consistent particle size distributions than those obtained from the old-corrugated containers with similar fine content, attributed to impurities like lignin, starch, inks, and adhesives in old containers.	Hossain et al. (2021)

Table 2.5. Continue.

Materials	Function	Making procedure	Results	Reference
Lignocellulosic nanofibrils from old corrugated container (LCNF-OCC; 90, 70% fines)		amplitude for 3 min. Nominal power was no mentioned. Then, wood particles were added to the suspensions. The top layer consisted of 0.2 wt% LCNF or CNF suspensions prepared with the same sonication process. The core layer suspension was deposited onto circular-cut printing paper using vacuum pressure for 15 min at 0.8 bar. The top layer was added and left to filter for 23 min. The wet materials were placed between two stainless steel plates of a hot press at 150°C and 0.015 bar for 5 min.	CNF or LCNF with smaller fibers created a stronger bond between wood particles and CNF/LCNF due to the larger surface area. Better bonding between CNF fibers and wood particles also led to lower pores formation in the material, resulting in higher fat resistivity. SEM images showed that the coated composites presented a layered structure, which may have contributed to the oil resistivity due to the inhibited oil fat diffusion on the composite.	Hossain et al. (2021)
Cellulose nanofibers obtained from Ginger tubers.	Transparent antimicrobial nanopaper development	The raw ginger fibers were soaked in a mixture of toluene and ethanol in a ratio of 2:1 for 48 h, 500 rpm at 50°C. Then, they were alkali-treated in 5% NaOH, dewaxed, and crushed/mashed with an electrical blender. The treated ginger fibers were bleached with a mixture of $NaClO_2$ and CH_3COOH in a ratio of 4:1 for 2 h, at 60°C and stirred at 500 rpm. The bleached ginger fibers suspension were hydrolyzed with 5M HCl at 50°C for 12 h. Fibrillation was performed using an ultrasonic cell crusher at 600W for 60 min at a maximum temperature of 60°C. The suspension was poured into a Teflon plate and oven dried for 20 h at 50°C for nanopaper formation.	The treated feed had a cellulose content of 88%. Ultrasonication reduced the fiber diameter to 54.3 nm and resulted in a transparent nanopaper with a thickness of 5 μm. X-ray diffraction: cellulose I diffraction pattern. Raw fiber had a crystallinity index of 26%, which increased to 67% after acid hydrolysis treatment. After ultrasonication for 60 min, the crystallinity index decreased to 48%, attributed to the increased molecular disorder in the cellulose structure. The samples had an inhibition zone diameters greater than 6 mm. The antimicrobial properties were attributed to the possible presence of bioactive compounds in the ginger fibers.	Abral et al. 2020

Table 2.5. Continue.

Materials	Function	Making procedure	Results	Reference
Cellulose nanofibers (CNF) copolymerized with polyacrylonitrile monomers. Chitosan	Chitosan films reinforcement	Raw diatom earth was crushed and dissolved in 2 M HCl with continuous stirring (350 rpm) for 1 h 25°C, and then washed and dried to obtain purified diatomite. For the polymerization reaction, 80 ml of 3 M acrylonitrile and 13.46 mM cerium ammonium nitrate were added dropwise (2 drops/*sec*) to 100 ml of 3% dw CNFs suspension for 10 min. The reaction was stopped after 1 h, washed, and dried. Then, diatomite at the concentrations of 10% (w/w) and 30% (w/w) based on final copolymer weight was added. The mixture was stirred at 35°C for 24 h. The obtained samples were filtered, washed, and oven-dried at 50°C. Chitosan-based nanocomposite films of CNF and copolymerized CNF with(out) diatomite were prepared by incorporating them into a 1% chitosan solution at concentrations of 1%, 2%, and 5%. Then, 20% glycerol based on chitosan weight was added. The mixture was stirred using at 12,000 rpm for 15 min, and then subjected to sonication (100 W for 10 min) to prevent any possible aggregation of diatomite and CNFs in the matrix. The film solutions were cast into petri dishes and dried at 30°C for 48 h.	SEM images showed partial homogeneous distribution of diatomite and CNFs in the chitosan matrix. Chitosan films' strength and water resistance were improved by using different amounts of CNFs/diatomite composite (1–5% for CNFs; 10% and 30% for diatomite). Concentration of CNFs/diatomite (1–5% and 10–30%) in the chitosan matrix improved the antioxidant activity. The increase of the diatomite content did not influence the antioxidant activity. The addition of CNFs/diatomite (5% and 30%) in the chitosan film decreased the water solubility from 30% to 21.06%. The produced composite combination can be potentially used as a coating for food packaging to prolong shelf life.	Mujtaba et al. (2021)
Cellulose nanofiber (CNF) obtained from *Phyllostachys pubescen* (moso bamboo)	Conductive nanocomposite development with potential uses for sensors, electromagnetic	Bamboo was treated with the lactic acid-ChCl DES at the molar ratio of 9:1 at 120°C for 3 h. The recovered cellulose was diluted with water (the concentration was not mentioned) for the refining process with a high-speed homogenizer 1 h and sonication to obtain CNFs.	DES based on urea and ChCl had no influence on the chemical structure of CNF except for a possible introduction of nitrogen atoms into the composite.	Liu et al. (2021)

Table 2.5. Continue.

Materials	Function	Making procedure	Results	Reference
Reduced graphene oxide	interference shielding, all-cellulose-based Triboelectric Nanogenerator, and supercapacitors applications	CNFs and graphene oxide sheets at mass ratios of 2:1, 1:1, and 1:2, respectively, and with a total mass of 30 mg were suspended in water and mixed with 20.00 g DES (ChCl + urea with a molar ratio of 1:1 prepared at 80°C). The mixture was stirred at room temperature for 15 min to obtain a homogeneous solution, and then, l-ascorbic acid (with a mass of 10x graphene oxide based) was added to reduce graphene oxide sheets for 1 h at 80°C. A CNFs and graphene oxide sheet gel was obtained by vacuum filtrating the suspension, and such gel was dried between hot plates under pressure for 2 h at 85°C.	The SEM images showed that the graphene sheets wrapped the surface of CNF, favoring the mechanical properties of the composite. The tensile strength of CNF and graphene oxide sheets at mass ratios of 2:1, 1:1, 1:2, and pure CNF were 37.67–46.95, 46.70–50.22, 31.80–40.21 and 17.43–23.03 MPa, respectively. The decrease in tensile strength of the ratio of 1:2 was attributed to the excess graphene materials, which weakened the crosslinking of fibers and facilitated the aggregation of graphene sheets. The sample with the 1:2 mass ratio had the highest electrical conductivity (26.47 $S \cdot cm^{-1}$). The maximum areal-specific capacitance of that sample reached 226.83 $mF \cdot cm^{-2}$ at a current density of 1 $mA \cdot cm^{-2}$.	Liu et al. (2021)
Chitosan TEMPO-oxidized cellulose nanofibers (CNF) Curcumin	Curcumin grafted CNF agent with potential application as an antibacterial or antioxidant component in food packaging. The developed film can be applied as a layer coating inside bottles for liquid foods or wrapping materials for solid foods such as meat and seafood.	1 g CNF dispersed into 30% v/v ethanol (300 mL). 0.65 g of 1-(3-Dimethylaminopropyl)-3-ethylcarbodiimide hydrochloride and 0.20 g of *N*-Hydroxysuccinimide were added to activate CNF carboxyl groups. After 1 h curcumin (0.10 g) was added to the mixture and stirred for 24 hours at room temperature and dark conditions for the grafting reaction. 2.0% w/v chitosan dissolved into an aqueous acetic acid solution (2.0% v/v) was prepared under continuous stirring at 800 rpm for 1.5 h. Curcumin-grafted CNF was dispersed in water and added to the chitosan solution (10, 17, 25 and 33% based on dry chitosan). The mixtures were homogenized for 20 min at 10,000 rpm.	Curcumin-grafted CNF was prepared by esterification. Carboxylated nanocellulose formed esters with hydroxyl-containing molecules to improve the stability of curcumin. Chitosan + 10 % curcumin-grafted CNF films created a smooth, uniform film with higher crystallinity, increasing it from 21.93% to 87.15%. The Water vapor transmission rate of chitosan films decreased by 6.0%. The UV blocking property was 2 times higher. The addition and the increase of curcumin-grafted CNF concentration decreased the tensile strength in films. The tensile strain at break remained consistent at around 4%.	Zhang et al. (2021)

Table 2.5. Continue.

Materials	Function	Making procedure	Results	Reference
		30 mL of the mixtures were cast on a plastic Petri dish (14x14 mm^2) and dried at room temperature for 24 h.	The films with(out) curcumin-grafted cellulose exhibited similar but significant antibacterial activity against *E. coli.*	Zhang et al. (2021)
TEMPO-oxidized cellulose nanofibers (CNF) Shikonin obtained from Dried roots of gromwell (*Lithospermum erythrorhizon*)	Development of CNF-based pH colorimetric indicator	A 10.0 wt% (based on CNF weight) shikonin ethanolic solution was added to a 200 mL aqueous CNF suspension (1 wt%) with 30 wt% glycerol (based on CNF weight). The mixture was agitated for 3 h. The film-forming solution was cast on a Teflon-coated glass plate and let dry for 72 hours.	Shikonin in CNF film showed distinctive pH-dependent color variations in the pH range of 1 to 12. Shikonin was evenly dispersed within the CNF matrix without forming aggregates. CNF cellulose I planes were detected in the XRD analysis, with no change in structure after adding shikonin. The crystallinity index of CNF and CNF/shikonin films were 65.8 and 65.6%, respectively, with no significant difference. The addition of glycerol to the CNF-based film did not significantly alter its functional groups. The CNF/shikonin film had similar peaks to the neat CNF film, with slight differences in intensity due to physical interactions between shikonin and CNF (van der Waals interactions and H-bonding). The moisture content (~5.3%), swelling ratio (~1850%), and water vapour permeability (0.55 10^{-9} g m/m^2.Pa.s) of the CNF film was not significantly affected by the shikonin addition. Shikonin significantly increased the tensile strength of the CNF film from 51.4±2.4 to 59.5±5.0 MPa, attributed to the development of interfacial interactions such H-bonding.	Roy et al. (2021)

Table 2.5. Continue.

Materials	Function	Making procedure	Results	Reference
Cellulose Nanofibers (CNF) Fatty acid chlorides (lauric, palmitic, and stearic acids)	Modification of premade CNF films to increase its hydrophobicity	200 ml of 1 % CNF solution were cast onto Petri dishes (14.2x1.5 cm) and air-dried at room temperature For the bulk modification, the CNF films were soaked in 100 ml of pyridine for 30 min at 110°C. Then, fatty acid chlorides were added, and the surface reaction was held for 90 min. Then, the films were withdrawn and dried at room temperature overnight. Unattached fatty acids were removed with Soxhlet extraction with ethanol for 24 h. For the surface modification, the CNF films were presoaked in a pyridine solution at 110°C; the films were then withdrawn, and thin layers of fatty acid chloride were immediately applied on the surfaces with a brush. The films were let to stand at room temperature overnight before the application the Soxhlet extraction of the unattached fatty acids.	Formation of an ester bond in all modified CNF films. Increase of peaks related to CH2 bending, CH_2 vibrations compounds containing a carbon chain with more than 4 CH_2 groups, and a decrease in the OH stretching peak. Contact angle analysis showed that the CNF had a contact angle of 57°, making it hydrophilic. Bulk-modified films prepared with lauric, palmitic, and stearic acids had contact angles of 114.19, 111.54, and 114.2, respectively. Surface-modified samples with lauric, palmitic, and stearic acids had contact angles of 108.7, 104.61, and 120.98, respectively. Thus, all modified CNF films had a hydrophobic behavior. All films prepared through bulk modification had lower tensile strength compared to surface modification, attributed to the swelling nature of the solvent used. Also, the fatty acid grafting may have resulted in the swelling and decreased H-bonding between fibers. The surface-modified films and the pure CNF film were not significantly different. Also, The Young's modulus of all surface-modified films and the unmodified films were not significantly different. The crystallinity indexes of the films were 70% for pure CNF films, and 57.30%, 62.90%, 65.91% for samples surface modified with laurate, palmitic, and stearic acids.	Balasubramaniam et al. (2020)

2.9 Sorption isotherms

Moisture sorption isotherm of a material describes the relationship between their equilibrium moisture content and equilibrium relative humidity (RH) or water activity (Aw) at a constant temperature and pressure. These isotherms provide information about the water vapor sorption mechanism and how materials interact with water (Rhim et al., 2009). To improve the barrier qualities of cellulose films, it is necessary to understand the moisture transport in that films (Bedane et al., 2015). Paper-based packaging materials are composed of cellulose fibers, which are porous and readily absorb moisture from the environment or high-moisture foods. Beyond a particular moisture content threshold, moisture absorption severely affects their mechanical and physical characteristics (Rhim et al., 2009).

The relationship between the equilibrium moisture content in paper and RH is described by a sigmoid shape known as the type II isotherm in the IUPAC 1985 manual (Sing el al., 1985; Kupczak et al., 2018). This description indicates a monolayer-multilayer physisorption process in which the adsorbed surface layer thickens progressively with increasing vapour pressure up to saturation. This adsorption process may be accompanied by a rapid increase in sorbed water at high RH values due to capillary condensation in the porous structure (Kupczak et al., 2018). Moisture diffusion in paper occurs through three main pathways: i) water vapor diffuses in the pore space at low RH; ii) water condenses and diffuses within cellulose fibers, and; iii) moisture exchange (adsorption or desorption) between the fibers and the pore space at high RH due to a more significant water condensation among the cellulosic matrix (Kupczak et al., 2018). The three-parameter sorption equation developed by Guggenheim, Andersen, and de Boer (GAB) had been extensively used to interpret the physisorption of water on paper, providing meaningful physical parameters like

monolayer capacity and energy parameters related to the net molar heat of adsorption (Kupczak et al., 2018).

Chapter 3. Wheat straw hydrolysis using pressurized mixtures of water + ethanol: Behavior of structural compounds

3.1 Introduction

Wheat, one of the most produced crops worldwide, is mainly used for human consumption. In fact, wheat was the fourth most produced crop in the world after sugar cane, maize, and rice, representing 8% of total crops produced globally in 2019 (FAO, 2021). According to FAOSTAT (2022), the main wheat producers in 2020 were China (134.2 million tonnes, MT), India (134.2 MT), and the Russian Federation (85.9 MT), followed by the USA (49.7 MT), and Canada (35.2 MT). In Canada, most of the wheat was produced in Saskatchewan (45%) and Alberta (32%) between 2017 and 2019. In lower quantities, wheat was also produced in Manitoba (15%), Ontario (6%), and Quebec (<1%) (USDA, 2022). Wheat production in Canada has been slowly increasing. The production of wheat between 2018 and 2019 was 32.30 MT while 35.20 MT were produced between 2020 and 2021, representing 34.45 and 35.33% of the total crop production in Canada, respectively. In addition, the area needed to seed wheat (all types) in Canada represents 32.30 and 32.41% of the total land used to seed crops during those periods, respectively (Government of Canada, 2022).

Only the wheat grain is used for human food. The residue-to-grain ratio of wheat, where residue includes straw, stubble, and chaff, is 1.66 kg of residue per kg of grain and depends on growing conditions, soil fertility, and wheat class and variety (Saskatchewan Agriculture Knowledge Centre, 2022). Thus, a large amount of biomass is produced when harvesting wheat. Furthermore, the estimated straw production is the highest for wheat than

for any other grain in Alberta (8,115 metric tonnes of wheat straw was produced in Alberta in 2018) (Budynski, 2020). In Canada, straw is mainly used as bedding material and feed for livestock. Farmers also take advantage of this agricultural residue by chopping and spreading it in their fields to add nutrients to the soil. The generally-accepted nutrient levels of wheat residue are K_2O (1.23-1.5%), N (0.55-0.68%), P_2O_5 (0.20-0.23%), and S (0.10-0.13%), where the nutrient content may vary depending on the farmer's fertilizer practices, degradation degree of the straw, and soil and climatic conditions (Saskatchewan Agriculture Knowledge Centre, 2022; Budynski, 2020). Wheat straw can also be baled and sold in markets for the production of medium-density fiberboard (Budynski, 2020). The average price of straw in Alberta between 2016 to 2018 was CAD $0.063 per kg of grain and the price for baling wheat straw in 2017 was estimated to be CAD $0.064–0.11 per kg of bale (Budynski, 2020).

Wheat straw is mainly composed of cellulose, hemicellulose, and lignin; the interest in such compounds has been growing due to their potential to be green precursors of valuable chemicals for human use. Thus, wheat straw represents an abundant, renewable, and low-cost by-product to produce value-added compounds (Cocero et al., 2018; Lou et al., 2022). In addition, cellulose, the main component of wheat straw, is an excellent candidate for food packaging development (Ciftci et al., 2018).

An example of such valuable compounds are cellulose nanofibers (CNF), which are cellulose-composed fibrils of typically <100 nm in diameter and a few micrometers in length (Huerta et al., 2020b). This biomaterial can be used to produce biodegradable food packaging. CNF are produced using hydrolysis methods to separate the three main components of lignocellulosic material (cellulose, hemicellulose, and lignin), followed by a

mechanical process, which disintegrates the big cellulose fibers into smaller cellulose fibrils of nano-scale dimensions (Patil et al., 2022). Commonly used hydrolysis treatments involve the use of corrosive and toxic solvents such as strong acids and bases, neutralization steps, and consequently the production of waste streams, among other drawbacks (Huerta et al., 2018b). Pressurized fluids, such as water and ethanol, represent a green alternative to commonly used hydrolysis treatments. Additionally, the hydrolysates, which contain oligo- and monosaccharides and phenols, are the co-products obtained from the pressurized fluid treatment and they are also considered to be value-added compounds (Huerta et al., 2018).

The cellulose content in biomass such as sugarcane bagasse, corn stover, canola straw, lupin hull, and wheat straw had been increased after pressurized water and ethanol treatents (Liu et al., 2003; Sasaki et al., 2003a; Huerta et al., 2019; Ciftci et al., 2015). Particularly, wheat straw has been hydrolyzed using subcritical and supercritical water in batch and continuous reactors, mainly for the production of biofuels like bioethanol and biogas (Petersen et al., 2009; Zhao et al., 2009; Abdelmoez et al., 2014; Reynolds et al., 2015; Rajput et al., 2018; Chen et al., 2021). Wheat bran had also been hydrolyzed by subcritical water treatment for phenolic compounds production (Sánchez-Bastardo et al., 2016; Pazo-Cepeda et al., 2020; Martín-Diana et al., 2021). To the best of my knowledge, there is only one study on the use of pressurized aqueous alcohol (ethanol and isopropanol) for treating wheat straw to produce bio-oils (Patil et al., 2014), which mostly focuses on the impact of this treatment on the oil production and does not provide information about the cellulose contents in the feed before and after the hydrolysis treatment.

This study aims to investigate the effect of pressurized fluid treatment (water + ethanol at different concentrations) on wheat straw to obtain a cellulose-rich solid residue.

The solid residue and liquid hydrolysates obtained from wheat straw after pressurized fluid treatment were analyzed to understand the behavior of the wheat straw compounds to select the best conditions for cellulose recovery.

3.2 Materials and methods

3.2.1 Materials

Wheat straw, kindly provided by Klaus Strenzke (University of Alberta, Edmonton, AB, Canada) was milled using a centrifugal mill (Retsch, Haan, Germany) with a sieve size of <1 mm. The size distribution of the particles was ≥300 μm (56% w/w), ≥250 μm (15% w/w), <250 μm (28% w/w). Milled wheat straw was stored in bags at ambient conditions.

Folin-Ciocalteau reagent, sodium carbonate, sulfuric acid (95.5%), phenol (99.9%), sulfuric acid (72%), hexane, gallic acid (99.9%), acetic acid, D-glucose, D-xylose and L-arabinose were purchased from Sigma-Aldrich (Oakville, ON, Canada). Milli-Q water was obtained after passing water through a Milli-Q water purification system (Millipore, Bedford, MA, USA). Ethanol (100 %; ethyl alcohol, anhydrous) was purchased from Greenfield Global Inc. (Brempton, ON, Canada).

3.2.2 Methods

3.2.2.1 Hydrolysis of wheat straw using subcritical water and pressurized ethanol + water mixtures

Fig. 3.1 shows the procedure followed for wheat straw hydrolysis and the characterization of the untreated wheat straw and its by-products. Approximately 3 g of wheat straw was mixed with approximately ~28 g glass beads. The feed was hydrolyzed using pressurized mixtures of water and ethanol at different concentrations (0%, 20%, 60%, 80%, and 100% v/v ethanol) in a semicontinuous subcritical water system at the optimum

conditions found by Huerta et al. (2018b) and Ciftci et al. (2015), which were 180°C, 50 bar, 5 mL/min and hydrolysis time was set for 60 min. The same equipment described by the aforementioned studies was used for wheat straw hydrolysis. The equipment consisted of an HPLC pump (Gilson 307, Villiers-le-Bel, France), an oven (Binder, Bohemia, NY, USA), a stainless steel high-pressure vessel (2.54 cm diameter × 10 cm length, volume of 50 mL, with inlet and outlet filters of 20 µm), a cooling system (Swagelok, Edmonton, AB, Canada), a digital pressure gauge, a back pressure regulator (Tescom, Elk River, MN, USA), and stainless steel tubing (Swagelok, Edmonton, AB, Canada).

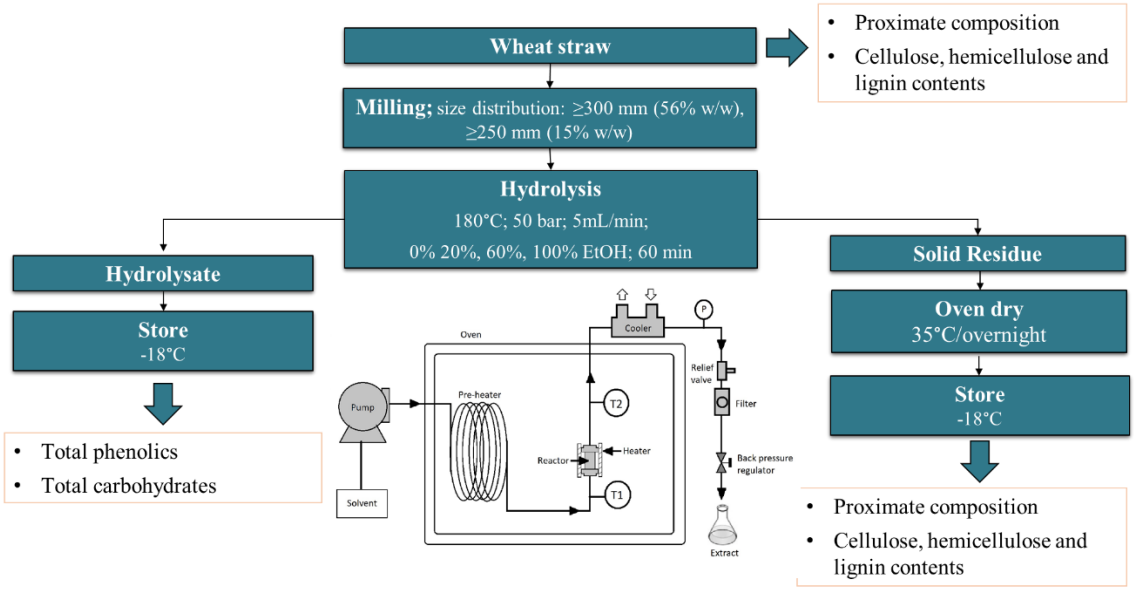

Fig 3.1. Flow chart for wheat straw hydrolysis and characterization.

During the pressurized fluid treatment, hydrolysates (pressurized water and ethanol + products such as sugars and phenols) were collected every 10 min. In total, six hydrolysate samples of 50 mL were collected. On the other hand, the solid residue (unhydrolyzed wheat straw) was removed from the reaction vessel at the end of the hydrolysis process. A mixture of the solid residue and glass beads was placed in a beaker with distilled water and the solid

residue was separated from the glass beads by decanting. Finally, the solid residue was separated from the distilled water by filtration through filter papers (# 1, GE Healthcare Life Sciences Whatman ™ Hardened 110 mm, Burlington, Massachusetts, USA) using the vacuum system. According to the SCW and pressurized 20% EtOH mass balances (Appendix A) the total mass loss (solid residue and solubles not removed in the hydrolysates) during the washing process was <4 % dw. Thus, that stream was considered negligible. The solid residue was dried in a convection oven at 30-35°C overnight. Then, the hydrolysates and solid residues were stored at -18°C until further analysis.

3.2.2.2 Solid residue analysis

3.2.2.2.1 Proximate composition

To determine the moisture content, 0.5 g sample was oven dried at 110°C overnight in a convection oven, then cooled in a desiccator before weight measurement in a digital balance (Satorius Lab Instruments GmbH & Co.; BCE2241-1S, Germany). The crude protein content of the solid residues was determined using a Leco nitrogen analyzer (Model FP-428, Leco instruments Ltd., Mississauga, ON, Canada). For calculations, a conversion factor (nitrogen-protein) of 6.25 was used. For the ash determination, 0.5 g of the sample was oven dried at 110°C overnight in a conversion oven and ashed at 500°C overnight in a muffle furnace (Model F-A1730, Thermolyne Corporation, Dubuque, IA, USA)). The lipid content of the solid residues was determined with the same method used by Strieder et al. (2022). Briefly, 0.5 g solid residue was placed into the test tube and weighed. Then, 10 mL hexane was added to the tube to extract and solubilize the lipids from the solid residue. Next, the solid residue + hexane mixture was allowed to rest for two days in a safety cabinet with intermittent shaking. After two days, the samples were centrifuged (10 min at 1500 rpm), and

the hexane was transferred as much as possible to another test tube using a Pasteur pipette. Finally, the hexane was removed using a stream of nitrogen at 50-60°C. The temperature was induced using a heater. The remaining extracts were weighted and used for lipid content calculations.

3.2.2.2.2 Lignin and structural carbohydrates

The acid-soluble and acid-insoluble lignin, and structural sugars in the solid residue were analyzed according to the NREL Laboratory Analytical Procedure "Determination of Structural Carbohydrates and Lignin in Biomass" as well as the method described by Huerta et al. (2018a), with some modifications. Briefly, 300 mg of the sample (untreated and hydrolyzed wheat straw) was placed in pressure tubes, and then, 3 mL of sulfuric acid (72%) was added. The residue + sulfuric acid mixture was placed in a water bath (Magnetic stirring hot plate Fisher Scientific; 411N3545; Ottawa, ON, Canada) at 30-45°C (temperature controlled with a mercury thermometer) for 60 min. During this period, residue + sulfuric acid was shaken every 5-10 min in a vortex (Fisher Scientific; model Genie 2). After 60 min, 84 mL of distilled water was added to the residue + sulfuric acid to dilute the concentration of the acid from 72% to 4%. Then, the diluted sample was autoclaved at 121°C for 60 min. Autoclaved samples were filtered through porcelain porous-bottom crucibles (CoorsTM #60531, Golden, CO, USA) using a vacuum system. The liquid phase was further used for the determination of acid-soluble lignin using a spectrophotometer (Molecular devices; SpectraMax M3; San Jose, California, USA) at the wavelength of 380 nm, and structural carbohydrates, as described further in this section. The solid residue product from the sulfuric acid hydrolysis was then dried in an oven (Fisher Scientific; Isotemp Oven 655G) at 105°C to determine the solids content and was ashed overnight in a muffle furnace (Model F-A1730,

Thermolyne Corporation, Dubuque, IA, USA), at 550°C to determine the acid-insoluble lignin content.

The liquid phase was used to determine the sugars that constitute the structural carbohydrates. The liquid phase was diluted in 0.005 M sulfuric acid at a 1:1 v/v ratio and then filtered with 0.2 µm filters. The diluted samples were analyzed using an HPLC system (Shimadzu Corp., Kyoto, Japan) equipped with an Aminex sugar HPX-87H column (300 mm x 7.8 mm; Bio-Rad, Hercules, CA, USA) and a refractive index detector (Waters 486, Milford, MA, USA) at the volumetric flow rate of 0.3 mL/min, using 0.005 M sulfuric acid as mobile phase, pressure of 45 bar isocratic mode, column temperature at 45°C, and the total analysis time of 60 min.

3.2.2.3 Hydrolysates analysis

The total phenolic content of hydrolysates was determined using the Folin-Ciocalteau method described by Sarkar et al. (2014). Briefly, 1.58 mL of distilled water, 20 µL of samples, and 100 µL of Folin-Ciocalteau reagent were mixed in a test tube with a vortex (Fisher Scientific; model Genie 2). Then, 300 µL of sodium carbonate at 20% was added and vortexed again. Next, the tubes were sealed with paraffin and incubated in a water bath at 40°C for 30 min. Finally, the total phenolic content in the samples expressed as gallic acid equivalents were read using a UV-Vis spectrophotometer (Molecular devices; SpectraMax M3; USA) at 765 nm. Also, a calibration curve (0-1000 µg gallic acid/mL solution) was prepared.

The total carbohydrate content of the hydrolysates was determined using the phenol-sulfuric method described by Dubois et al. (1956). Before the assay, samples were properly diluted with Milli-Q water. Diluted samples (2 mL) were placed in test tubes and mixed with

20 µL of aqueous phenol solution (80%). Then, 5 mL of 96% sulfuric acid was added. The samples were allowed to stand for 10 min, and then shaken in a vortex and incubated in a water bath at 30-25°C for 15 min. Finally, the samples absorbances were measured using a spectrophotometer (Molecular devices; SpectraMax M3; San Jose, California, USA) at 490 nm. Also, a calibration curve (0.029 - 0.111 mg glucose/mL solution) was prepared.

For the brown color determination, a similar procedure as the one used by Ajandouz & Puigserver (1999) was used. Samples were diluted in water as necessary and then centrifuged (Fisher Scientific; AccuSpin 400) for 20 min at 15 xg to eliminate turbidity from the samples, and measured using UV-Vis spectrophotometer (Molecular devices; Spectra Max M3; San Jose, CA, USA) at 420 nm.

The pH was measured for each hydrolyzed sample using a pH meter (Fisher Scientific; Accumet AB 200; Singapore).

3.2.2.4 Statistical analysis

All experiments were performed in duplicates. Results were presented using the average and standard deviations of data obtained from the respective analysis. Statistically significant differences were determined using one-way ANOVA and Tukey's test at a 95 % confidence interval. Statistical analysis was performed using the program Minitab version 18 (Minitab Inc., State College, PA, USA).

3.3 Results and discussion

3.3.1 Solid residue

3.3.1.1 Proximate composition

Table 3.1 compares the proximate composition of the untreated wheat straw used in different studies and the present study. Overall, the results of all studies, including those presented here, are similar with some variations, especially in the carbohydrate and ash contents. Those variations may be mainly attributed to the ratio of tissue components in the analyzed samples and growing conditions, which are not mentioned in those studies. Different wheat cultivars may also explain those variations. Collins et al. (2014) evaluated the content of structural carbohydrates, lignin, and phenolics in different tissues (internodes, nodes, leaves, and ears) of 90 wheat straw cultivars. They found that the level of sugars (structural carbohydrates) of the same tissues among different cultivars showed little variations, yet significant; however, the different tissue concentrations in the samples resulted in large variations in the structural carbohydrates and lignin contents. Glucose, the most abundant sugar in wheat straw, was higher in the internode (29–44% w/w) and the lowest in leaf tissue (22–35% w/w) while the lignin showed the highest content in the internode (13–20% w/w) and the lowest in the node (11–19% w/w). In addition, Duguid et al. (2007) studied the structural carbohydrates, lignin, and ash of wheat straw tissues (chaff, leaves, nodes, and internodes) before and after alkali and acid pre-treatments. Chaff and leaves had the highest ash content and the lowest lignin content (approximately 10.8 and 15.0%, respectively) while the nodes and internodes presented the lower ash content and higher lignin content (2.6 and 19.5%, respectively).

Table 3.1. Proximate composition analysis of wheat straw.

Moisture (%)	Protein (%)	Lipids (%)	Ash (%)	Carbohydrates (%)	Specie	Reference
n/m	4.4 (dw)	n/m	6.2 (dw)	~84.7 (dw)	*T. aestivum* cv. Apache	Silva et al. (2011)
5.58 (ww)	n/m	n/m	17.4 (dw)	93 (dw)	*Triticum aestivum*	Montero et al. (2016)
7.7±0.5 (ww)	n/m	n/m	5.3±1.1 (wt)	n/m	*Triticum*	García et al. (2014)
n/m	2-6 (dw)	n/m	0-2 (dw)	≥ 63 (dw)	*T. aestivum*	Zhang et al. (2022)
n/m	n/m	2 (Lipophilic content, dw)	6.6 (dw)	n/m	*Triticum durum* var. Carioca	del Río et al. (2013)
n/m	n/m	1–3 (dw)	n/m	n/m	n/m	Deswarte et al. (2006)
4.87±0.73 (ww)	5.59±0.14 (ww)	1.16±0.01 (ww)	8.90±0.15 (ww)	79.96±0.70 (ww)	*T. aestivum*	This study

n/m = not mentioned, ww = wet weight, dw = dry weght.

Also, the leaves had the lowest glucan contents (approximately 30%), while the internodes had the highest glucan content (approximately 38%) (Collins et al., 2014).

Table 3.2 shows the proximate composition of untreated wheat straw and wheat straw solid residue after treatment with subcritical water (SCW). The moisture contents of SCW-treated and untreated wheat straw showed no significant difference. However, the moisture content average is slightly lower in the SCW-treated wheat straw due to the drying step after the hydrolysis treatment. SCW treatment significantly ($p<0.05$) reduced the protein content of the wheat straw due to possible protein extraction and/or hydrolysis. The protein content was also significantly ($p<0.05$) reduced after the SCW treatment. Sereewatthanawut et al. (2008) studied the effect of SCW on deoiled rice bran protein fraction at 100-220°C for 5–30 min in a batch reactor. They found that proteins and amino acids were solubilized into the reaction media. The increase of the ionization constant in liquid pressurized hot water resulted in an increase of hydronium and hydroxide ions concentration in the reaction media, which further broke peptide bonds in proteins, producing soluble peptides and amino acids.

The optimal conditions were 200°C for 30 min, where the hydrolysates presented protein and amino acid concentrations of 219±26 and 8.0±1.6 mg/g of rice bran, respectively (rice bran before deoiling had 12% protein content while deoiled rice bran protein content was 19%). Additionally, Vo and Saldaña (2023) evaluated the time, temperature, and protein:pectin ratio on the hydrolysis of pea protein concentrate (the feed had a protein content of 51%). They found that the hydrolysates of pea protein treated with SCW at 180°C, 50 bar after 60 min in a batch reactor had approximately 400 mg protein/peptide/amino per g pea protein concentrate while the degree of hydrolysis of SCW treatment was approximately 27%. Depending on the time and temperature of the process, soluble proteins may degrade into carboxylic acids such as acetic, propionic, and formic acids (Sereewatthanawut et al. 2008). However, due to the mild temperature used in the present study, and according to the results of Sereewatthanawut et al. (2008) and Vo and Saldaña (2023), it can be concluded that the degradation of soluble proteins might not be significant in this study.

Table 3.2. Proximate composition of untreated wheat straw and solid residue after SCW hydrolysis treatment.

	Untreated wheat straw		Treated wheat straw	
	% wet weight	**% dry weight**	**% wet weight**	**% dry weight**
Moisture	4.87±0.73^{A}	n/a	3.01±0.30^{A}	n/a
Protein	5.59±0.14^{A}	5.87±0.19^{A}	3.52±0.63^{B}	3.63±0.64^{B}
Ash	8.90±0.15^{A}	9.37±0.10^{A}	4.73±0.26^{B}	4.88±0.28^{B}
Lipid	1.16±0.01^{A}	1.23±0.01^{A}	0.89±0.06^{B}	0.92±0.05^{B}
Carbohydrate	79.96±0.70^{B}	83.53±0.11^{B}	87.85±.12^{A}	90.57±.41^{A}
Structural carbohydrates + lignin	–	79.89	–	95.4

Carbohydrate = 100 - lipid + ash + protein + moisture*; *if applicable; n/a = non-applicable. $^{A-B}$ Values in the same line and same basis (wet or dry) represent significant differences at $p<0.05$. Untreated (wet basis) data previously shown in Table 3.1.

The lipid content significantly ($p<0.05$) decreased after the SCW treatment. However, lipid on the treated and untreated samples was the lowest proximate component of the samples, indicating that the change in lipids after the SCW treatment had the lowest effect on the increase of the carbohydrate content in the SCW-treated samples. Oil extraction using SCW has been reported by Pourali et al. (2009a), who studied the inactivation of lipases and the extraction of oil from rice bran using SCW at 120-240°C for 10-20 min in a batch reactor. SCW at 160°C for 10 min and 200°C for 10 min extracted 174 and 196 mg rice bran oil/g dry matter, respectively. The optimum conditions for oil extraction with SCW were 240°C for 10 min, which yielded 240 mg rice bran oil/g dry matter. Soxhlet extraction with hexane at 72°C for 4 h achieved an extraction yield of 266 mg rice bran oil/g dry matter. Therefore, SCW can be used to extract oil because the water at temperature and pressure near the critical point presents a lower dielectric constant, which increases the solubilization of non-polar

compounds like lipids (Toor et al., 2011). In addition, samples treated with SCW at 160°C for 10 min had 6.2% free fatty acid, which showed no increase after 12 weeks (Pourali et al., 2009a). Therefore, it can be concluded that the reduction in the lipid content after the SCW treatment may be due to their extraction.

SCW treatment significantly ($p<0.05$) reduced the ash content of wheat straw due to possible solubilization of minerals in the hydrolysates. In addition, ash had the highest change after the SCW treatment. Le et al. (2014) studied the distribution of minerals in wheat straw after SCW treatment as a function of operating conditions such as time (14, 18, or 22 min), temperature (170°C, 183°C or 196°C), and pH (adjusted with the addition of H_2SO_4 and NH_4OH to pH 2 and 10, respectively). According to their results, ash recovery after the SCW treatment was in the range of 40-60%. Potassium, the most abundant mineral (13.4 g/kg untreated wheat straw dw), was mostly solubilized in the reaction media (recovery range of 4-11 %). The removal of other minerals such as silicon (12.4 g/kg DM; recovery of 56-89%), calcium (4.0 g/kg DM; recovery of 30-73%), and phosphorous (1.7 g/kg DM; recovery of 3-72%), also contributed to the reduction of the ash content in wheat straw. They concluded that the studied SCW treatment conditions, particularly pH, influenced the contents of water-soluble minerals such as phosphorous, magnesium, potassium, manganese, zinc, and calcium in the solid residue.

As a proximate component, carbohydrate content represents the rest of 100% minus the sum of the other proximate compounds. Such value resembled the wheat straw's cellulose, hemicellulose, and lignin contents. The carbohydrate content of the wheat straw residue increased after the SCW treatment. According to the mass balance of the process (see appendix A), the percentage of ash, protein, and lipid (i.e., other compounds in the mass balance) of the wheat straw removed into the hydrolysates was 72.07%. On the other hand,

42.41% of the carbohydrate fraction was removed from the solid residue. As a result, the carbohydrate content in the SCW-treated sample increased while the contents of the other compounds were reduced. In the literature, there is limited discussion and studies about the effect of SCW on carbohydrate content (as part of the proximate composition analysis) of biomass, and thus, no information on wheat straw. On the other hand, there are abundant studies on the effect of SCW on the cellulose, hemicellulose, and lignin contents on different feeds. The results of such analysis in this study are presented in the next sections.

3.3.1.2 Lignin and structural carbohydrates

Table 3.3 shows a comparison of cellulose, hemicellulose, and lignin contents of untreated wheat straw obtained from the literature and this study for different wheat varieties. The lignin and structural carbohydrates contents obtained in this study are similar to those obtained in other studies, with some variations, which might be due to the same reasons for the proximate composition variations.

Fig. 3.2 shows the results for the structural carbohydrates and lignin contents of the wheat straw before and after pressurized fluid treatments with different ethanol (EtOH) concentrations. Hemicellulose content was determined based on the xylose and arabinose contents in the wheat straw. The SCW treatment and 20% EtOH treatments showed the lowest content of hemicellulose (Fig. 3.2). Untreated samples and samples treated with 60% and 100% EtOH showed no significant difference, which may be due to the different removal degree of lignin and cellulose from the wheat straw, resulting in the similar hemicellulose content of these samples. The lower hemicellulose content in SCW and 20% EtOH-treated wheat straw may be due to the higher concentration of water in the reaction media, which allowed higher depolymerization of the hemicellulose.

Table 3.3. Lignin and structural carbohydrate contents of wheat straw (% dw).

Cellulose	Hemicellulose	Lignin	Specie	Reference
34.6±0.2	29.3±0.3	21.3±0.3	*Triticum aestivum* L.	Naik et al. (2010)
32.60	22.60	16.80	*Triticum aestivum* var. Thunderbird Whole Plant #154	Cherubini et al. (2010)
37.43±0.22	~22.06	18.38±0.16	Canadian Prairie spring wheat (*Triticum aestivum*)	Fu (2011)
28.80	39.10	18.60	n/m	Demirbaş (1997)
33.61±0.87	~22.36	18.40±2.20	*Triticum aestivum* var. Thunderbird	Templeton et al. (2016)
36.72±0.14	22.60±0.05	20.52±0.44	*T. aestivum*	This study

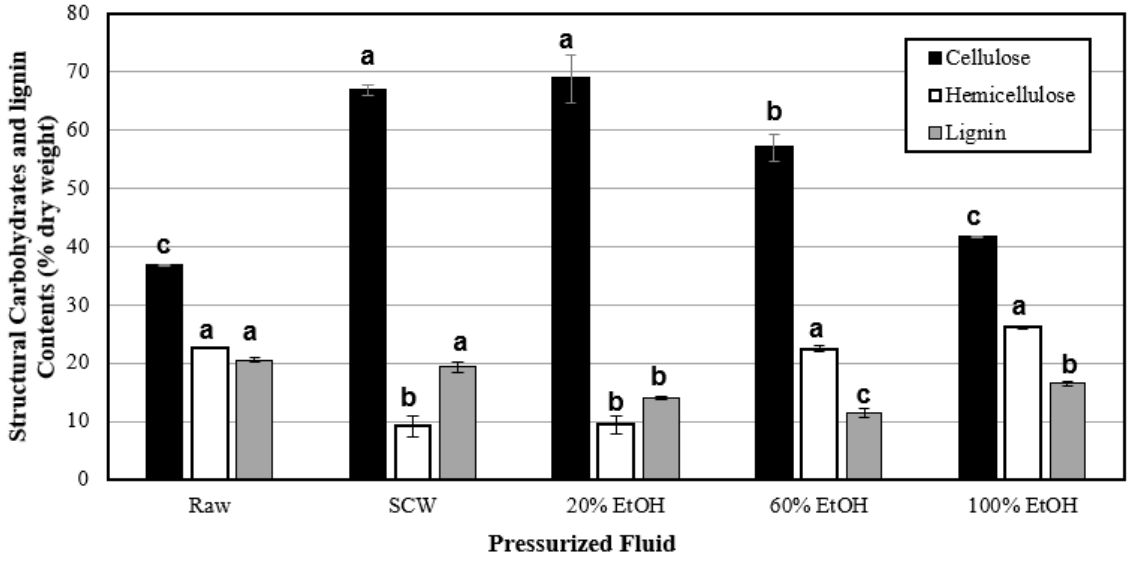

Fig 3.2. Effect of ethanol concentration on the structural carbohydrates and lignin content of wheat straw before and after treatment with pressurized water + ethanol (EtOH) at 180°C, 50 bar, and 5 mL/min. [a-c]Values on bars of the same color represent significant differences at $p<0.05$. Data in the appendix section (Table B.1).

On the other hand, the higher hemicellulose concentration of 60% and 100% EtOH may be due to the predominant concentration of EtOH in the reaction media, allowing a lower production of hydronium and hydroxide ions, thus, limiting hemicellulose depolymerization. The mass balance suggested that hemicellulose of wheat straw was the compound with the highest reduction of 80.27% total hemicellulose content after the SCW treatment (See Appendix A).

Of the three most important components in lignocellulosic biomass, hemicellulose was the most prone to hydrolyze and be removed by SCW due to their lower structural recalcitrance and higher solubility of its reaction products in the reaction media. Hemicellulose depolymerization released acidic groups (mainly acetyl groups) and produced carbohydrates with a lower polymerization degree, which depending on the operational conditions, were further reduced in length and/or degraded into other compounds (Prado et al., 2016; Cocero et al., 2018). Ciftci et al. (2015) studied the effect of SCW on sweet blue lupin hull at different conditions of temperature, pressure, flow rates, and initial pH values (160–220°C, 50–200 bar, 2–10 mL/min, pH 2–12, respectively). They found that the temperature, flow rate, and pH had a significant effect on hemicellulose depolymerization, and the optimal conditions were 180°C, 50 bar, 5 mL/min, and pH 6.2, achieving a hemicellulose sugars yield of 85.5% w/w in the hydrolysates. Pressure did not have a significant effect on the hemicellulose depolymerization. The release of ionic products from water at subcritical conditions caused the hydrolysis of glycosidic linkages of hemicellulose and released the O-acetyl group and other acid moieties from hemicellulose, forming acetic and uronic acids. The low hemicellulose sugar yields on hydrolysates obtained after SCW treatment at 160°C (60.8–64.2% w/w) indicated low depolymerization of hemicellulose. The

drastic yield decrease at 200, and 220°C (sugars yields of 70.7–73% w/w at 5 mL/min, pH 6.2) compared to the optimum temperature (180°C), indicated the decomposition of hemicellulosic sugars and formation of furfural and hydroxymethyl-furfural (HMF) from the dehydration of pentoses and hexoses, respectively (Ciftci et al., 2015). The pH values of 2.6 and 6.2 resulted in the highest hemicellulose sugar yields (84.5 and 85.5% w/w at 180°C, 50 bar, 5 mL/min) due to the catalyst effect of acids in the reaction media and acids derived from hemicellulose depolymerization. High flow rate (7.5 and 10 mL/min at 180°C, 50 bar, and pH values of 6.2) resulted in lower hemicellulose yield (approximately 79.5 and 78.5 % w/w) due to the reduced contact time of the sample in the SCW conditions while lower flow rates (<5 mL/min) increased the degradation of sugars due to increased contact time, also resulting in lower hemicellulose yield (81.5% w/w). As this thesis used the same optimum conditions of temperature, pressure, pH, and volumetric flow found by Ciftci et al. (2015) for the pressurized fluid treatments, high hemicellulose yield with minimal production of furfural and hydroxymethyl-furfural (HMF) in the hydrolysates are expected. However, the detailed quantification of structural sugars and their degradation by-products is beyond these thesis boundaries Their future analysis is encouraged to assess and describe these co-products applications.

Lignin was determined as the sum of acid-soluble lignin and acid-insoluble lignin, according to the NREL methodology. Samples treated with 60% EtOH had the lowest percentages of total lignin, followed by 20% and 100% EtOH-treated samples with no significant difference (Fig. 3.2). The SCW-treated wheat straw and the untreated wheat straw had the highest lignin contents and presented no significant difference between them. In the literature, most of the studies that focus on lignin depolymerization using hydrothermal treatments employed high temperatures near or above the critical point of water (T =

374.15°C and P = 221 bar). Yong et al. (2013) studied the kinetics of lignin (alkali lignin isolated from Norway Spruces) conversion behavior under subcritical (300−370°C) and supercritical (390−450°C) water treatments at 250 bar for 0.5, 2, 5, and 10 s in a continuous system. Total decomposition occurred rapidly under hydrothermal treatment (approximately 10 s at 300°C) and the increased temperature improved the lignin depolymerization, which was mostly attributed to the breakdown of the β-aryl ether (β-O-4) linkages. The main depolymerization reactions induced by the hydrothermal treatments were ionic and radical. However, the predominance of one of such reactions varied according to the temperature used in the treatment. In the SCW treatment, initial decomposition occurred due to the radical reaction; nevertheless, the ionic reactions were predominant due to the high ionic products from water under the subcritical domain. Additionally, SCW treatment showed a higher yield of total organic carbon in the liquid effluent and a significantly lower char (re-polymerized lignin, solid stream) yield than the supercritical water treatment. The results suggested that the high amount of low molecular weight products generated from lignin due to the high-temperature treatment consequently crosslinked, resulting in char formation. The literature also mentioned that carbohydrate degradation products such as organic acids and furfural might contribute to lignin re-polymerization (Prado et al, 2016).

Several studies reported that the lignin concentration increased in the solid residue after the SCW treatment of biomass (Cocero et al., 2018; Prado et al., 2016). For instance, Chen et al. (2021) studied the optimization of SCW treatment and high solid hydrolysis using wheat straw as feed for its further conversion to bioethanol. They found that the optimum conditions were 220.5°C for 22 min with a substrate loading of 2.5% (w/v). The SCW treatment reduced the hemicellulose content by 18.37% while increasing the cellulose and lignin contents by 25.92 and 8.81%, respectively. Also, Petersen et al. (2009) optimized the

hydrothermal continuous pilot-scale system for the conversion of wheat straw sugar into bioethanol operated at 185, 195, and 205°C for 6, 9, and 12 min with a constant flow rate of 50 kg/h. The optimal conditions were 195°C for 6 to 12 min, which achieved a recovery of 70% hemicellulose, 93-94% of cellulose in the solid residue, and at least 90% of lignin in the solid residue.

Nevertheless, the flow rate might considerably influence the removal of lignin. Liu et al. (2003) studied the effect of flow rate on the SCW treatment of corn stover in a semi-batch system at 180, 200, and 220°C for 12 and 16 min, focusing on flow rates of 1, and 10 mL/min, and no flow. The authors mentioned that the removal of xylan, a by-product of the hemicellulose hydrolysis, suggested that the flow rate of 5 mL/min provided no further insights than flow rates of 1 and 10 mL/min. Thus, such conditions were not included further in their study. When the equipment was operated at static conditions (0 mL/min), the lignin removal was less than 30% (all conditions) while high flow rates achieved a lignin reduction of up to 75% (220°C, 10 mL/min, 12 min). At 180°C after 16 min, the SCW treatment resulted in a lignin removal of approximately 25, 34, and 16%, at flow rates of 1 and 10 mL/min, and no flow rate, respectively. Liu et al. (2003) also reported a linear relationship between the lignin and xylan removal from corn stover at the studied temperatures and flow rates except at static conditions. Hemicellulose and lignin in biomass are naturally linked, and thus, the authors proposed that the relationship between lignin and xylan removal was due to the release of hemicellulose oligomers, which might be linked to lignin fragments (oligomer-lignin compounds), promoting lignin fragments solubilization in the reaction media. The longer residence time of such compounds in the reactor, as a consequence of low or no flow rate, resulted in the separation of hemicellulose oligomers and lignin fragments. The former could be further hydrolyzed by the SCW, resulting in short-chain oligomers,

monomers, and degradation products while the latter could precipitate due to their low solubility and/or be further depolymerized and the shorter fragments could react to form char.

The partial hydrolysis of oligomer-lignin compounds could explain the high removal of lignin in the semicontinuous reactor, especially at higher flow rates and temperatures. Therefore, high lignin content of the solid residue in the studies of Chen et al. (2021) and Petersen et al. (2009) might be due to a residence time that allowed a high degree of depolymerization of oligomer-lignin compounds which could lead to the precipitation of large lignin fragments and char formation. The findings of Liu et al. (2003) could also explain why the lignin content of the solid residue in the present study showed no significant difference from the untreated sample even though hemicellulose and other proximate compounds were removed from the sample. In addition, the mass balance of the lignin suggested a 53.92% of lignin removal from the solid fraction after the SCW treatment (see appendix A).

In this study, the higher hemicellulose concentration in the solid residue of 60% and 100% EtOH treatments was attributed to the predominant concentration of EtOH in the reaction media, allowing a lower production of hydronium and hydroxide ions, thus, limiting hemicellulose depolymerization. On the other hand, the EtOH concentration in the reaction media favored the solubilization of lignin fragments. Huerta et al. (2018) studied the effect of pressurized aqueous EtOH (PAE) (20–100% v/v) and SCW in barley and canola straws at 140–220 °C, and 50–200 bar. They found that the PAE treatments were more efficient for the removal of lignin, having a total lignin removal of 40% for SCW and 54, 61, and 50% for PAE at 20, 60, and 100% EtOH, respectively, at operational conditions of 180 °C, 50 bar and 5 mL/ min for 40 min. As a result, the synergistic effect of water and EtOH present in the reaction media may explain the high removal of lignin in the water + EtOH -treated samples.

Earlier, Sarkar et al. (2014) evaluated the production of phenolics and carbohydrates from barley hull (BT 584) in aqueous ethanol solid–liquid batch extraction, pressurized water, pressurized aqueous ethanol, and pressurized aqueous N-methyl-2-hydroxyethylammonium acetate. Additionally, the authors studied the solubility of ferulic acid and glucose during the pressurized fluid treatments. The authors proposed that the high depolymerization of carbohydrates was mostly attributed to the interaction and steric effect of cation/anion, especially those produced from water autoionization (H^+ and OH^-). Nonetheless, lignin hydrolysis produced alkyl-aromatic radicals that were not stabilized by OH^- ions, resulting in char formation. However, in the pressurized aqueous EtOH treatment, the ion products were H^+ and $CH_3CH_2O^-$, and the anion improved the radical stabilization, and consequently, allowed the depolymerization of lignin into phenolic compounds, as described in the following mechanism proposed by Sarkar et al. (2014).

1) Autohydrolysis of the fluid

$$H_2O + CA \overset{P,T}{\longleftrightarrow} H^+ + OH^- + C^+ + A^- \qquad \text{Eq. (3.1)}$$

2) Hydrolysis of the biomass

$$RA\_O\_Lig + C^+ + A^- \overset{H^+,OH^-}{\longleftrightarrow} RA\_O^- + C^+ + Lig^+ + A^- \qquad \text{Eq. (3.2)}$$

$$R\_O\_Ch + C^+ + A^- \overset{H^+,OH^-}{\longleftrightarrow} R\_O^- + C^+ + Ch^{\cdot} + A^- \qquad \text{Eq. (3.3)}$$

3) Stabilization of ionic species from biomass

$$RA—O^- + C^+ + Lig^+ + A^- \leftrightarrow [RA—O\cdot + A^-] + e^- + Lig^+ + C^+ \qquad \text{Eq. (3.4)}$$

$$R—O^- + C^+ + Ch^+ + A^- \leftrightarrow [R—O^- + C^+ + A^- + Ch^+] \qquad \text{Eq. (3.5)}$$

4) Products

$$[RA—O\bullet + A^-] \leftrightarrow R—O\bullet \ldots A^- \leftrightarrow \text{products}\,(RA—OH,\ RA—O—RA) + A^- \quad \text{Eq. (3.4)}$$

$$[R—O^- + C^+ + A^- + Ch^-] \leftrightarrow \text{products}\,(R—OH) + C^+ + A^- \quad \text{Eq. (3.5)}$$

where, C^+ = cation (H^+), A^- = the anion ($CH_3CH_2O^-$), CA = cosolvents (EtOH), Lig = Lignin, Ch = cellulose/hemicellulose.

Cellulose content was determined based on the glucose content of the wheat straw. According to the results, SCW treatment and 20% EtOH showed no significant difference and the highest concentrations of glucose, followed by 60% EtOH, and 100% EtOH (Fig. 3.2). In addition, 100% EtOH-treated samples and untreated samples showed no significant difference in their cellulose contents. However, samples treated with SCW and 20% EtOH showed almost twice the cellulose content compared to the untreated sample. Liu et al. (2023) recently studied the effect of SCW and PAE hydrolysis (180–220 °C for 40 min, ethanol concentrations of 20–100% (v/v), 50–200 bar, and flow rate of 5 mL/min) in the lignin and cellulose contents on hydrolyzed barley straw. They found that the cellulose content significantly increased after the 100% EtOH treatment at 180°C (41.79%), 200°C (43.35%), and 220°C (40.64%) compared to the untreated sample (34.33%). Nevertheless, those cellulose contents were lower than those obtained after SCW, 20% EtOH, and 60% EtOH, which was attributed to a higher removal of the hemicellulose and lignin fractions after those hydrolysis treatments.

Additionally, the literature mentioned that SCW at temperatures below 230°C induced minimal cellulose hydrolysis due to its high stability (Prado et al., 2016). Sasaki et al. (2003a) studied the fractionation of sugarcane bagasse using hot pressurized water in a semi-batch equipment. During the hydrothermal treatment, the temperature was not constant

and increased at the rate of 0.51°C/min up to 330°C during the process. The authors found that hemicellulose and lignin were mainly removed at temperatures of 200 to 230°C. Approximately 60% of the initial bagasse was removed from the samples and mainly comprised of organic compounds derived from hemicellulose and lignin with very small traces of glucose and cellobiose. Cellulose was depolymerized at 230 to 280°C. At this temperature range, approximately 30% of the initial bagasse was removed and the hydrolysate contained cellobiose and a few aromatic compounds. The cellulose fraction in the solid residue presented no change in the cellulose I structure.

Later, Sasaki et al., (2003b) studied the production of cellulose II from microcrystalline cellulose (cellulose I) using hot pressurized water in a continuous microreactor at 320-400°C, 250-330 bar, and an operational time of 0.02-0.6 s. The hydrothermal treatment consisted of a combination of rapid heating and quick quenching processes. After the treatment, the solid and liquid fractions were separated by decantation. The cellulose II and other cellulose hydrolysis products were recovered from the liquid fraction. They found that cellulose I could dissolve in near- and supercritical water, forming cellulose II (60 to 80% yield, polymerization degree of 30-50 at 355−400°C and 0.02−0.22 s). Cellulose I crystal dissolved into the near- and supercritical water due to the cleavage of intermolecular H-bonds, and the resulting carbohydrates aggregated and recrystallized into cellulose II after the hydrothermal treatment. Therefore, the increase in the cellulose content of the samples in this study was attributed to the minimum effect of the pressurized fluid treatment on the cellulose structure and the depolymerization and/or removal of hemicellulose, lignin, and other compounds such as proteins, ash, lipids, etc. According to the mass balance of the hydrolysis system, the total cellulose of wheat straw had a reduction

of 11.06% after the SCW treatment; thus, cellulose was the compound that was the least affected by the SCW treatment (see appendix A).

Overall, water in the reaction media mainly affected the removal of hemicellulose while EtOH mainly affected the removal of lignin (Fig. 3.2). The SCW and 20% EtOH treated samples showed the highest removal of hemicellulose. However, comparing those two samples, 20% EtOH showed a higher removal of lignin. These results suggest that 20% EtOH treatment was the best treatment for cellulose recovery from wheat straw in this study.

3.3.1 Hydrolysates characterization

3.3.1.1 Total phenolics

Fig. 3.3 shows the total phenolic content represented as gallic acid equivalents (GAE) of wheat straw obtained at different EtOH concentrations. Total phenolics obtained from the hydrolysis treatments may be an indicator of the breackdown of lignin (Cocero et al., 2018). According to the results, the total phenolic content in the samples treated with SCW and pressurized 60% EtOH had no significant difference and the highest phenolic content, followed by 20% and 100% EtOH. Interestingly, the phenolics content in the hydrolysates did not resemble the lignin solubilized into the hydrolysates. This behavior resembled the results obtained by Huerta et al. (2018), who studied the effect of EtOH concentration of pressurized liquid water + EtOH treatment in barley and canola straws. Pazo-Cepeda et al. (2020) also studied the extraction of total phenolic compounds and ferulic acid from wheat bran using PAE at different temperatures (130, 145, and 160°C), EtOH contents (20, 50, and 80%), and times (20, 40, and 60 min). They found that 20% EtOH, 160°C, and 40 min was the optimum condition for ferulic acid extraction (226.8 ± 1.4 µg ferulic acid/g). Moreover, an increase in the EtOH in the reaction media reduced the ferulic acid extraction. However, the total phenolic content in the hydrolysates was not significantly

affected by the EtOH content (~8 mg GAE/g). It was attributed to the coextraction of other phenolic compounds at different EtOH concentrations. Such phenolic compounds were not further identified by Pazo-Cepeda et al. (2020). Also, the authors did not specify the temperature and time conditions for the EtOH effect study.

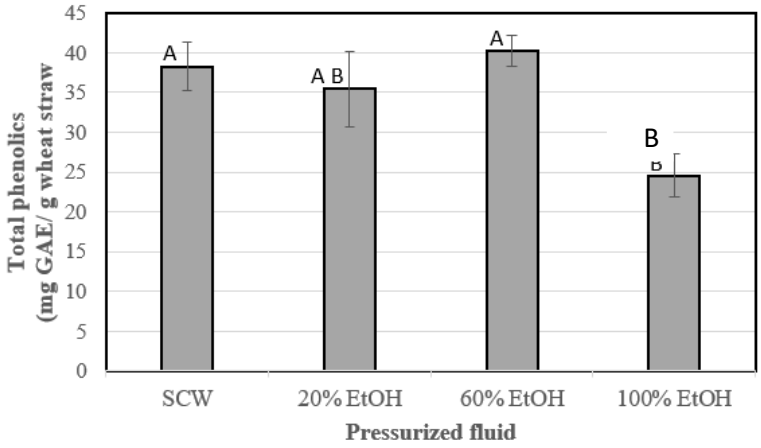

Fig 3.3. Effect of ethanol concentration on the total phenolic content of wheat straw hydrolysates using pressurized water + ethanol (EtOH) at 180°C, 50 bar, and 5 mL/min. [A-B]Values represent significant differences at $p < 0.05$. Data in the appendix section (Table B.2).

In addition, Appel et al. (2001) studied the response of the Folin-Denis assay to high-purity tannin extracts obtained from 16 different woody plants and three commercial polyphenol standards and concluded that the reactivates used in the Folin-type essays provided an overall idea of the redox activity of the phenolics in the extracts. Appel et al. (2001) also concluded that Folin-type essays may also provide information about the relative amount of phenolics compounds, but only when standards of expected analytes in the sample are used. The results on total phenolics in the present study were expressed in gallic acid equivalents (GAE) while the use of other phenolic compounds could be more appropriate to

elucidate the content of phenolics in wheat straw using this assay. For instance, ferulic acid and p-coumaric acid are considered as the major phenolics in wheat straw (Pan et al., 1998). Thus, it is concluded that the results represent the equivalence of the redox activity of the compounds in the hydrolysates with the redox activity of gallic acid rather than the total quantity of phenolics.

3.3.1.2 Total carbohydrates

Fig. 3.4 shows the total carbohydrates represented in glucose equivalents (GE) in wheat straw hydrolysates obtained at different EtOH concentrations. Hydrolysates treated with pressurized 20% EtOH and SCW showed the highest carbohydrate content, followed by pressurized 60% and 100% EtOH treatments, which may be due to the higher proportion of water in the solution media. Thus, more H^+ and OH^- ions were produced, increasing the structural carbohydrates hydrolysis, and obtaining higher quantities of monosaccharides and oligosaccharides in the hydrolysates. These results were congruent with the results mentioned above, in which higher sugar concentrations were found in hydrolysates after SCW and 20% EtOH treatments. Huerta et al. (2018) also studied the total carbohydrate contents in hydrolysates obtained from barley and canola straws hydrolysis. The highest total carbohydrate concentration of barley and canola straws hydrolysates (527.6±0.5 and 442.7±14.8 mg glucose equivalents/g straw) was reached at 180 °C, 50 bar, and EtOH concentration of 20%. Such conditions were also found to achieve the highest carbohydrate concentration in wheat straw hydrolysates. Additionally, Liu et al. (2023) reported the sugar content in the hydrolysates obtained after barley straw SCW and PAE hydrolysis at 180–220 °C for 40 min, ethanol concentrations of 20–100% (v/v), 50–200 bar, and flow rate of 5 mL/min. They reported the highest yield of reducing sugars in hydrolysates obtained after SCW hydrolysis at 200 °C/50 bar/40 min, followed by 20% EtOH, 60% EtOH, and 100%

EtOH. That behavior was attributed to the sugar antisolvent effect of ethanol, which limited the sugars solubility in the reaction media.

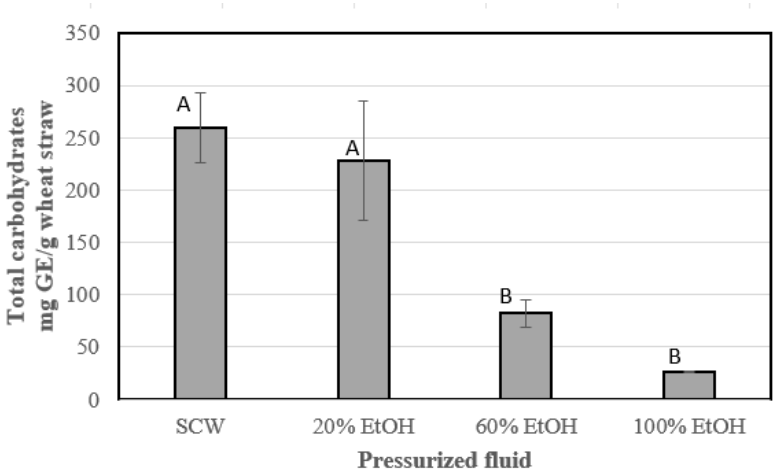

Fig 3.4. Effect of ethanol concentration on the total carbohydrate content of wheat straw hydrolysates using pressurized water + ethanol (EtOH) at 180°C, 50 bar, and 5 mL/min. [A-B]Values represent significant differences at $p<0.05$. Data in the appendix section (Table B.2).

3.3.1.3 pH

Fig. 3.5 shows the average pH of wheat straw hydrolysates collected at different EtOH-concentration treatments. Samples treated with SCW, and 20% EtOH had no significant differences. Furthermore, samples treated with SCW, and 20% EtOH showed significantly ($p<0.05$) lower pH values than those treated with 60% EtOH and 100% EtOH. Samples treated with 60% EtOH and 100% EtOH had no significant differences. There was congruence between the pH and the total carbohydrate values in the hydrolysates as the decrease in pH may be an indicator of straw depolymerization (Cocero et al., 2018).

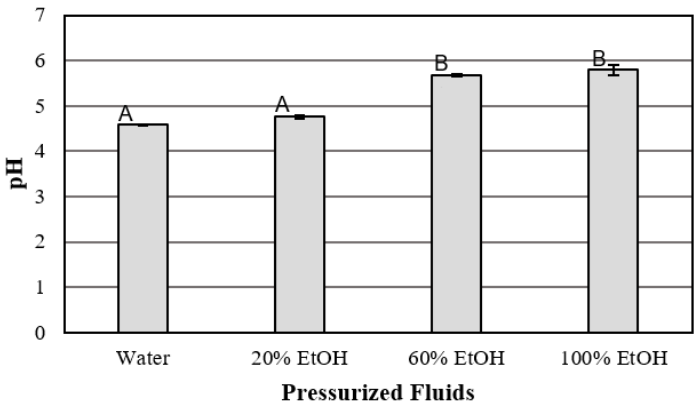

Fig 3.5. Effect of ethanol concentration on pH of wheat straw using pressurized water + ethanol (EtOH) at 180°C, 50 bar, and 5 mL/min. $^{A-B}$ Values represent significant differences at $p < 0.05$. Data in the appendix section (Table B.2).

Prado et al. (2014) hydrolyzed sugarcane bagasse using SCW in a semi-batch system at different temperatures (213, 251, and 290°C) and flow rates (11, 22, 33, 44, and 55 mL/min) for 30–48 min and presented the change in pH as a function of time. Overall, the pH of the hydrolysates at different times ranged from 3.3 to 6.5. The highest pH was achieved at the beginning of the treatment. At 194 to 214°C, the minimum pH values (approximately 3.5 to 4) were achieved after 10 to 20 min and then slowly increased until the end of the process. At 213 to 290°C, a similar trend was observed with minimal pH (approximately 3.3 to 4) after around 5 min. The low pH was attributed to the carbohydrate fraction degradation. Additionally, Pourali et al. (2009b) hydrolyzed rice bran using SCW at 100 to 360°C for 5 min in a batch reactor. The study included the change in pH as a function of temperature and the concentration of different organic acids (acetic acid, formic acid, glycolic acid, levulinic acid, and citric acid) in the hydrolysates. There was a change in the pH of the reaction media due to the formation of water-soluble organic acids. The pH was stable up to 240°C, where the minimum pH value of 4.6 was obtained. As discussed earlier, such organic acids were

mainly the result of the released acidic moiety from the hemicellulose. However, some sugars can also be converted into organic acids, such as acetic and formic acids at operational temperatures greater than 220°C (Vo and Saldaña, 2023). Other organic acids that can be released from biomass include lactic and uronic acids (Cocero et al, 2018).

3.3.1.4 Brown color

Fig. 3.6 shows the average brown color of wheat straw hydrolysates collected at different times and EtOH concentrations. Brown color analysis may indicate non-enzymatic reaction (e.g., carbohydrate degradation and Maillard reactions) products, such as furfural, 5-hydroxymethyl-furfural (5-HMF), and phenolic content degradation, which contribute to the dark-brown color of the samples (Sarkar et al., 2014; Ciftci et al., 2015). In this study, samples treated with SCW, and 100% EtOH did not present any significant differences. As well, comparing samples treated with 20% EtOH and 60% EtOH did not present significant differences but showed a significantly ($p<0.05$) higher brown color than those treated with SCW and 100% EtOH, suggesting that EtOH concentrations between 20 and 60% in the reaction media favored non-enzymatic browning reactions.

The brown color of hydrolysates obtained from barley straw (10.7% protein wet basis) and canola straw (12.8% protein wet basis), after SCW and pressurized aqueous EtOH treatments at 180°C, 50 bar, and 5 mL/min was also analyzed by Huerta et al. (2018). They found a similar trend between the brown color and the total carbohydrate content of the samples, in which the hydrolysate with higher carbohydrate content also had a higher brown color index. Huerta et al. (2018) also found that the brown color values of hydrolysates had similar trend as their total carbohydrates contents as a function of EtOH concentration at 180 °C, 50 bar, and 5mL/min. Such findings were not consistent with the results obtained in this study, because the highest carbohydrate content was obtained with the SCW and

pressurized 20% EtOH treatments while the 20% EtOH and 60% EtOH achieved the highest brown color in the hydrolysates from wheat straw hydrolysis.

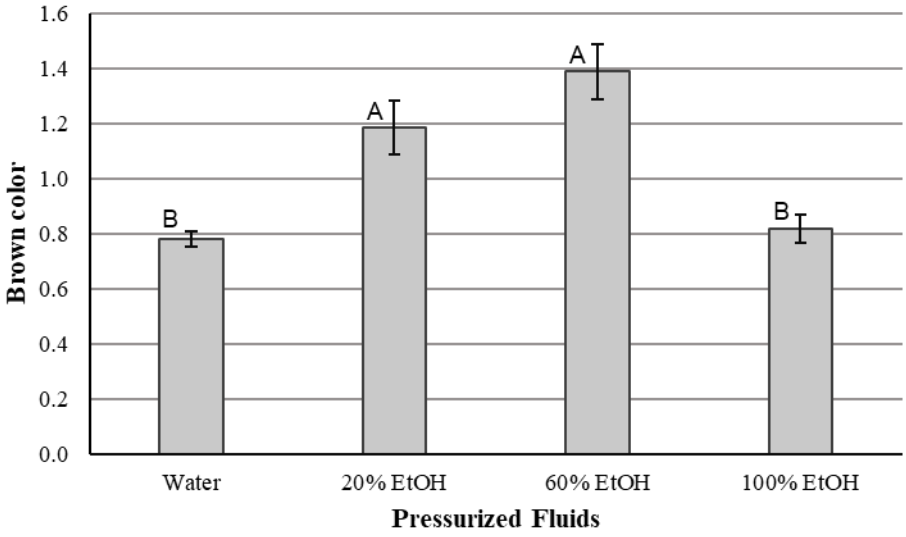

Fig 3.6. Effect of ethanol concentration on the brown color of wheat straw hydrolysates using pressurized water + ethanol (EtOH) at 180°C, 50 bar, and 5 mL/min. $^{A-B}$ Values represent significant differences at $p<0.05$. Data in the appendix section (Table B.2).

However, Huerta et al. (2018) did not specify whether the brown color of the samples was measured with any intermediate steps. The samples in this study were centrifugated prior to the color analysis to remove non-soluble compounds of the hydrolysates that provided turbidity to the sample, and thus, might have interfered with the measurement. The lack of the centrifugation step could explain the different behavior among these results and the results obtained in the aforementioned studies. In addition, dehydration promotes biomass monomer decomposition (Toor et al., 2011). A reaction media with less water might promote such reactions and could be an explanation of why hydrolysates obtained from aqueous EtOH up to 60% had higher brown colorations than those obtained with SCW.

3.4 Conclusions

Cellulose-enriched solid residues were obtained from milled wheat straw after SCW and pressurized water + EtOH hydrolysis. In the hydrolysates, samples treated with SCW and water + EtOH showed no significant difference in phenolic content expressed as gallic acid equivalents. Samples treated with SCW and 20% EtOH showed the highest total carbohydrate content and the lowest pH, indicating the depolymerization of the hemicellulose. In the solid residue, pressurized fluid treatment greatly reduced the ash, crude protein, and lipid contents of wheat straw, more than the carbohydrate portion, thus the carbohydrate content after the SCW treatment was higher than the untreated wheat straw. Samples treated with pressurized 60 showed the lowest total lignin content as the EtOH content in the reaction media influenced the lignin removal from the wheat straw due to the formed anion ($CH_3CH_2O^-$) influence.

On the other hand, samples treated with SCW and 20% EtOH showed the highest cellulose content and lower hemicellulose content as the high-water content in the reaction media allowed the higher H^+ and OH^- ion production for lignocellulosic biomass depolymerization. SCW and pressurized 20% EtOH treated samples showed the highest removal of hemicellulose. However, among those two samples, the 20% EtOH treated showed a higher removal of lignin, with the potential for further processing to obtain CNF.

Chapter 4: Sustainable cellulose-based micro/nanopaper development

4.1 Introduction

Food packaging have four basic functions: i) containment, ii) communication, iii) protection, and iv) convenience (Robertson, 2009; Cachon et al., 2019). An increase in the demand for food containers in the food industry is forecasted (Marketsandmarkets, 2018).

Plastics, paper board, metal, and glass are the most common materials for food packaging development (Grandviewresearch, 2021). Plastic containers are conventionally fabricated with petroplastic materials like (polyethylene terephthalate, high-density polyethylene, polyvinyl chloride, low-density polyethylene, polypropylene, and polystyrene) mainly due to their low price, good moisture barrier properties, and strong sealing capacity (Hahladakis et al., 2018; Grandviewresearch, 2021). However, consumers' and governments' concerns for society and the environment's welfare have been increasing in the last decades. Therefore, finding a replacement for plastic as a food packaging material to reduce plastic production and waste, and thus, reduce their consequences to society and the environment is needed (Montoya Sánchez et al., 2022; Garrido-Romero et al., 2022). Paper-based materials, which are mainly composed of cellulose, represented 33% of total sales in 2022 in the packaging market. These materials have been presented as an attractive option for petroplastics replacement due to design, printability, and sustainability advancements. Other advantages of paper-based materials are eco-friendliness and ease of recyclability (Grandviewresearch, 2021).

To produce paper-based materials, plant-based sources first require mechanical treatment for particle size reduction, hydrolysis (e.g., SCW, pressurized aqueous ethanol, acid and alkali treatments) and delignification (also known as bleaching) to isolate cellulose. Then, cellulose fibrillation is an additional process for the generation of CNF.

Chemical bleaching is conventionally achieved using chlorinated chemicals and oxidizers such as sodium chlorite ($NaClO_2$) and hydrogen peroxide (H_2O_2) under acidic and alkaline conditions, respectively. Acidified sodium chlorite (ASC) and alkaline hydrogen peroxide (AHP) are some delignification methods (Fang et al., 1999; Sun et al., 2000; Nan et al., 2018). Earlier, Ciftci et al. (2018) mentioned that the material's cellulose content was minimally impacted by the ASC method when lignin content is ≥1%. However, using chlorinated compounds for the ASC method results in the emission of poisonous and carcinogenic pollutants, which severely affect the environment (Zhao et al., 2018). Compared to ASC, AHP is considered more environmentally friendly. Nevertheless, AHP negatively affects the cellulose fraction under non-optimized conditions, causing swelling, low crystallinity, and raising water intake (Fang et al., 1999; Sun et al., 2000).

For the fibrillation process, the most commonly implemented methods are mechanical treatments, such as grinding, high-pressure homogenization, and microfluidization (Huerta et al., 2020b; Redlinger-Pohn et al., 2022). However, those methods require multiple repetitions to achieve cellulosic fibers with small and desired diameter sizes. Additionally, high-pressure homogenization commonly results in equipment clogging, which requires either a pre-treatment to minimize fiber size or treatment of dispersions with low cellulose concentration (Huerta et al., 2020b). In comparison to the aforementioned fibrillation methods, high-intensity ultrasound (HIUS) is a clean and quick

technique, with good performance on the cellulose nanofibrillation due to the sonic cavitation phenomena (Huerta et al., 2020b; Wu et al., 2021).

Some additives used in cellulose-containing materials include calcium carbonate and glycerol. Calcium carbonate is currently the most popular filler in the pulp and paper industry and is used to reduce supply costs and improve properties such as opacity, whiteness, and porosity (Gill et al., 1995; Sáenz et al., 2023; Hu et al., 2022). Also, glycerol is one of the most widely utilized plasticizers to produce film composites, and is used to improve flexibility, workability, and distensibility (Vieira et al., 2011).

The study of moisture sorption isotherms provides information about the interactions of the material with moisture (Rhim et al., 2009). As cellulose-based packaging materials readily absorb moisture from the environment or high-moisture foods, that study may provide valuable information to improve cellulosic materials' water barrier properties (Bedane et al., 2015). The Guggenheim, Andersen, and de Boer (GAB) sorption equation has been used to interpret paper water sorption behavior, providing meaningful parameters like the monolayer moisture content and energy parameters related to the net molar heat of adsorption (Kupczak et al., 2018).

Using natural, renewable, and biodegradable compounds like cellulose as a matrix material in food packaging systems may contribute to the reduction of petroplastics waste and fulfillment of the production of food containers. Therefore, this study aims to develop a micro/nanopaper made of cellulose sourced from wheat straw hydrolyzed with pressurized mixtures of water and EtOH, bleached, and fibrillated with HIUS with the potential for food packaging development. To achieve this objective, The effect of bleaching treatments (ASC

and AHP) on pressurized 20% EtOH treated wheat straw, as well as the effect of HIUS treatment and the addition of calcium carbonate and glycerol were analyzed.

4.2 Materials and methods

4.2.1 Materials

Wheat straw, kindly provided by Dr. Klaus Strenzke (University of Alberta, Edmonton, AB, Canada), was milled using a centrifugal mill (Retsch, Haan, Germany). Milled wheat straw was stored in bags at ambient conditions. The proximate composition and particle size of the wheat straw sample used in this chapter are the same as reported in Chapter 3.

Sodium hydroxide (≥99.0 %), hydrogen peroxide (30%), acetic acid (≥99.7%), D-glucose (≥99.9 %), D-xylose (≥99.7%), L-arabinose (≥99.7%), sodium chlorite (80%), NaCl (≥99 %), KCl (≥99 %), LiCl (≥99 %), glycerol (≥99%), and calcium carbonate (≥99 %) were purchased from Sigma Aldrich (Oakville, ON, Canada). Milli-Q water was obtained after passing water through a Milli-Q water purification system (Millipore, Bedford, MA, USA). Ethanol (100%; ethyl alcohol, anhydrous) was purchased from Greenfield Global Inc. (Brempton, ON, Canada).

4.2.2 Methods

4.2.2.1 Hydrolysis of wheat straw using pressurized 20% aqueous ethanol

Wheat straw was hydrolyzed using a pressurized mixture of water and ethanol (20% v/v ethanol) for 1 h at 180°C, 50 bar, and a flow rate of 5 mL/min in the semicontinuous high-pressure equipment as described in Section 3.2.2.1. These conditions produced solid residues with the highest cellulose and lower lignin contents, as discussed in the Chapter 3. The proximate composition of the solid residue is presented in Appendix A (table A.8).

4.2.2.2 Bleaching of the hydrolyzed solid residues

After hydrolysis, the wheat straw residue was bleached using acidified sodium chlorite (ASC) and alkaline hydrogen peroxide (AHP). For the ASC bleaching, the procedure followed by Huerta et al. (2018) was slightly modified. Briefly, 8 g of wheat straw residue was mixed with 1.7% ASC solution (pH = 3.99) at a 1:10 w/w residue:ASC solution ratio. The bleaching temperature was 77.5±2.5°C and the total time was 2 h. These methodologies at such conditions, except for time, had been extensively studied in our research group. In this thesis, different processing times were selected as it was observed that samples achieved a bright white color at bleaching times lower than 3 h.

For the AHP method, 8 g of wheat straw residue was mixed with AHP at a 1:10 w/w ratio. AHP was prepared by mixing 1% w/w sodium hydroxide with 20% w/w hydrogen peroxide. The effect of bleaching treatment at different times (1, 2, and 2.5 h) was studied. The proposed times were selected based on color observations, similar to the ASC bleaching process. After bleaching, the solid residue was washed with tap water until the pH reached 6-7. Finally, the bleached solid residue was dried overnight at 35°C and stored at -18°C until further use. This AHP bleaching method was found to be optimum to bleach barley straw in our research group (paper in publishing process).

4.2.2.3 Micro/nanopaper formation and characterization

Fig. 4.1 shows a graphic representation of the overall procedure for cellulosic micro/nanopapers formation and characterization.

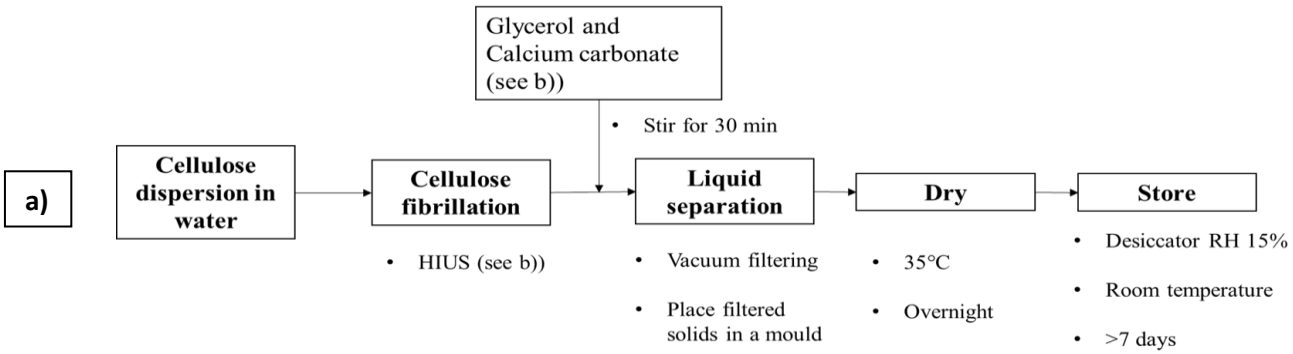

Studied conditions:

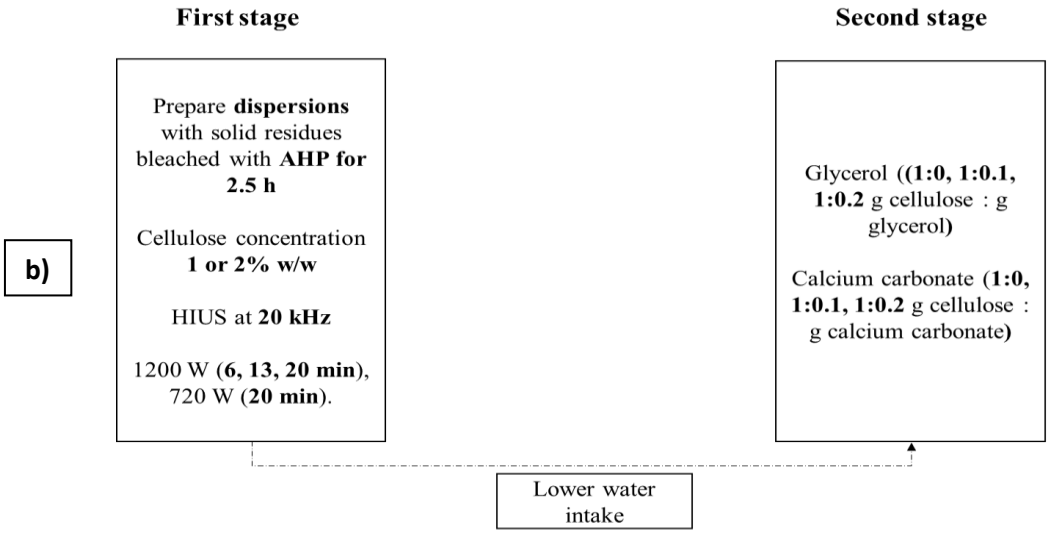

Characterization:

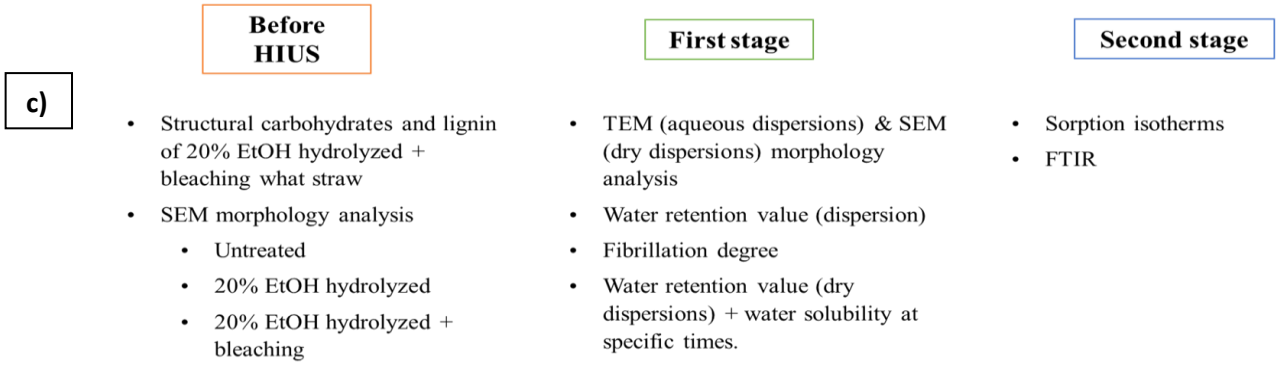

Fig. 4.1. Procedure for micro/nanopapers formation: a) overall procedure for material formation, b) stages and process conditions for micro/nanopaper study and selection, and c) Characterization analysis of samples produced in each stage.

In the first stage, after bleaching the hydrolyzed wheat straw with AHP for 2.5 h, the cellulose-enriched solid residue was dispersed in 30 mL of Milli-Q water at concentrations of 1% and 2% w/v. Suspensions were treated with high-intensity ultrasound (HIUS) to fibrillate the cellulose fibers using an ultrasonic processor (Model No. FS-1200N, Shanghai Sonxi Ultrasonics Instrument Co., Shanghai, ZJ, China) with a 20 mm diameter probe at 20 kHz and nominal powers of 720 W (20 min) and 1200 W (6, 13, and 20 min).

Samples were analyzed before and after oven drying. Characterization before drying included fiber diameter size analysis with TEM and SEM, water retention value (WRV_w) of the wet dispersion, and fibrillation degree. Characterization after drying involved the WRV_d to evaluate the water intake of the dried micro/nanopapers. Dried samples were prepared by the solvent casting method by pouring 30 mL (one batch) of the HIUS-treated dispersions in a petri dish (diameter ~ 5 cm) covered with canola oil and drying the poured dispersion at 35°C for 2 days. The samples and characterization analysis until this point are regarded as the first stage.

To improve the physicochemical characteristics of the micro/nanopapers, glycerol (1:0, 1:0.1, 1:0.2 g cellulose:g glycerol) and calcium carbonate (1:0, 1:0.1, 1:0.2 g cellulose:g calcium carbonate) were added to the dispersions to produce the second-stage micro/nanopapers. The HIUS process at 1200 W for 6 min was selected for second-stage micro/nanopapers for practical reasons. Glycerol was used as a plasticizer and calcium carbonate was used as filler. The second-stage micro/nanopapers were prepared with the vacuum filtration method for practical reasons. Approximately 18 g of the HIUS-treated dispersions were placed in 25 mL beakers, and glycerol and calcium carbonate at the aforementioned concentrations were added. Dispersions with(out) glycerol and calcium

carbonate were stirred for 30 min and then poured into a vacuum filtering system to remove the water for approximately 15 min. The beakers that contained the dispersions with(out) glycerol and calcium carbonate were rinsed, and the content was also poured into the vacuum filtering system to minimize sample loss. The funnel had a diameter of ~5 cm with filter paper Whatman # 1 at the bottom of the funnel. The solid phase of the dispersion was removed from the funnel and filter paper and dried in an oven (Fisher Scientific; Isotemp Oven 655G) at ~35°C overnight and stored in a desiccator at ~21°C and RH of 15%. Lastly, sorption isotherms and FT-IR analysis were performed to study the second-stage produced materials.

4.2.2.4 Lignin and structural carbohydrates

Lignin and structural carbohydrates of bleached solid residues were analyzed using the same procedure described in Section 3.2.2.3.2 of Chapter 3.

4.2.2.5 Morphology

The microstructure of the bleached solid residues was analyzed with a scanning electron microscope (SEM) while the fibril diameter size of the HIUS-treated dispersion was analyzed with transmission electron microscope (TEM) and SEM.

For SEM analysis, untreated, hydrolyzed, and hydrolyzed and bleached (ASC 2 h, AHP 2.5, AHP 2 h, and AHP 1 h) samples were adhered to a stub (Electron Microscopy Sciences Cat. # 75230; Hatfield, Philadelphia, USA) using an adhesive carbon sticker, then sputter coated with carbon using a hummer 6.2 sputter coater (Anatech Ltd. Au/Pd coating) and imaged using the SEM equipment (EVO 10 model operating at 15 kV, Carl Zeiss Canada Ltd., Toronto, ON, Canada). First-stage dried dispersions (prepared with the solving casting

method were also analyzed with the SEM equipment by cutting a ~3 x 3 mm^2 square of the sample, adhering it to a stub, and sputter coating before SEM analysis.

For the TEM analysis, wet dispersions were diluted as required. A drop of the diluted sample was placed on a grid and allowed to adhere for 2 min. The excess liquid was then blotted off with a filter paper, and the dried sample in the grind was stained with 4% uranyl acetate before imaging with the TEM equipment (Morgagni 268 model operating at 80 kV, FEI company, Hillsboro, Oregon, USA; with a Gatan Orius CCD Camera). Samples analyzed with TEM just included the AHP 2.5h bleached solid residues treated with HIUS at a concentration of 1% and power of 1200 W for 6, 13, and 20 min.

The fiber size was determined using the method described by Huerta et al. (2020b) with slight modifications. Briefly, 4 photos were taken with the TEM equipment, then using the ImageJ software, a total of one hundred measurements of fiber diameters in the nanoscale were taken to calculate the average diameter and size distribution.

4.2.2.6 Fibrillation yield

The fibrillation yield was determined and calculated according to Huerta et al. (2020b). Briefly, samples were diluted to 0.2 wt%, then centrifuged at 1800x*g* for 20 min. The supernatant was separated by decanting, and the solid was dried at 100°C until constant weight. The nanofibril content in the cellulosic material was calculated using the following equation:

$$Nanofibril\ content\ (wt\%) = \left(1 - \left(\frac{Weight\ of\ dried\ sediment\ [g]}{Weight\ of\ cellulosic\ fiber\ before\ centrifugation\ [g]}\right)\right) \times\ cellulose\ content\ \times\ 100\ \% \quad \text{Eq. (4.1)}$$

4.2.2.7 Water retention value (WRV_w) of the dispersion

The water retention value of the wet dispersions was measured according to the method reported by Huerta et al. (2020b). Briefly, dispersions were centrifuged at 900x*g* for 30 min at 20°C. The supernatant was separated by decanting, and the solid was dried at 105°C in a convection oven until constant weight. The WRV of the dispersions was calculated using Eq. 4.2:

$$WRVw\ (\%) = \frac{Dried\ pellet - wet\ pellet}{Wet\ pellet} x\ 100\% \qquad Eq.4.2$$

4.2.2.8 Water retention value (WRV_d) of the dried materials

The WRV was determined following the methodology described by Manzocco et al. (2022) with some modifications. Approximately 1/6 (~0.055 g) of the first-stage dried dispersions, previously stored in the desiccator (RH = 15% for ≥7 days, were placed in a beaker with 100 mL of Milli-Q water at room temperature of 22°C. After certain time intervals (0.5, 1, 3, 5, 7, 9, 11, 13, and 15 min), samples were removed from the beaker, the excess of water was carefully removed with Kimtech Kimwipes delicate-task wipers, and sample weight was recorded. The experiment was stopped when the constant weight was reached within a 5% error. Water retention values were calculated using Eq. 4.3.

$$WRV\ (\%) = \frac{Final\ weight - Initial\ weight}{Initial\ weight} x\ 100\% \qquad Eq.4.3$$

The initial weight is the weight of the dry sample before analysis and the final weight is the weight of the sample placed in the beaker with water after a certain time interval.

4.2.2.9 Micro/nanopaper water solubility

This analysis was performed as a complement to the WRV_d study to show that the changes in the sample weight were mainly due to the intake of water and not due to the cellulosic fibrils re-dispersion into the water media during the WRV analysis.

The first-stage dried dispersions solubility in water was analyzed following the method reported by Zhao et al. (2019) with some modifications. Approximately 1/6 of the dried sample (~0.055 g), previously stored in the desiccator (RH = 15% for ≥7 days) was placed in a beaker with 100 mL of Milli-Q water at room temperature of 22°C. After certain intervals of time (0.5 and 15 min), samples were removed from the beaker, and the excess of water was carefully removed with Kimtech Kimwipes delicate-task wipers. Finally, the samples were dried at 105°C in a convection oven until samples reached constant weight. Also, the moisture content of samples before placing them in the beaker with 100 mL of Milli-Q water was determined as in Section 3.2.2.2.1, Chapter 3. The water solubility was calculated using Eq. 4.4:

$$Water\ solubility\ (\%) = \frac{M_0 - M_f}{M_0} x\ 100\% \qquad Eq.(4.4)$$

where, M_0 represents the weight (dw) of the dry material before placing them in the beaker with Milli-Q water and M_f of the dry samples after placing it in the beaker with Milli-Q water for a certain time interval.

4.2.2.10 Interactions of cellulose, calcium carbonate and glycerol by Fourier-transform infrared spectroscopy (FT-IR)

Chemical properties and interactions of the second-stage micro/nanopapers were studied using FT-IR spectroscopy (FT-IR-iS50, Thermo Fisher Scientific, Waltham, MA, USA) in the range of 4000 to 400 m^{-1}.

4.2.2.11 Monolayer moisture content and GAB parameters analysis by sorption isotherms

The second-stage micro/nanopaper water binding capacity at different relative humidities (RH) was analyzed according to the methodology described by Yoshida et al. (2014) with slight modifications. First, micro/nanopapers with(out) glycerol and calcium carbonate were prepared as described in Section 4.2.2.3. Then, the micro/nanopapers were stored in a desiccator (RH = 15% for ≥7 days), and then cut into 4 pieces (~0.04 g each). The pieces of samples were then placed in chambers at 21 ± 1°C. Each chamber had different aqueous salt solutions with different water activities (13.41 molal LiCl (A_w = 26%), 8.57 molal LiCl (A_w = 50%), 6 molal NaCl (A_w = 76%), and 0.5 molal KCl (A_w = 98%)). Samples were maintained in the chamber until a constant weight was reached (±5%). The weight and the moisture content on a dry weight basis of each sample were determined as in Section 3.2.2.2.1, Chapter 3. Then, the micro/nanopapers' sorption isotherms were estimated using the Guggenheim, Anderson, and de Boer (GAB) isotherm equation:

$$X = \frac{X_m * C * k * A_w}{(1 - k * A_w) * (1 - k * A_w + C * k * A_w)} \qquad Eq. 4.5$$

where, X is the dry basis moisture content, X_m is the monolayer moisture content, C is a constant related to thermal effects and k is the GAB constant related to the properties of multilayer water molecules with respect to the bulk liquid. The GAB parameters were estimated by non-linear regression. Samples were analyzed at least in duplicates.

4.2.3.12 Statistical analysis

All experiments were performed in duplicates. Results were presented using the average and standard deviations of data obtained from the respective analysis. There is an exemption for the structural carbohydrates and lignin contents results for ASC, where two samples obtained from one experiment were analyzed. Statistically significant differences were determined using one-way (ANOVA) and Tukey's test at a 95 % confidence interval. Statistical analysis was performed using the program Minitab version 18 (Minitab Inc., State College, PA, USA).

4.3 Results and discussion

4.3.1 Structural carbohydrates and lignin

Fig. 4.2 shows the effect of bleaching treatments with ASC for 2 h and AHP for 1, 2, and 2.5 h after pressurized 20% EtOH treatment of wheat straw. The cellulose contents of hydrolyzed wheat straw after bleaching with ASC for 2 h (87.34±2.72% dw) and AHP for 1 h (80.52±1.98% dw), 2 h (83.14±0.18% dw), and 2.5 h (85.48±0.65% dw) showed no significant difference. Bleaching treatments with ASC and AHP at different times achieved a significant cellulose increase compared to the 20% EtOH-treated wheat straw (68.79±3.43% dw). Also, the cellulose contents after 20% EtOH treatment and bleaching treatments (ASC for 2 h and AHP for 1, 2, and 2.5 h) increased more than twice compared to the untreated wheat straw (35.62±0.14% dw). Hemicellulose contents of samples before and after bleaching with ASC for 2 h (8.99±0.00% dw) and AHP for 1 h (9.31±0.32% dw), 2 h (9.68±0.11% dw), and 2.5 h (9.77±1.48% dw) showed no significant difference.

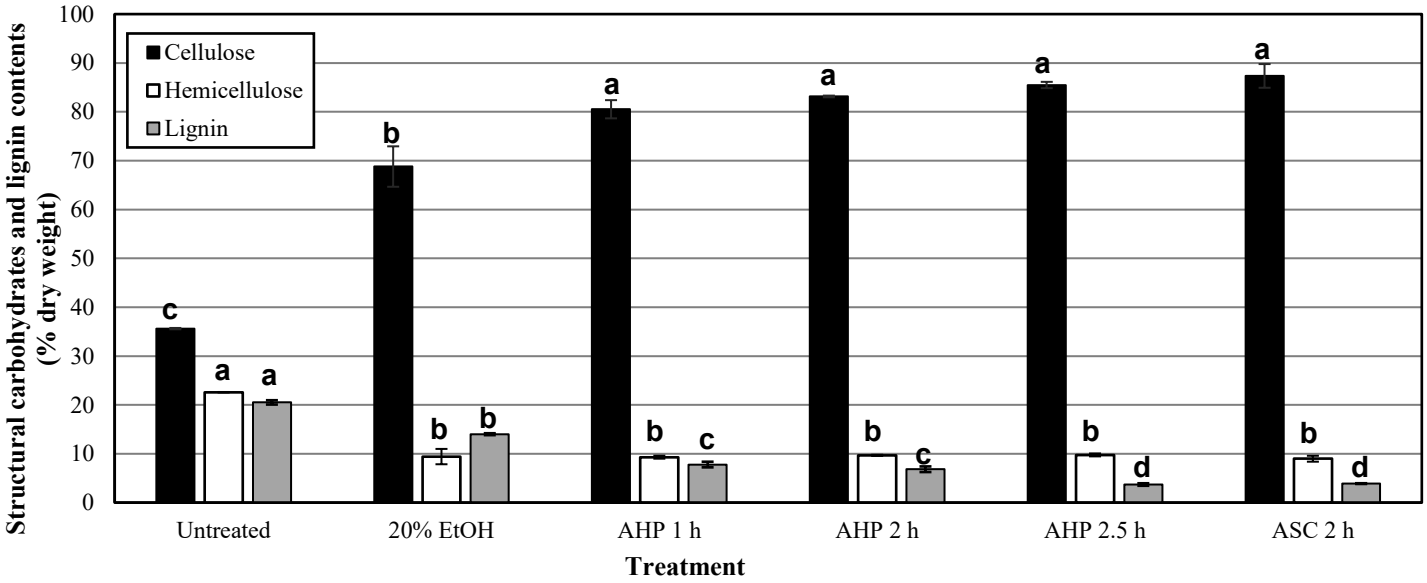

Fig. 4.2. Untreated, pressurized 20% EtOH and pressurized 20% EtOH+ bleaching (acidified sodium chlorite* (ASC*) for 2 h and alkaline hydrogen peroxide (AHP) for 1, 2, and 2.5 h) treated samples composition. [a-d]Different letters on bars in the same color represent significant differences at $p < 0.05$. *ASC bleaching results obtained from two samples obtained from one experiment. Data in the appendix section (Table C.1).

The initial feed (untreated wheat straw) had a lignin content of 20.52±0.44% dw that further decreased after the hydrolysis and bleaching treatments (Fig. 4.2). The lignin content in hydrolyzed wheat straw after treatments with ASC 2 h and AHP 2.5 h were not significantly ($p<0.05$) different and reduced from 14.01±0.19 to 3.90±0.07 and 3.71±0.25% dw, respectively, compared with the 20% EtOH treated wheat straw. Hydrolyzed wheat straw bleached with AHP after 2 h and 1 h had a significantly ($p<0.05$) higher lignin content than the aforementioned samples, achieving a lignin content reduction from 14.13±0.19 to 6.84±0.61 and 7.80±0.61% dw compared with the 20% EtOH treated wheat straw, respectively. Also, wheat straw bleached with AHP after 2 h and 1 h were not significantly ($p<0.05$) different. The mass balance of hydrolyzed and bleached wheat straw is presented

in Appendix A. The values obtained for cellulose and hemicellulose presented inconsistencies probably due to solid residue loss during the bleaching solvent change and recovery steps. Therefore, the mass balance is not further discussed in this section. However, lignin was the most affected compound, with a reduction of more than half in all the bleaching treatments and times, according to the mass balance.

During the AHP treatment, the hydroperoxy anion eliminates chromophore groups present in lignin through its reaction with quinones, non-conjugated carbonyl groups, and double bonds, resulting in the formation of carboxyl fragments. Additionally, hydroxyl radicals and superoxide radicals are responsible for the delignification of lignocellulosic materials through lignin oxidation (Fang et al., 1999; Sun et al., 2000). As for the ASC treatment, the delignification mechanism is still not well understood. Nevertheless, it is well accepted that $NaClO_2$ is unstable under acidic conditions, leading to the formation of chlorine dioxide and chloride anions, responsible for the breaking of ether and carbon-carbon bonds between lignin and the carbohydrate portion, removing the lignin fraction from the lignocellulosic material (Nan et al., 2018).

Previously, Ciftci et al. (2018) studied the cellulose isolation from lupin hull and canola straw using NaOH at concentrations of 5–20% w/w, at 25–99°C, for 2–10 h, and ASC at the concentration of 1.7% w/w, 75°C for 2–6 h. The optimal conditions for the NaOH treatment were 15% NaOH at 99°C for 6 h. After the optimized NaOH treatment, the lignin contents of the lupin hull and canola straw samples were 4.7 ± 0.2 and 12.3 ± 0.2 %, respectively. Also, they found that the ASC treatment removed non-cellulosic material, obtaining a white color solid residue in both lupin hull and canola straw treated with 15% NaOH at 99°C for 6 h. The solid residue obtained from the lupin hull and canola straw turned

white after 2 h and 4 h, respectively (Ciftci et al., 2018). After those times, the lignin content in the lupin hull and canola straw were 2.9 ± 0.4 % and 8.5 ± 0.7 %, respectively. Also, the lignin content of treated canola straw was 10.8 ± 0.5 % after 2 h. Based on the findings of that research, it can be inferred that the amount of lignin in the lignocellulosic solid residue treated with ASC varies, depending on the feed for cellulose isolation, even if the treatment time is the same.

Additionally, Huerta (2020c) isolated cellulose from canola straw treated with PAE at the concentration of 20% ethanol, 180°C, 5 mL/min, for 40 min using 1.7% ASC at the same conditions as in Ciftci et al. (2018). Huerta (2019) found that the lignin content after the PAE treatments increased from 18.2±0.1 to 20.0±0.4 %. After 6 h of ASC treatment, the lignin content was reduced from 20.0±0.4 % to 8.0±0.2 %. Such lignin concentrations differ from the findings of Ciftci et al. (2018). According to Ciftci et al. (2018), the NaOH hydrolyzed canola straw had a lignin content of 12.3 ± 0.2 %, and after 6 h of ASC treatment, the lignin content was reduced to 7.9 ± 0.3 %. Even though the initial lignin content in the PAE-treated canola straw was almost twice as high as the lignin content of the NaOH treated samples, the lignin contents of those samples were similar after 6 h ASC treatment. Thus, it is also concluded that the hydrolysis treatment (NaOH vs PAE) may also influence the lignin concentration changes during the ASC treatment. Therefore, the different results achieved by Ciftci et al. (2018), Huerta (2019), and the results presented in this study might be due to differences in the pretreatment types and cellulose straw sources.

Overall, hydrolyzed wheat straw bleached with ASC for 2 h and AHP for 1, 2, and 2.5 h had similar cellulose contents. However, ASC for 2 h and AHP for 2.5 h had low lignin contents compared to the other treatments. Due to the similar cellulose and lignin contents,

short processing time difference, and low environmental impact, the AHP for 2.5 h treatment was selected as the best bleaching treatment to be used for further micro/nanopapers production and characterization.

4.3.2 Morphology of the bleached and unbleached solid residue by SEM

Fig. 4.3 shows the microstructures of wheat straw before and after hydrolysis with pressurized 20% EtOH at 180°C, 50 bar, 5 mL/min for 60 min and microstructures obtained after bleaching treatments with ASC for 2 h and AHP for 2.5, 2, and 1 h. In all SEM images, non-homogeneous sizes of treated and untreated wheat straw were observed. In nature, cellulose forms fibrils that are bundled together into microfibrils, which are surrounded by hemicellulose, lignin, ash, proteins, and lipids, among other compounds. In Fig. 4.3a, raw milled wheat straw had a fibrous, yet smooth surface. After the hydrolysis treatment, the wheat straw surface had a slightly more fibrous surface (Fig. 4.3b). Similar morphology was found in wheat straw pretreated with 6% w/w NaOH, at 150°C for 120 min and treated by hot water at 150°C for 120 min, which had a Klason lignin and holocellulose contents of 7.12% and 77.32%, and 21. 33% and 73.61%, respectively (Malik. et al., 2020). Initial feed had 22.38 % Klason lignin and 70.11 % holocellulose. Malik. et al., (2020) concluded that both treatments partially destroyed the wheat straw surface. However, the hot water treated sample presented lower damage, and the changes were mainly due to the partial removal of hemicellulose. The alkali-treated sample presented more open structure and square-like patterns due to the removal of hemicellulose and lignin, with further swelling of the cellulose structure. The surface of wheat straw hydrolyzed with pressurized aqueous ethanol at the concentration of 20% ethanol slightly changed in comparison with the untreated wheat straw. However, the cracked structures of the samples in this study resembled the patterns reported

in the samples of Malik. et al. (2020). Thus, it could be concluded that the changes in hydrolyzed wheat straw in this study might be due to the removal of hemicellulose and lignin with less cellulose swelling, in comparison to the finding of Malik et al. (2020).

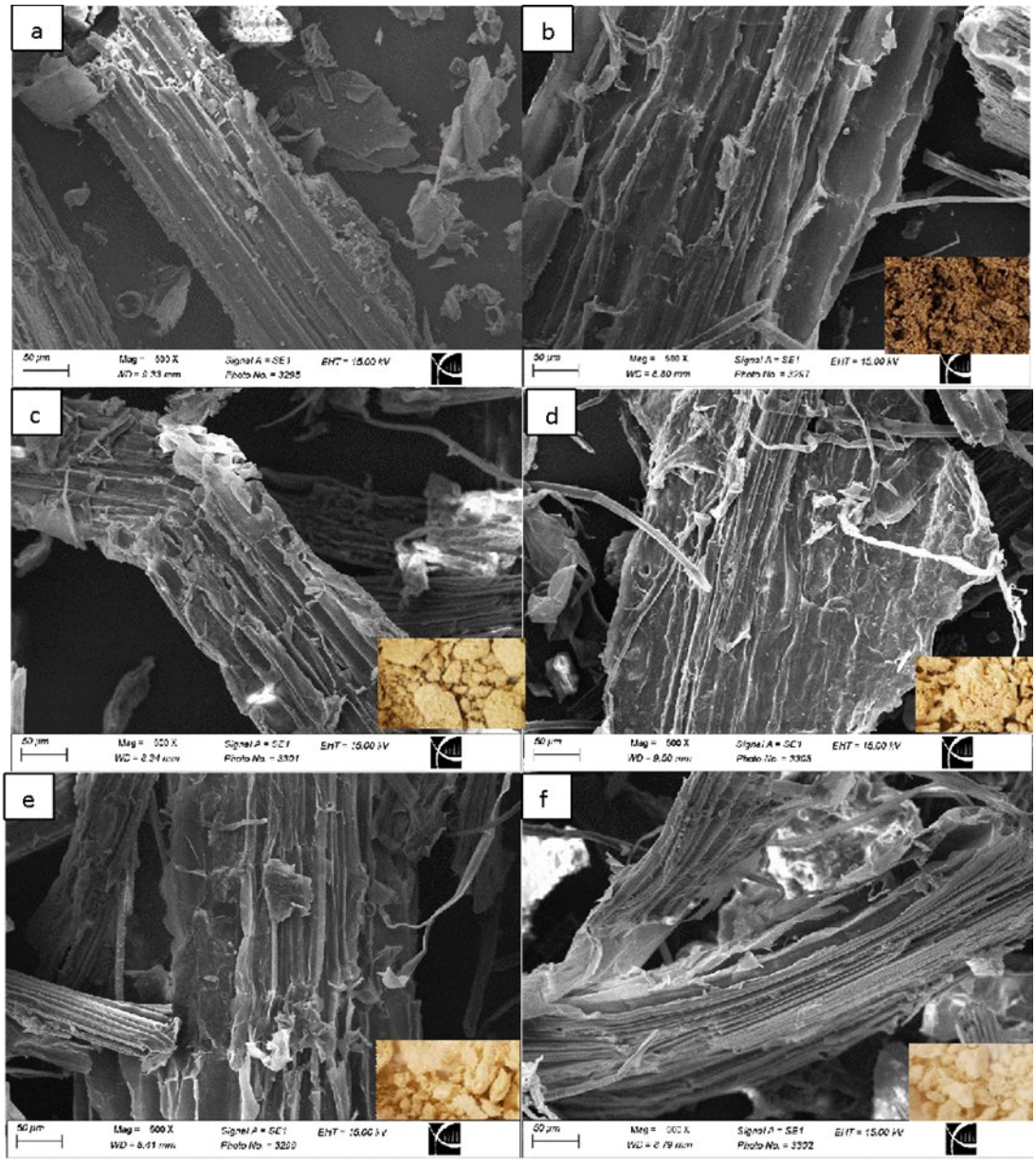

Fig. 4.3. SEM pictures of (a) untreated wheat straw, (b) 20% EtOH treated wheat straw, and (c) AHP 1h, (d) AHP 2h, (e) AHP 2.5h, and (f) ASC 2h. AHP: alkaline hydrogen peroxide, and ASC: acidified sodium chlorite.

The bleaching treatments with ASC for 2 h and AHP for 1, 2, and 2.5 h greatly contributed to the removal of lignin as discussed before (Fig. 4.3f). As a result, wheat straw surface after the hydrolysis and bleaching treatments showed a higher cracked and fibrous appearance compared to the raw and hydrolysis-treated wheat straw (Fig. 4.3c-f).

4.3.3 Morphology analysis of the HIUS-treated wet dispersions

Fig. 4.4 shows the morphology of wet dispersions treated with HIUS at 1200 W for 6, 13, and 20 min. This figure revealed that fibrillated cellulose consisted of fibers with a wide range of diameters both in the nano- and micro-range. Fibers in the micro-range were observed as wide-black structures with a diameter > 4-6 μm. Several nanofibrils were attached to those wide-black structures at the same spot, and they were coming out in a web-like manner.

Fig. 4.5 shows the diameter size distribution of cellulosic fibers with diameters <1 μm of wet dispersions analyzed with TEM. The average diameters of the fibers obtained after dispersion in water at 1% and HIUS treatment for 6, 13, and 20 min were 30, 25, and 21 nm, respectively. The average diameter of the fibers obtained after dispersion in water at 2% and HIUS treatment at 1200W for 13 min was 47nm. Also, samples prepared at the concentration of 1% had a high proportion of fibers with a diameter below 30 nm. Dispersions with 2% treated by HIUS at 1200 W and 13 min resulted in higher diameter fiber production than that with 1% at the same conditions, suggesting that the bleached solid residue concentration in the dispersion also affects the fibrillation process.

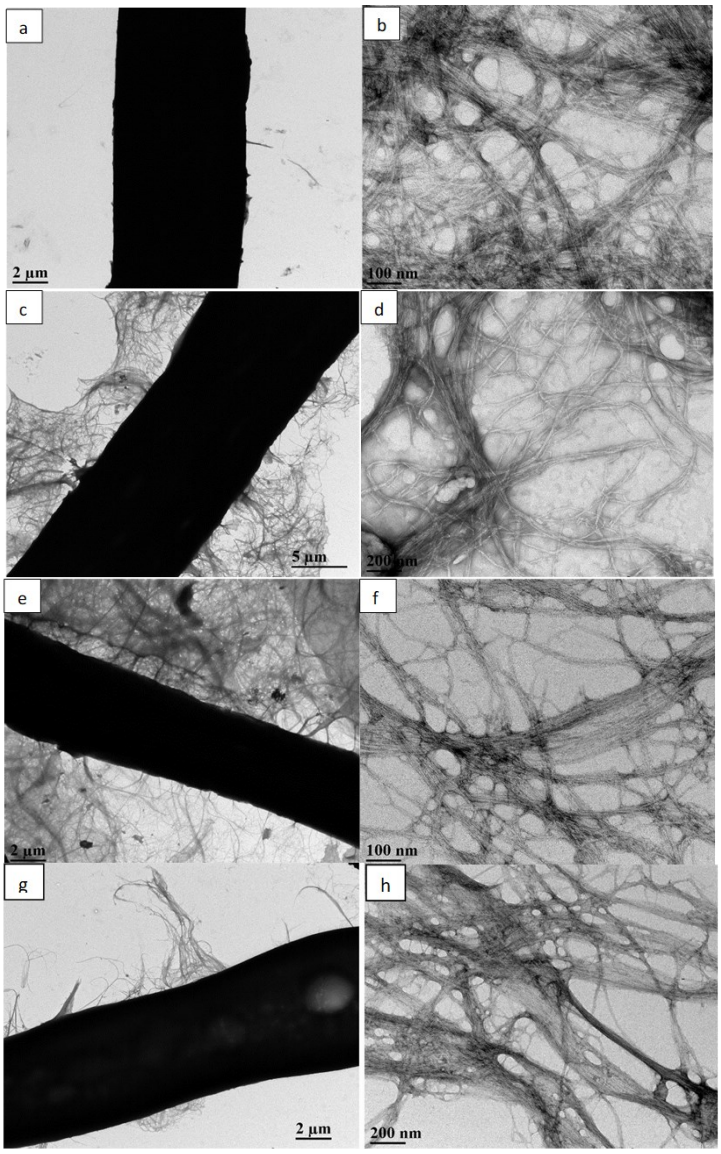

Fig.4.4. TEM pictures of wet dispersions of hydrolyzed wheat straw bleached with AHP for 2.5 h and fibrillated with HIUS at 1200 W and 20 Hz for 6 min (a, b), 13 min (c, d), and 20 min (e, f) at the concentration of 1%, and 13 min (g, h) at the concentration of 2%.

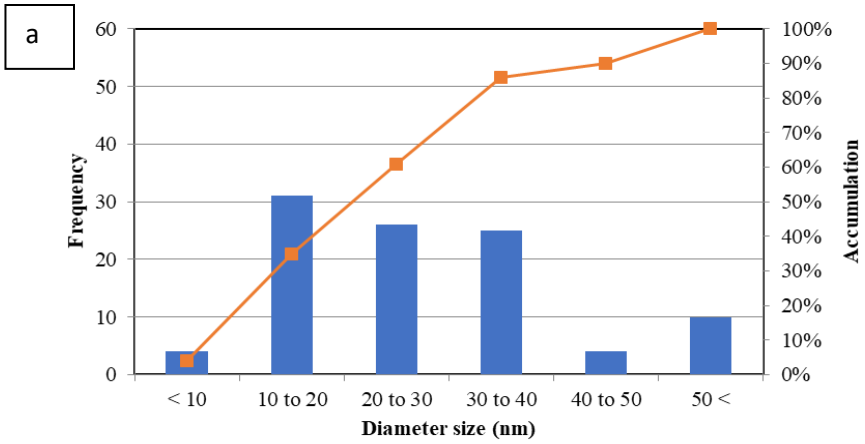
a
60
50
40
30
20
10
0
Frequency
100%
90%
80%
70%
60%
50%
40%
30%
20%
10%
0%
Accumulation
< 10
10 to 20
20 to 30
30 to 40
40 to 50
50 <
Diameter size (nm)

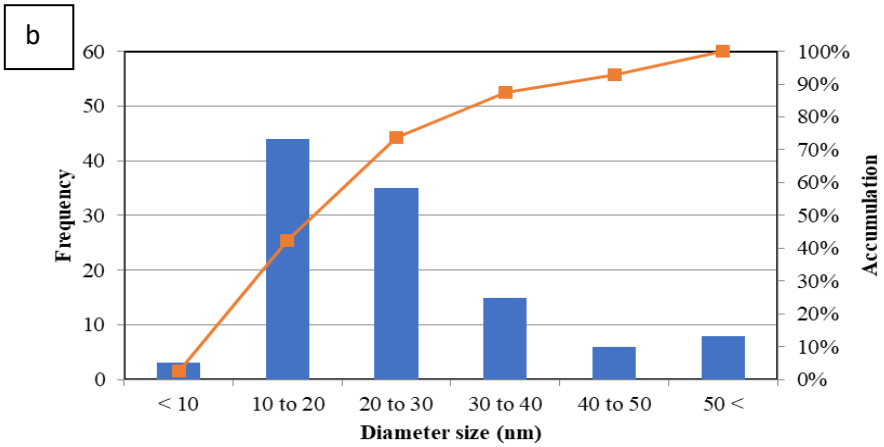
b
60
50
40
30
20
10
0
Frequency
100%
90%
80%
70%
60%
50%
40%
30%
20%
10%
0%
Accumulation
< 10
10 to 20
20 to 30
30 to 40
40 to 50
50 <
Diameter size (nm)

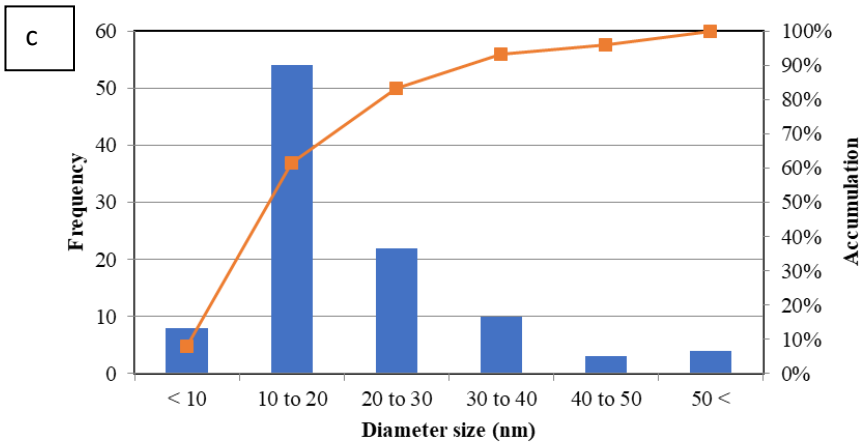
c
60
50
40
30
20
10
0
Frequency
100%
90%
80%
70%
60%
50%
40%
30%
20%
10%
0%
Accumulation
< 10
10 to 20
20 to 30
30 to 40
40 to 50
50 <
Diameter size (nm)

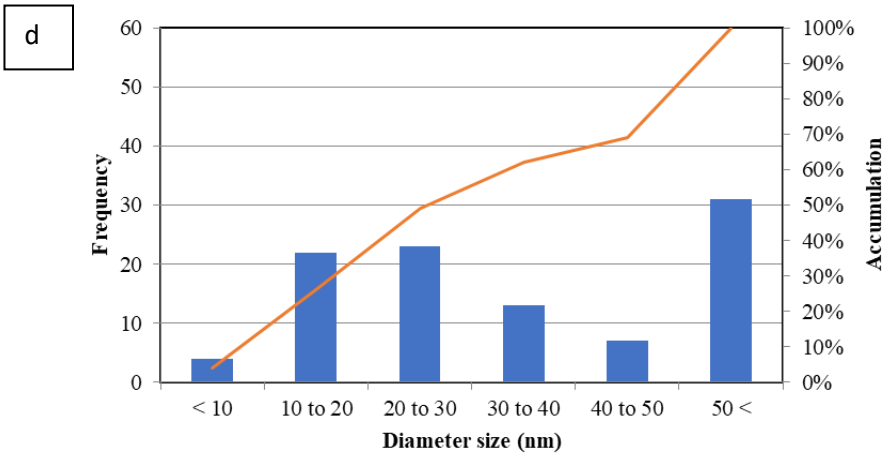

Fig. 4.5. Size distribution of solid residue bleached with AHP for 2.5 h, dispersed in water at concentrations of 1%, and fibrillated with HIUS at 1200 W for 6 min (a), 13 min (b), and 20 min (c); and solid residue bleached with AHP for 2.5 h, dispersed in water at concentrations of 2%, and fibrillated with HIUS at 1200 W for 13 min (d). Data in the appendix section (Table C.2).

As the TEM equipment was limited to a maximum amplification of 5 µm, the dried sample morphology in the micro-range fibrils was challenging to analyze. Thus, SEM images were taken to analyze the morphology of micro-range fibrils. Fig. 4.6 shows the morphologies of the micro/nanopapers obtained after casting and drying the aforementioned wet dispersions. It can be observed that the fibers aggregated after the drying process, thus the analysis of individual nanofibrils, especially those with small diameters, was challenging. Nevertheless, discernible fibers presented diameter size in the micro-range of ~2-~23 µm. Also, the morphology of those fibers presented kinks, which could be attributed to the HIUS fibrillation mechanism.

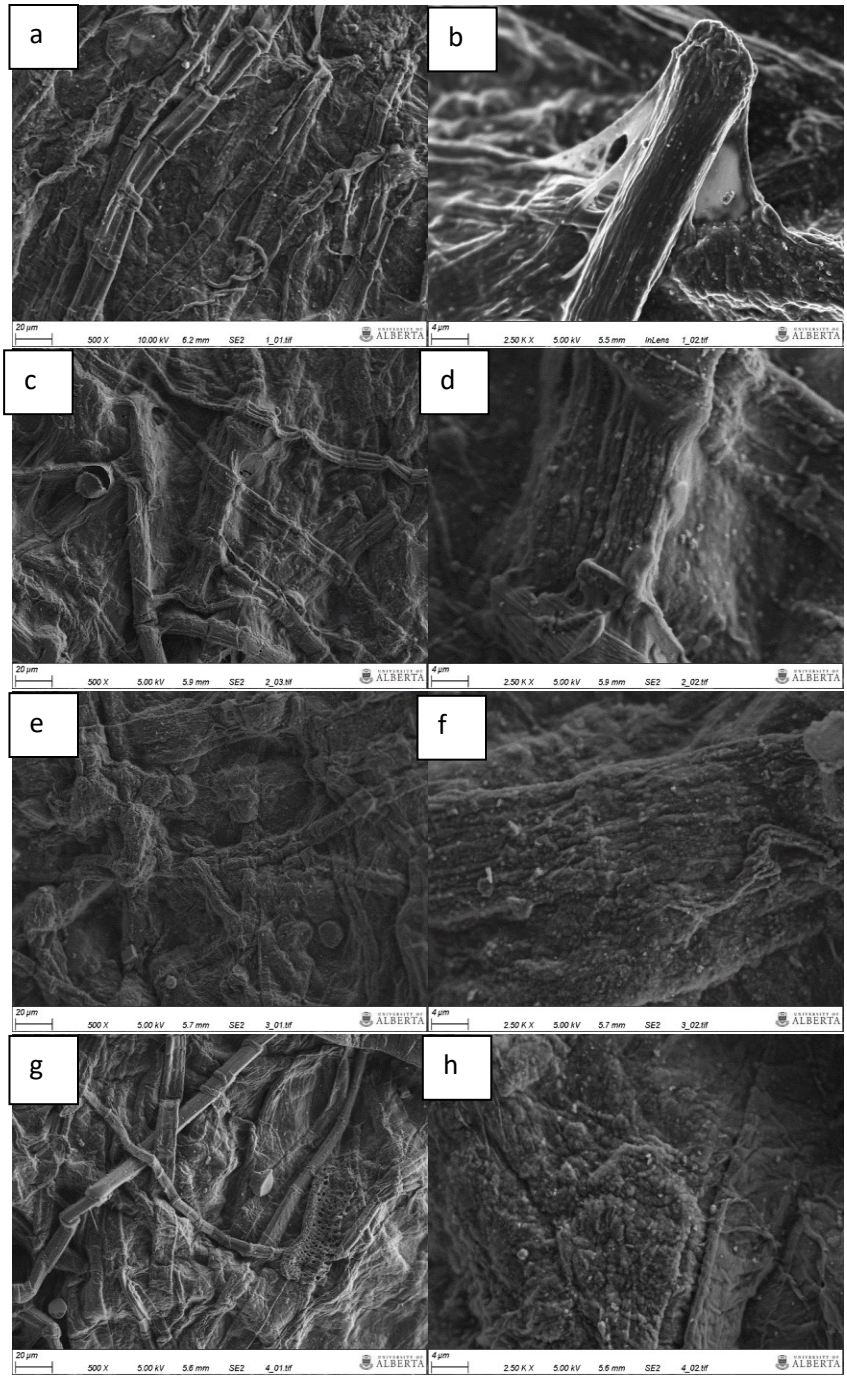

Fig. 4.6. SEM pictures of dried first stage micro/nanopapers composed of hydrolyzed wheat straw bleached with AHP for 2.5 h and fibrillated with HIUS at 1200 W and 20 Hz for 6 min (a, b), 13 min (c, d), and 20 min (e-f), at the concentration of 1%, and 13 min at the concentration of 2 % (g-h) prepared by solvent casting.

Redlinger-Pohn et al. (2022) studied the effect of hydrodynamic and acoustic cavitation on enzymatically and chemically modified cellulose fiber pulp by TEMPO oxidation and carboxymethylation. They concluded that the main mechanism for the fragmentation and fibrillation of cellulose fibres into CNF would be microstreaming, which is the localized hydrodynamic forces produced by fast fluid flow in or out caused by cavitation bubbles. Due to the large diameters of cellulosic fibres compared to the cavitation bubbles, the cellulose fibrils would bend into the cavity rather than reorienting in the collapsing cavity, resulting in the stretching and bending of fibres. Bending cellulose fibrils can result in deformation failure and molecular damage to the fibrils, such as kinks and delamination. Kinks are alterations in the direction of the fibril axis. Redlinger-Pohn et al. (2022) hypothesized that the first stages of cellulose fibre fibrillation involved bending and delamination. Further fibrillation mechanism that resulted in shortening of the fibrils may have involved bending and scission-induced breakage. Additionally, it was concluded that the chemically modified cellulose was easier to fibrillate than non-modified cellulose due to weaker fibril cohesion, requiring lower mechanical forces (i.e., stronger bending) to bend and delaminate fibrils within the cellulosic fibers.

4.3.4 Fibrillation yield

Fig. 4.7 shows the fibrillation yield of bleached and hydrolyzed wheat straw, dispersed in water at the concentrations of 1% and 2%, and treated with HIUS at 1200 W for 6, 13, and 20 min. Bleached samples dispersed at a concentration of 1% and treated with HIUS at 1200 W for 6, 13, and 20 min showed no significant difference.

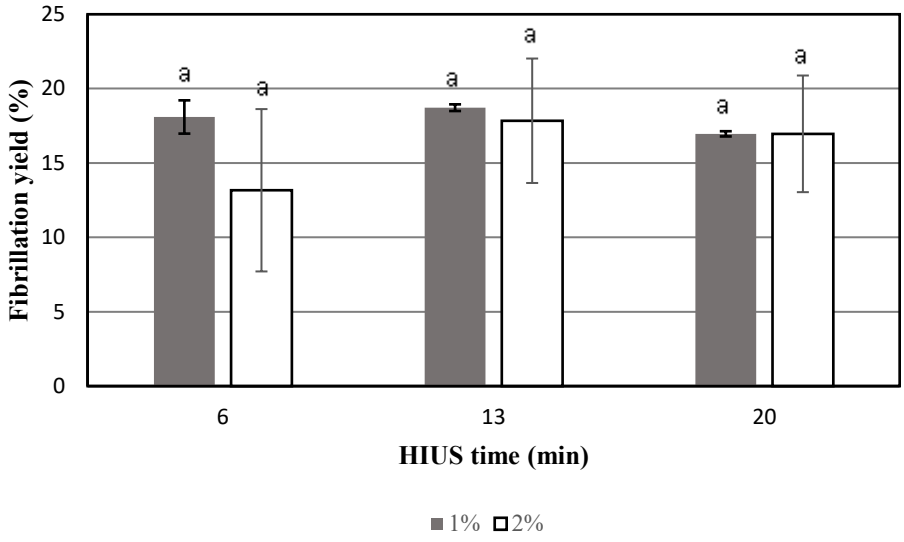

Fig. 4.7. Fibrillation yield of HIUS treated dispersions of bleached wheat straw at concentrations of 1% and 2% at 1200 W. [a]Bars with different letters represent significant differences at $p < 0.05$. Data in the appendix section (Table C.3).

The method used in this study to measure the fibrillation yield was based on the separation and aggregation of fibers of different sizes through centrifugation. Such method was used and validated by Jiang et al. (2018), who separated fibrils made from bagasse solid residue with different lignin contents with the same method of centrifugation used in this study at the same conditions. The fibrillation process was applied to cellulose isolated from bagasse at the concentrations of 2 and 2.3 % w/v, and the fibrillation process was carried out using a SuperMassColloider at 1500 rpm with a gap between grinding stones adjusted to − 100 μm from motion zero position for 0.5-7 h. The process was stopped for 20 min every 1.5 h to minimize the water evaporation. They analyzed the fibril morphologies, sizes and transparencies. They found that non-centrifuged samples consisted of a mixture of fibrils with a variety of diameters. On the other hand, fibrils in the nanoscale were effectively separated from fibrils with diameters mostly in micron range > 100 nm after centrifugation,

which were precipitated at the bottom as a solid while nanofibrils stayed in the supernatant fraction. However, underestimations were reported, attributed to nanofibril aggregation to sheets/bundles due to H-bonding among fibrils, which were pronounced by a momentary high concentration of fibrils during centrifugation.

Comparison of the fibrillation yield of wheat straw in this study and the literature was challenging due to scarce studies reporting fibrillation yield for wheat straw. Also, different conditions for fibrillation yield and different pretreatment and fibrillation treatments were used. For instance, Espinosa et al. (2016) produced lignocellulosic nanofibers from cellulose isolated from wheat straw, which was previously treated with soda pulping, passed through a pulp disintegrator, and beated. The high-pressure homogenization was performed at 60–70°C, with 1.5 % dispersion passed 4 times at 300 bar, 3 times at 600 bar, and 3 times at 900 bar. The fibrillation yield was determined by centrifuging a 0.2 wt% suspension at 4500 rpm for 20 min. The feed had cellulose, hemicellulose, and lignin contents of 73.0, 16.3, and 2.8 %, resectively. The lignocellulosic nanofibers produced in that study had a fibrillation yield of 55.6 %, which was higher than the results obtained in this study.

The same research group later compared the high-pressure homogenizer twin-screw extruder, and ultra-fine grinder in the production of lignocellulosic nanofibers from the same feed pretreated at the same conditions, except for the pulp disintegrator step (Espinosa et al., 2019). Ultra-fine grinding was performed with 2 wt% dispersion, 2500 rpm for 2.5 h, maximum gap between the two disks of −10, pulp passed for 1 s 60 times/h through the nip zone) while the twin-screw extruder was carried out with 18–20 wt% dispersion, L/D ratio = 4, 10°C, 400 rpm. The twin-screw extrusion process was performed with(out) enzymatic pretreatment of feed with endoglucanase. The fibrillation yields of such treatments were

35.8 ± 1.20, 15.17 ± 4.20, and 42.31 ± 0.01 % for the ultra-fine grinder, twin-screw extruder, and twin-screw extruder + enzymatic pretreated samples, respectively. Thus, different mechanical treatments resulted in different fibrillation yields.

Among the studies in our research group, Huerta et al. (2020b) analyzed the fibrillation yield of cellulose isolated from canola straw using HIUS treatment at 20 kHz in a continuous mode at different nominal powers of 240, 720, and 1200 W, for 8 min, and a cellulose concentration of 1 %. They used two feeds, one containing high lignin (70.73±1.00% cellulose, 4.90±1.03% hemicellulose, and 18.22±0.18 lignin%), and the other containing low lignin (81.92±1.05% cellulose, 3.68±0.06% hemicellulose, and 7.98±0.22% lignin). The conditions for fibrillation yield and hydrolysis reported by Huerta et al. (2020b) were similar to the ones followed in this study. They found that the low lignin and the high lignin feeds had maximum fibrillation yields of 46 and 40 wt% at the nominal power of 1200 W, respectively. Such results were almost twice the fibrillation yields achieved in this study for all investigated conditions. This study analyzed the treatment time effect on cellulose isolated from wheat straw. As discussed earlier, treatment times from 6 to 20 min at concentrations of 1 and 2 % showed no significant difference, suggesting that the cellulose isolated from wheat straw required a more intense fibrillation process than the canola straw studied by Huerta et al. (2020b). Additionally, some of the nano-fibrils were attached to bigger fibrils, as shown in the TEM analysis of the dispersions and the SEM analysis of the dried micro/nanopapers. This behavior may have contributed to the fibril's aggregation during centrifugation, explaining the lower fibrillation yields in this study.

4.3.5 Water retention value (WRV_w) of wet dispersions

The WRV_w is a measurement used to assess the fibrillation degree. This value reflects the fibers' ability to hold water, which typically increases due to increased fiber swelling caused by increased external surface area resulting from cellulose external fibrillation through delamination (Gu et al., 2018). Fig. 4.8 shows the WRV_w of bleached solid residue dispersions at the concentrations of 1% and 2% and treated with HIUS at 1200 W for 6 min, 13 min, and 20 min. Samples dispersed with a concentration of 2% and treated with HIUS at 1200 W for 6 min, 13 min, and 20 min showed no significant difference. Samples dispersed with a concentration of 1% and treated with HIUS at 1200 W significantly ($p<0.05$) increased with HIUS treatment time.

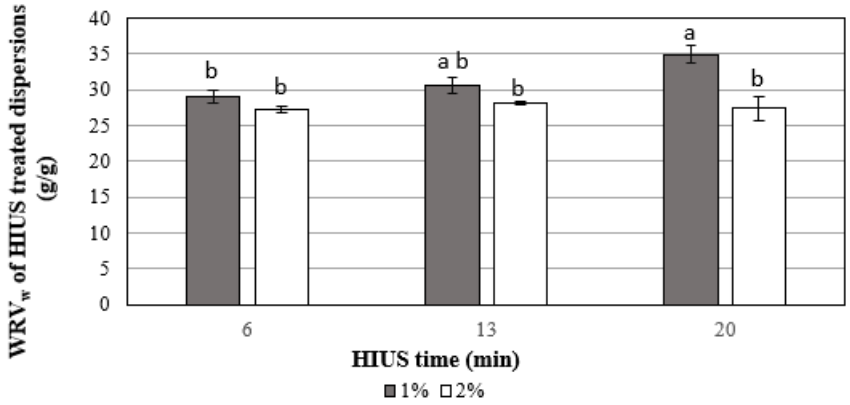

Fig. 4.8. WRV_w of HIUS treated dispersions of bleached solid residue at concentrations of 1% and 2%. HIUS treatments conditions were HIUS at 1200 W for 6, 13, 20 min. [a,b]Different letters on bars of the same color represent significant differences at $p < 0.05$. Data in the appendix section (Table C.3).

The procedure for WRV_w followed in this study was similar to that described by Huerta et al. (2020b), who studied the effect of HIUS treatment on cellulose isolated from canola straw. High lignin samples were treated with ASC for 2 h while the low lignin samples were treated with ASC for 6 h. They reported that the WRV_w for high and low lignin contents

varied from 17.08 ± 1.23 to 33.77 ± 0.88 and 31.72 ± 1.51 to 81.85 ± 1.06, respectively, for all analyzed HIUS conditions. The ranges obtained for high lignin samples by Huerta et al. (2020b) were close to those obtained in this study.

Recently, Redlinger-Pohn et al. (2022) concluded that the chemically modified cellulose was easier to fibrillate than non-modified cellulose due to weaker fibril cohesion. Their results suggested that different levels of H-bonding among the cellulose structure affected the ability of the mechanical treatment to fibrillate cellulose. Thus, it was concluded that the cellulose isolated from wheat straw previously pretreated with 20 % aqueous ethanol and bleached with AHP, as described in this study, presented stronger H-bonding that led to the production of fibres with a wide diameter range from nano to the micro sizes. Additionally, the HIUS treated dispersions presented lower values for fibrillation yield and WRV compared to the results reported for canola straw (Huerta et al., 2020b). Fibrils obtained in this study and by Huerta et al. (2020b) differed in untreated particle size, cellulose straw source, and bleaching treatment. Thus, it would be interesting to study the effect of untreated particle size, cellulose straw source, and bleaching treatment on HIUS fibrillation of cellulose to better understand this promising fibrillation process.

4.3.6 WRV_d and water solubility of stage one dried materials

Fig. 4.9 shows the WRV_d of dried samples dispersed in water at concentrations of 1% and 2% fibrillated with HIUS at 1200 W for 6, 13, 20 min and 720 W for 20 min. At 0.5 min, the dried materials had almost reached the maximum WRV_d, and the WRV_d was considered constant for all samples up to 15 min. All samples treated with HIUS rapidly absorbed water and the WRV_d was stable after 1 min. Samples treated with the same HIUS power and time, but different dispersion concentrations showed no difference except those

treated with HIUS at 720 W for 20 min, where the WRV_d of samples at 2% were significantly ($p<0.05$) higher than those at 1%.

It is suggested in the literature that paper porosity increases the water interactions with cellulosic fibrils. Recently, Saini et al. (2022) studied the conversion of rice straw into paperboard with the addition of a coating of CNF extracted from the rice straw. Strands of rice straw were cut into pieces of 2 to 4 cm in length, soaked in water for ~ 3 h at 140°C, and beated. The paperboard sheets were made with a manual hand sheet former. As for the CNF production, chopped rice straw was further ground, sieved, and extractives removed. The sample underwent chlorite-based bleaching and alkali treatment to remove lignin and hemicelluloses, respectively. Cellulose, hemicellulose, and lignin contents of the final solid residue were not specified. The isolated cellulose was then dispersed in water at the concentration of 0.05%, placed in an ice bath, and treated with a high-speed homogenizer at 12000 rpm for 2 cycles each of 10 min with a 10 min break. Sonication treatment was also employed (12 mm diameter probe at 20 Hz and 600 W for 30 min in an ice bath). The nano-fibril suspension was centrifuged (7000 rpm for 10 min) to remove microfibers. The supernatant was concentrated to 0.83 wt%, and the rice straw paperboard was coated with the CNF suspension with an automatic rod coater. Saini et al. (2022) found that the $Cobb_{60}$ value, which measures water absorption capacity, significantly decreased with the increasing amount of the CNF coating from 0 to 4 g/m^2. Such results were attributed to the reduction of roughness and porosity by filling up pores and decreasing intra-fiber spaces with the addition of CNF, resulting in the decrease of the permeability of water.

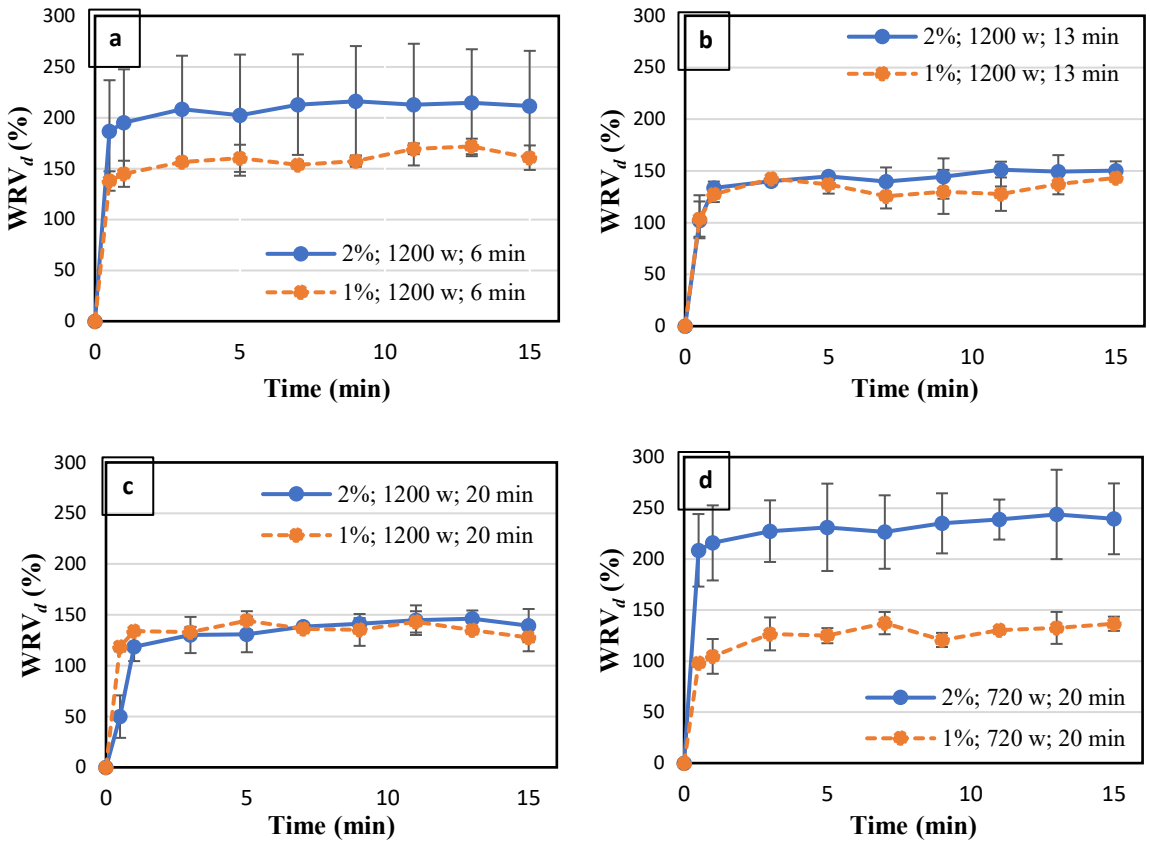

Fig. 4.9. WRV$_d$ of dry solid residues bleached with AHP for 2.5 h dispersed in water at concentrations of 1% and 2% fibrillated with HIUS at 1200 W for (a) 6, (b) 13, (c) 20 min and (d) 720 W for 20 min. Data in the appendix section (Table C.4).

Therefore, the fact that the WRV$_d$ of the sample treated with HIUS at 720 W for 20 min at the concentration of 2% was significantly ($p<0.05$) higher that of the one treated at the same conditions at the concentration of 1 %, was attributed to a lower degree of fibrillation, which achieved fibrils with larger diameter that resulted in micro/nanopapers with higher roughness and porosity. Additionally, the fact that samples treated with HIUS at 720 W for 20 min were the only ones that presented significant difference in terms of cellulose concentration was attributed to a lower power output from the HIUS equipment, which caused lower cavitation effect during the treatment. As known, cavitation causes turbulence in the water media, generating a mixing effect. It was also observed that

dispersions treated with HIUS power of 720 W produced lower mixing effect than 1200 W. Thus, materials prepared at 720 W were not homogeneously fibrillated, especially those prepared at the concentrations of 2%.

Figs. 4.10 show the comparison of the WRV of dried samples dispersed in water at concentrations of 1% fibrillated with HIUS at 1200 W for 6, 13, and 20 min and 720 W for 20 min. Samples treated with HIUS for 6, 13, and 20 min at 1200 W showed no significant difference. These results are congruent with the ones obtained for the fibrillation yield, which indicated no significant difference for HIUS fibrillation at 1200 W for 6, 13, and 20 min at the concentrations of 1 and 2 %. Table 4.1 shows the water solubility of cellulosic materials treated at ambient conditions for 0.5 and 15 min. Such times were selected from the WRV results of the dried samples (Fig. 4.9). At 0.5 min, the WRV showed the highest increase in all the samples while 15 min samples reached constant WRV. Therefore, those were the most representative times from the WRV results. The solubilities of the samples in water confirmed that the change in the weight of the samples during the WRV analysis were attributed only to the water intake, and not due to cellulose fibers re-dispersion in water. The solubility of all samples in water placed in the beaker with 100 mL of water for 0.5 and 15 min at 22°C can be considered negligible (Fig. 4.10e). The solubility behavior was attributed to the aggregation of the fibers caused by the drying process (Nagarajan et al., 2021).

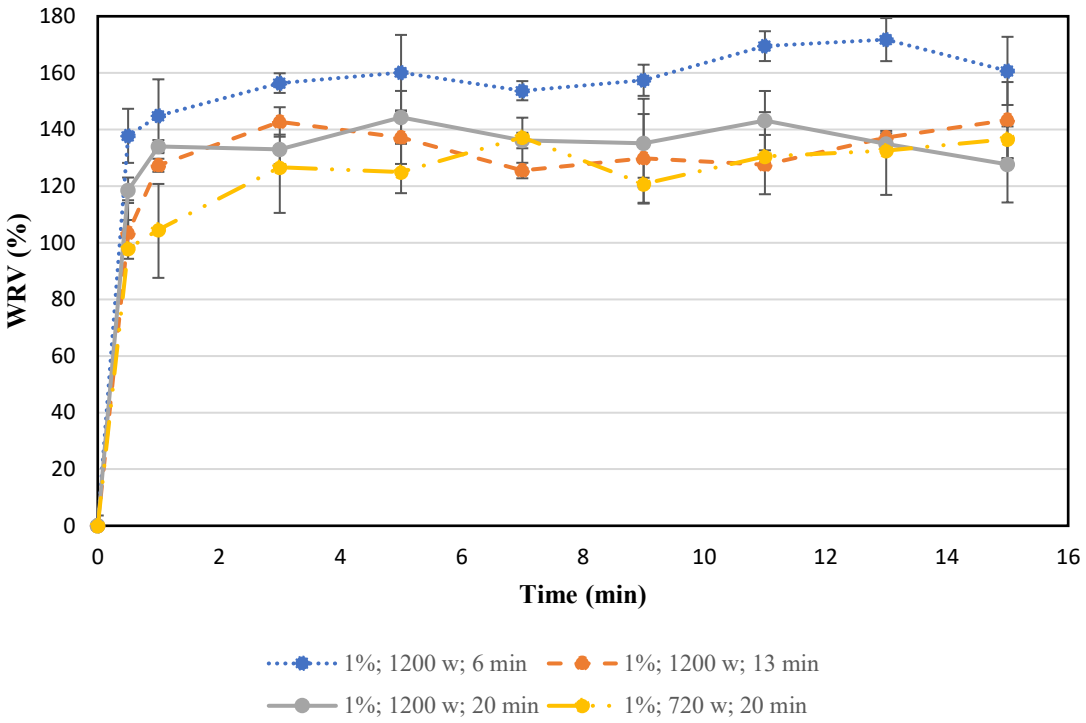

Fig. 4.10. Comparison of WRV of dry solid residues bleached with AHP for 2.5 h dispersed in water at concentrations of 1% fibrillated with HIUS at 1200 W for 6, 13, and 20 min. Data in the appendix section (Table C.5).

Table 4.1 Water solubility at room conditions and different immersion times of cellulosic materials at the concentration of 1% treated at 1200 W for 6, 13, and 20 min**.**

Water solubility (%)		
	Immersion time (min)	
	0.5	15
6 min	Traces	Traces
13 min	Traces	Traces
20 min	Traces	Traces

4.3.7 Evaluation of dried micro/nanopapers with(out) glycerin and calcium carbonate

The HIUS treatment of dispersions at different times (6, 13, 20 min) had no significant effect on the WRV_d and fibrillation yields. Even though WRV_w of 1% bleached solid residue dispersions increased with time, such values did not show a high difference as the dispersions previously reported by Huerta et al., (2020b), who produced CNF from

treated canola straw with similar lignin contents as the ones presented in this study. Thus, the HIUS treatment at 1200 W for 6 min was used for the second stage of analysis for practical matters.

4.3.7.1 Interactions of cellulose, calcium carbonate and glycerol by Fourier-transform infrared spectroscopy (FT-IR)

Fig. 4.11 shows the FT-IR spectra of micro/nanopapers prepared with different ratios of bleached solid residue:calcium carbonate (1:0, 1:0.1, 1:0.2 w/w). The FT-IR spectra peaks observed in the control samples were the typical peaks that represented cellulose-rich residue from lignocellulosic biomass. The hydroxyl groups of polysaccharides and lignin produced a broad band at 3326 cm^{-1} (Huerta et al., 2019). Signals at 2920 and 2848 cm^{-1} were related to the C-H stretch in the methyl and methylene groups of lignin. The absorption band around 2920 cm^{-1} was also related to the C−H stretching vibrations in cellulose and hemicellulose (Liu et al., 2017). The peak near 1600 cm^{-1} was attributed to the C-C aromatic skeletal vibration and C=O stretching in lignin (Huerta et al. 2019). Peaks around 1734 and 1240 cm^{-1} were associated with hemicellulose's carboxylic acid and carbonyl groups of xylan, and the peak around 1367 cm^{-1} was related to lignin's phenolic hydroxyl groups (Huerta et al., 2019). Bands near 1160 cm^{-1} were attributed to the stretching of cellulose and hemicellulose's C−O−C asymmetrical bond, and bands near 1030 and 1000 cm^{-1} were related to C−O, C=C, and C−C−O stretching of cellulose, hemicellulose, and lignin (Aryal et al., 2022). Strong peaks at 1064 and 1030 cm^{-1} indicated C–O stretching at carbons C-3 and C-6, and C–C stretching of the carbohydrate fraction (Liu at al., 2006). Lastly, peaks at 992 and 897 cm^{-1} indicated the C−H glycosidic linkage of cellulose (Liu et al., 2017).

Peaks of samples prepared with 1:0.1 and 1:0.2 w/w cellulose: calcium carbonate showed similar patterns as those observed in the control. Two peaks around 870 and 712 cm^{-1} appeared in the micro/nanopaper with calcium carbonate at the ratio of 1:0.1 w/w, which are typical bands of calcium carbonate, representing the bending's in-plane and out of plane of the CO_3 group (Song et al., 2022). Also, peaks around 1200 and 1490 cm^{-1} in that sample were intensified, which was attributed to a third band of calcium carbonate, representing the stretching vibrations of the CO_3 group at 1400 cm^{-1} (Song et al., 2022). On the other hand, the micro/nanopaper with calcium carbonate at the ratio of 1:0.2 w/w had more intense peaks around 1030 and 3330 cm^{-1} in comparison with the control, which are characteristics of the carbohydrate fraction. As discussed before, peaks at 1030 and 3330 cm^{-1} represented C–O stretching at carbons C-3 and C-6, and C–C stretching of the carbohydrate fraction and the O-H stretch of the hydroxyl groups, respectively. Recently, Sáenz Ezquerro et al. (2023) studied the chemical interactions between cellulose and calcium carbonate nanoparticles. They prepared and characterized a full atomistic model of an amorphous cellulose + calcium carbonate nanocomposite. Amorphous cellulose consisted of the formation of cellulose oligomers with a degree of polymerization of 40. Then, 38 oligomers were randomly added in the simulation cell to form the model of the neat amorphous cellulose matrix. The calcium carbonate nanoparticles were based on the crystalline structure of calcite. As the whole system was simulated under the periodic boundary conditions, it was implicitly comparable to a system with an infinite number of nanoparticles.

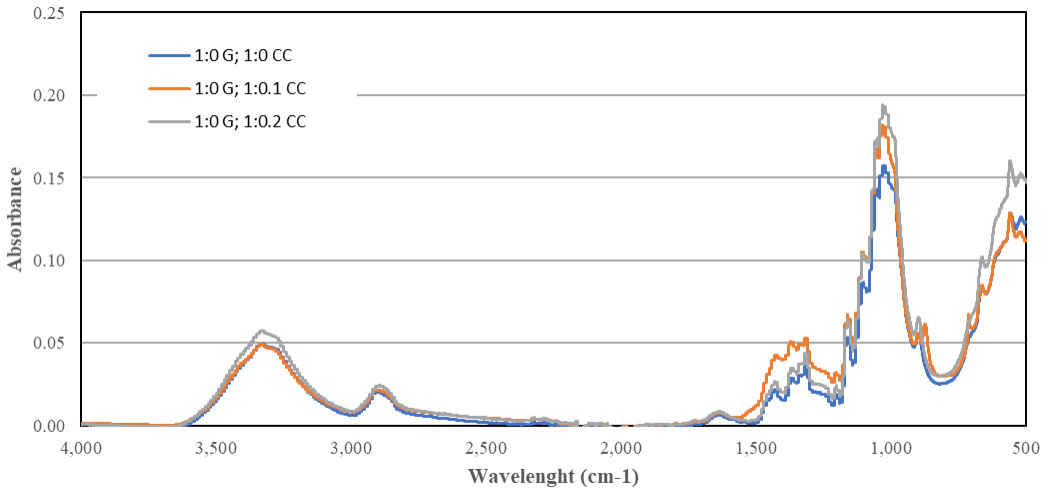

Fig. 4.11. FT-IR of second stage micro/nanopapers without glycerol (G) and with different contents of calcium carbonate (CC).

Sáenz Ezquerro et al. (2023) concluded that cellulose and calcium carbonate interacted via electrostatic attraction between hydroxyl groups and the oxygen on the carbonate ions and calcium ions and oxygen atoms in cellulose. Furthermore, Song et al. (2022) produced a filler for paper making using a mechanical co-refining process. They combined TEMPO-oxidized CNF and precipitated calcium carbonate (PCC) in a ratio of 3:40 w/w, respectively. The FT-IR analysis showed that the hydroxyl peak shifted and broadened, indicating interactions between OH- groups and calcium ion between CNF and PCC. However, they did not mention changes in other CNF peaks. Song et al. (2022) and this study differed as Song et al. (2022) employed TEMPO-oxidized CNF at lower concentrations compared to PCC. Thus, some differences in the FT-IR spectra results could be expected. Therefore, interactions among cellulose and calcium carbonate could explain the higher transmittance levels among the control and the calcium carbonate added micro/nanopapers bands around 1030 and 3330 cm^{-1}. However, the reason for why the micro/nanopaper with

calcium carbonate at the ratio of 1:0.2 w/w did not present the typical peaks for calcium carbonate is unknown at this point. Thus, further investigations are suggested to clarify this behavior.

In addition, Sáenz Ezquerro et al. (2023) investigated the H-bond interactions and torsional angles of amorphous cellulose matrix before and after the addition of calcium carbonate nanoparticles to understand the cellulose nanocomposites' mechanical properties within and beyond the elastic limit via molecular dynamics simulations. Calcium carbonate nanoparticles led to an increase in the rigidity of the composite system due to their electrostatic interactions being more significant than the van der Waals component. The presence of calcium carbonate nanoparticles also resulted in higher values of plastic deformation in the composite compared to the neat cellulose matrix, indicating a decrease in the flexibility of the material under applied force. The higher plastic deformations were attributed to a reduction of the overall H-bond capacity and the disrupted H-bond networks in the cellulose composites caused by the addition of the calcium carbonate nanoparticles. Interestingly, the authors also noticed that the interaction evolution and cellulose conformation during the deformation process remained unaffected by the presence of the nanoparticles (Sáenz Ezquerro et al., 2023).

4.3.7.2 Monolayer moisture content and GAB parameters analysis by sorption isotherms

Fig. 4.12a-d shows the sorption isotherm data for micro/nanopapers made of cellulose isolated from wheat straw pretreated with 20 % aqueous EtOH, bleached with AHP for 2.5 h, and fibrillated with HIUS at 1200 W for 6 min with(out) glycerol and/or calcium carbonate at 22°C. For the second-stage micro/nanopaper formation, the cellulosic fibrils with(out) glycerol and/or calcium carbonate were separated from water using vacuum

filtration, and consequently dried with a convection oven. Such methodology was selected for practical reasons.

The control (without glycerol and calcium carbonate) showed similar values as those reported in the literature for cellulose (Kupczak et al., 2018) and paper (Bedane et al., 2015). Earlier, Kupczak et al. (2018) studied the equilibrium moisture contents of historical paper and cardboard specimens dated to between seventeenth and twentieth centuries as a function of the RH (0-85 %) and determined the GAB model parameters at 24°C. They found that the minimum and maximum values of moisture contents at RH of 25 % were ~ 2.5 and ~5 %, respectively. Those values were achieved by a machine-made paper material sample and paperboard in a bookbinding, respectively. At RH of 80 %, the minimum and maximum values for moistures contents were ~6 and ~13 %, respectively. Additionally, the values for X_m and the parameters C, and k were 4.39 %, 13.3, and 0.72, respectively, for paper materials made of rags, gelatine sized, and 4.66 %, 13.1, and 0.64 for machine-made paper materials.

Bedane et al. (2015) also determined the GAB parameters at 25°C of cellulosic materials, such as bleached kraft paper, TEMPO-oxidized nanofibrillated cellulose, cellulose film from bleached kraft pulp, cotton linter, and microcrystalline film. The values for X_m, C, and k were 4.12-11.93, 2.26-9.63, and 0.53-0.67, respectively. The closest values for the GAB parameter to the ones obtained in this study (X_m = 5.39, K = 0.7, and C = 11.67 for the control), were those obtained for the bleached kraft paper (X_m = 4.12, K = 0.67, and C = 9.62). The lower X_m, C, and K values in comparison with those for the micro/nanopapers prepared in this thesis could be attributed to the higher temperature used by Bedane et al. (2015) (25°C vs 21°C), paper fibre source and composition, and the processes involved in the paper making (Rhim et al., 2009). Bedane et al. (2015) did not provide information about

the fibre source, composition or paper making process of the bleached kraft paper but mentioned that it was donated by Limerick Pulp & Paper at the University of New Brunswick.

When the control was compared with samples without calcium carbonate and glycerol at the ratios of 1:0.1 and 1:0.2 w/w (Fig. 4.12a), it was observed that all the measured Aw points were not significantly ($p<0.05$) different. Similarly, samples with different ratios of glycerol (1:0, 1:0.1, and 1:0.2 w/w based on cellulose) at fixed calcium carbonate concentrations (Fig. 4.12c-d) showed no significant difference. This behavior was attributed to minimal interactions between cellulose and glycerol due to the implementation of the vacuum filtration method to develop the micro/nanopapers, which removed the water media that solubilized the glycerol. It is suggested to produce micro/nanopapers using the solvent-casting method in future studies to better understand the effect of glycerol on the cellulosic materials.

When the control was compared with samples without glycerol and calcium carbonate at the ratios of 1:0.1 and 1:0.2 w/w (Fig. 4.12b), it was observed that all the measured Aw points were not significantly ($p<0.05$) different, except for Aw = 0.78. Therefore, the GAB fitting model was applied to those data sets for parameter analysis. Fig. 4.13 shows the GAB model fitting for micro/nanopapers prepared with different calcium carbonate ratios (1:0, 1:0.1, 1:0.2 w/w) without glycerol. Table 4.2 shows the fitting parameters of the GAB model, respectively. The curves obtained from the GAB model showed R^2 values of 0.97, 0.92, and 0.91 for samples prepared with calcium carbonate at the ratios of 1:0, 1:0.1, and 1:02 w/w, respectively, showing a satisfactory fitting.

Furthermore, the addition of calcium carbonate into the cellulosic micro/nanopapers resulted in the decrease of the X_m value and the increase of C and k values. The reduction on the micro/nanopapers X_m value may indicate a decrease in the number of available binding sites between water molecules and the micro/nanopapers. On the other hand, C and k parameters are related to the differential enthalpy magnitudes in the upper layers and monolayer, and sorbate's pure liquid, respectively (Bedane et al. 2015). Earlier, Rhim et al. (2009) reported accurate values of C and k for biological constituents as 4-40, and 0.7-0.9 (without exceeding 1), respectively. An increase of the C value would indicate stronger interactions of the micro/nanopaper with the upper layers and monolayer of water. The k values close to 1 may suggest that the bulk water has similar behavior to pure liquid (Bedane et al. 2015; Portugal et al., 2010). Thus, the results suggest that the addition of calcium carbonate enhanced the interactions between the micro/nanopaper matrix with the monolayer water and reduced the organization in multilayer water molecules (Quirijns et al., 2005). A more exhaustive study of the micro/nanopaper porosity properties might provide better insights on the effect of the surface properties of the micro/nanopaper with(out) calcium carbonate.

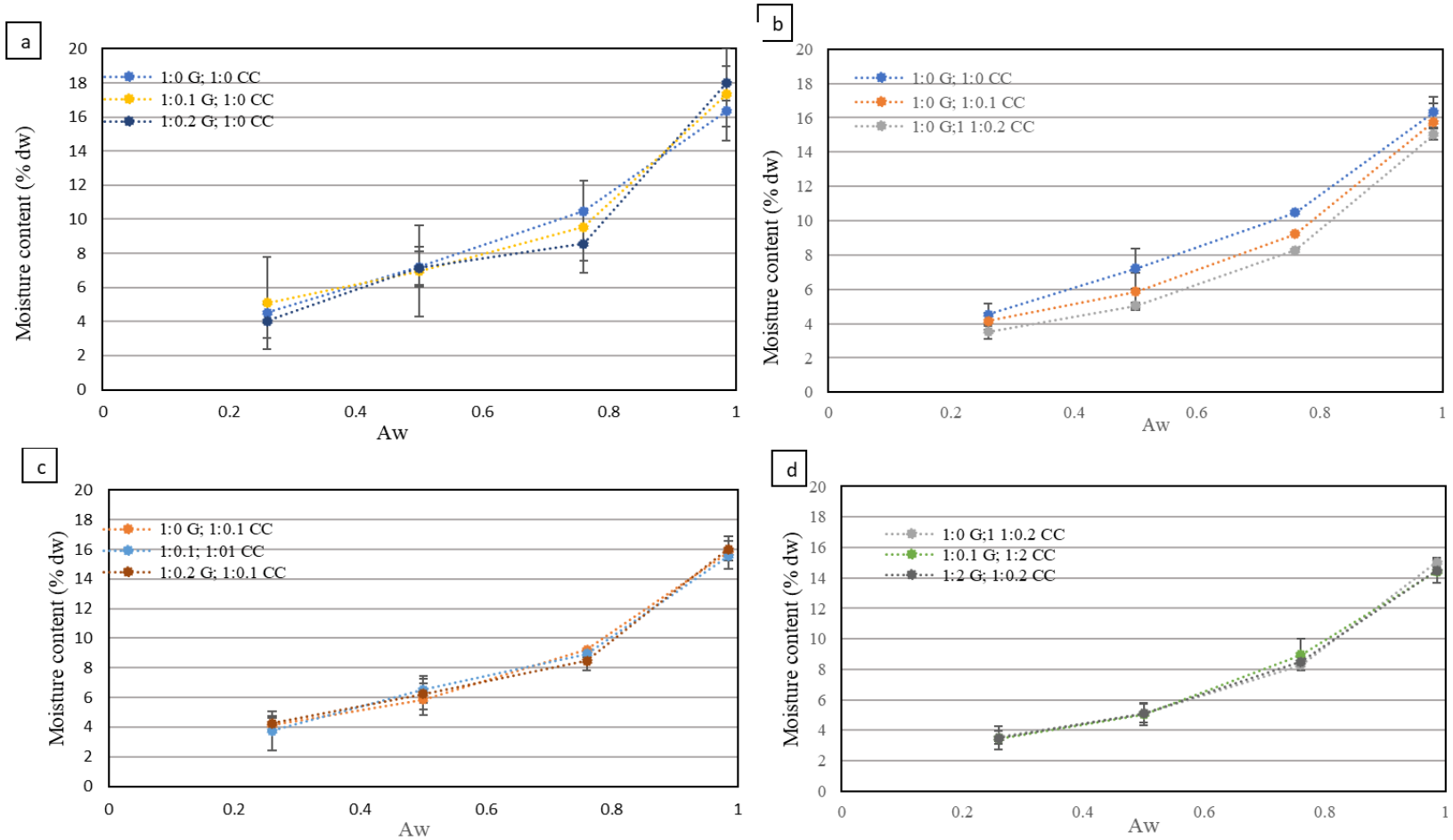

Fig. 4.12. Sorption isotherms for second stage micro/nanopapers prepared with(out) glycerol and/or calcium carbonate at 22°C: (a) different ratios of glycerol on micro/nanopapers without calcium carbonate, (b) different ratios calcium carbonate on micro/nanopapers without glycerol, (c) different ratios of glycerol on micro/nanopapers at the ratio of 1:0.1 w/w calcium carbonate, (d) different ratios of glycerol on micro/nanopapers with 1:0.2 w/w calcium carbonate. Ratios are expressed as w/w based on cellulose. Data in the appendix section (Table C.6 and Table C.7).

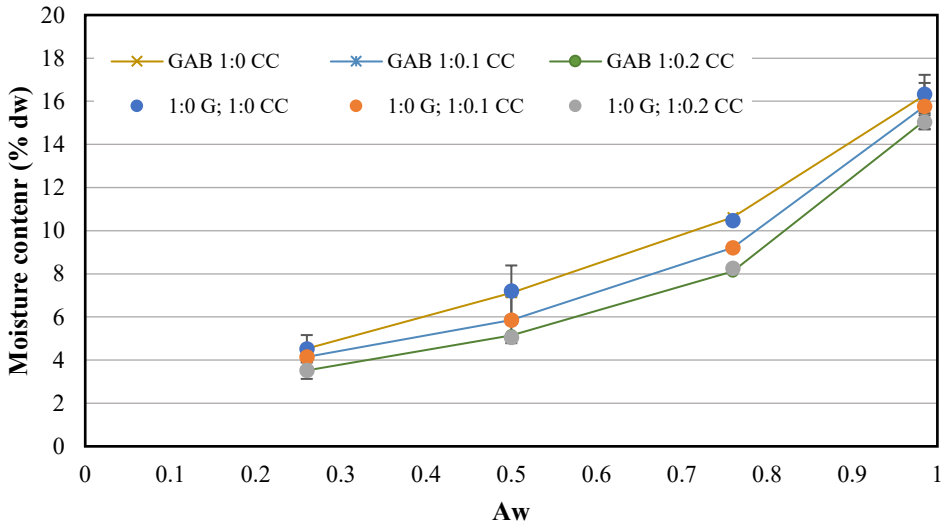

Fig. 4.13. GAB model fitting for second stage micro/nanopapers prepared with calcium carbonate at different concentrations. Data in the appendix section (Table C.8).

Table 4.2. Calculated parameters for GAB fitting.

	1:0 G; 1:0 CC	1:0 G; 1:0.1 CC	1:0 G; 1:0.20 CC
X_m	5.39	3.79	3.22
k	0.70	0.78	0.81
C	11.67	34.67	31.59
R^2	0.97	0.92	0.91

X_m monolayer moisture content, C: constant related to thermal effects, and k: GAB constant related to the properties of multilayer water molecules.

4.4 Conclusions

To the best of my knowledge, this is the first time for the production of micro/nanopaper via HIUS with cellulose isolated from wheat straw using pressurized 20 % EtOH and AHP. The cellulose content after pressurized 20% EtOH treatment and bleaching treatments (ASC 2 h and AHP 2.5 h) increased more than twice compared to the untreated wheat straw. Hydrolyzed wheat straw treated with AHP for 1 and 2 h showed no significantly ($p<0.05$) different lignin content. Thus, AHP for 2.5 h was used for the bleaching treatment

for the production of cellulose-rich solid residue used for further cellulosic materials development.

Further dispersion of the bleached solid residue at 1% and HIUS treatment at 1200 W for 6, 13, and 20 min resulted in micro- and nanofibers with a wide range of diameter sizes. The average diameters of the nanofibrils (<1 μm) ranged from 21 nm to 30 nm whereas the microfibril diameters (>1 μm) were in the range of 2 μm to 23 μm. Additionally, the fibrillation yield and WRV_d analysis showed no significant difference among cellulosic fibrils dispersed at the concentrations of 1 and 2 % treated at 1200 W for 6, 13, and 20 min. The sorption isotherm analysis results implied that the addition of calcium carbonate in the cellulosic micro/nanopapers produced a significant change in the water interactions with the cellulosic matrix. Finally, the FT-IR spectra suggested interactions among the calcium carbonate molecules and hydroxyl and oxygen-containing groups in the cellulose structure, which may have influenced the equilibrium moisture content of the micro/nanopaper.

Chapter 5. Conclusions and recommendations

5.1 Conclusions

The increase in the demand for food containers and convenience foods, the growing concerns related to petroplastics use, and the consequent single use plastic ban in Canada resulted in the increased interest for petroplastics replacement with renewable and biodegradable materials like cellulose. Thus, the main objective of this thesis was to study and develop sustainable micro/nanopapers using cellulose isolated from wheat straw, an abundant and low-cost by-product from the agricultural sector.

5.1.1 Hydrolysis of wheat straw

The first objective in Chapter 3 of this thesis evaluated the effect of pressurized EtOH and water mixtures at different concentrations (0 to 100 % EtOH) and optimized conditions of 180°C, 50 bar, and 5 mL/min for cellulose isolation from wheat straw. After treating milled wheat straw with SCW and pressurized water + EtOH treatments milled, solid residues with the highest cellulose content and the highest hemicellulose removal were obtained. Notably, 20% pressurized EtOH treatment yielded higher lignin removal than SCW, indicating a potential for micro/nanopaper production.

The lower pH values and the higher carbohydrate contents of the hydrolysates produced from the SCW and pressurised 20% EtOH treatments indicated higher hemicellulose depolymerization degree than pressurized 60 and 100% EtOH treatments. Additionally, samples treated with SCW and pressurized aqueous EtOH up to 60% EtOH showed the highest the phenolic content reported as gallic acid equivalents (GAE) with no significant difference. Those results suggested that SCW and pressurised 20% EtOH have

potential to produce valuable co-products such as sugars and phenolic compounds along with the obtention of cellulose-enriched solid residues.

5.1.2 Micro/nanopaper formation

The second objective in Chapter 4 of this thesis focused on further cellulose purification using bleaching treatments, including ASC and AHP at different times, followed by cellulose fibrillation to form micro/nanopaper with potential for food packaging applications. The effects of the addition of glycerol and calcium carbonate on the formation of micro/nanopapers were also studied.

After pressurized 20% EtOH and ASC for 2 h and AHP for 2.5 h treatments, the solid residues had the highest cellulose contents (more than twice compared to the untreated feed) and the lowest lignin contents. The AHP treatment for 2.5 h was selected for micro/nanopapers development due to the lower environmental impact compared to the ASC treatment.

The bleached solid residue was then fibrillated using HIUS at the concentration of 1% and at 1200 W for 6, 13, and 20 min, resulting in micro/nanofibers production. The average fibril diameters in the nano-range varied from 21 nm to 30 nm while the observed fibril diameters in the micro-range varied from 2 μm to 23 μm. As the fibrillation yield, and WRV_d analysis of fibrillated cellulose dispersed at 1% and 2% concentration treated at 1200 W for 6, 13, and 20 min showed no significant difference, the HIUS treatment at 1200 W for 6 min was chosen for further production of the micro/nanomaterial formation for practical reasons.

Finally, glycerol and calcium carbonate were added to the fibrillated dispersions, stirred for 30 min, and vacuum filtered to remove the liquid phase. The solid phase was removed from the vacuum system and dried in a convection oven to form micro/nanopapers with(out) glycerol and calcium carbonate. The sorption isotherm analysis indicated that the glycerol did not cause any significant change, ascribed to the implementation of the vacuum filtration method to develop the micro/nanopapers, which removed the water media that solubilized the glycerol. On the other hand, the addition of calcium carbonate caused a significant change in the cellulosic material interactions with water, which was also reflected by the chemical properties and interactions analysis.

In summary, the approach involving pressurized 20% EtOH hydrolysis, followed by AHP bleaching and HIUS fibrillation was a promising method to develop micro/nanopapers, with potential food packaging applications. This thesis represents an advance in the understanding of cellulose isolation from Alberta' wheat straw, an abundant agricultural waste, using green solvents such as pressurized water and ethanol and a more eco-friendly alternative to ASC bleaching. The study also provides information about the formation of other valuable co-products, such as phenolics, carbohydrates, and minerals, representing a further step for the achievement of a circular economy in the wheat production and processing industry and the generation of sustainable goods for human use. Furthermore, this thesis also contributed to the understanding of the HIUS fibrillation of the cellulose isolated from wheat straw, the further development of micro/nanopapers, and the effect of the addition of calcium carbonate in those micro/nanopapers. The findings will provide useful information to the Canadian agri-food industry for the development and usage of sustainable

cellulose-based food packaging, contributing to the mitigation of petroplastics waste and providing an alternative for single-use plastics made of petroplastics.

5.2 Recommendations

5.2.1 Hydrolysis of wheat straw

- The degree of polymerization of carbohydrates in the hydrolysates and the degree of hydrolysis of the SCW and pressurized water + ethanol can be further analyzed using HPLC to characterize the carbohydrates and phenolic compounds coproducts sourced from the hydrolysates.
- The kinetics data of the hydrolysis treatment using pressurized 20% ethanol at 180°C, 50 bar, and 5 mL/min can be analyzed for cellulose enrichment to provide the optimal time for processing.
- The identification of minerals in the solid residue and hydrolysates after the pressurized fluid treatment can be performed to further understand the effect of the SCW and the 20 % EtOH treatments on the wheat straw mineral content, which may also be considered as a co-product obtained from the hydrolysis treatments.
- Individual phenolic compounds in the hydrolysates can be determined using HPLC to provide more accurate information about the effect of the SCW and pressurized water + ethanol treatment at different concentrations obtained from wheat straw.
- The ion formation behavior in pressurized water + ethanol reaction media was theorized based on the contributions of previous research (Sarkar et al., 2014). However, a study of the ion formation in the pressurized 20% EtOH reaction media at the conditions studied in this thesis can be performed to better understand the effect of the pressurized 20% EtOH treatment on the wheat straw components.

- Scale-up of the wheat straw hydrolysis process can be implemented to increase the production of solid residue to further produce fibrillated cellulose and implement its use in various applications in our research group and industry.

5.2.2 Micro/nanomaterial formation

- A more rigorous study of the kinetics for cellulose isolation sourced from wheat straw with AHP bleaching treatment at different times used in this thesis (e.g., 2-4 h) can be performed for the optimization of the bleaching process with AHP. Additionally, the cellulose isolated after those times can be HIUS fibrillated to study the effect of the bleaching treatment time on the nanofiber production.
- HIUS treatment of isolated cellulose in this thesis achieved a lower fibrillation degree than in a previous study in our research group, even though similar hydrolysis and fibrillation treatments were used (Huerta et al., 2020b). To understand the different results, further studies on the effect of different straw feeds, bleaching treatments and time (ASC 6 h vs AHP 2.5 h) and cellulose particle size on the isolated cellulose fibrillation are suggested.
- No effect of the glycerol addition on the micro/nanomaterials was observed due to the solubilization of glycerol on the dispersion water and their further removal during the vacuum filtration process in the second stage of Chapter 4. Thus, the formation of micro/nanomaterials added with calcium carbonate and glycerol with the solvent casting method can be performed to elucidate the effect of glycerol on the cellulosic matrix.
- The identification of other strategies to increase the fibrillation yield of cellulose isolated from wheat straw is encouraged. Some suggestions could be the

implementation of an additional treatment before HIUS, which could be chemical (e.g., acid hydrolysis), mechanical (e.g., beating) or enzymatic (e.g., endoglucanases) treatment.

- Also, the implementation of strategies to reduce the hydrophilicity of the micro/nanomaterials is needed to expand the applications of such sustainable materials. Some examples could be the combination of cellulosic fibers with hydrophobic polymers like PLA and the chemical modification of cellulose with fatty acids.

- The further measurement of the mechanical properties of the micro/nanopapers with different equilibrium moisture contents due to the exposure at different RH is also encouraged to provide valuable insights on the micro/nanopapers applications as food containers.

- Scale-up of the HIUS fibrillation process can be implemented to increase the production of fibrillated cellulose and implement its use in various applications in our research group and industry.

References

Abdelmoez, W., Nage, S. M., Bastawess, A., Ihab, A., & Yoshida, H. (2014). Subcritical water technology for wheat straw hydrolysis to produce value added products. *Journal of Cleaner Production*, 70, 68-77. https://doi.org/10.1016/j.jclepro.2014.02.011

Abral, H., Ariksa, J., Mahardika, M., Handayani, D., Aminah, I., Sandrawati, N., & Ilyas, R. A. (2020). Transparent and antimicrobial cellulose film from ginger nanofiber. *Food Hydrocolloids*, 98,105266. https://doi.org/10.1016/j.foodhyd.2019.105266

Ajandouz, E.H., & Puigserver, A. (1999). Nonenzymatic browning reaction of essential amino acids: effect of pH on caramelization and Maillard reaction kinetics. *Journal of Agricultural and Food Chemistry*, 47, 1786-1793. https://doi.org/10.1021/jf980928z

Al Omari, M. M. H., Rashid, I. S., Qinna, N. A., Jaber, A. M., & Badwan, A. A. (2016). Calcium carbonate. *Profiles of drug substances, excipients and related methodology*, 41, 31-132. https://doi.org/10.1016/bs.podrm.2015.11.003

Alemdar, A., & Sain, M. (2008). Isolation and characterization of nanofibers from agricultural residues–Wheat straw and soy hulls. *Bioresource Technology*, 99(6), 1664-1671. https://doi.org/10.1016/j.biortech.2007.04.029

Alle, M., Bandi, R., Lee, S., & Kim, J. (2020). Chapter 3. Recent trends in isolation of cellulose nanocrystals and nanofibrils from various forest wood and nonwood products and their application. In *Nanomaterials for Agriculture and Forestry Applications*. Elsevier Science. ISBN: 978-0-12-817852-2. https://doi.org/10.1016/B978-0-12-817852-2.00003-2

Appel, H. M., Govenor, H. L., D'ascenzo, M., Siska, E., & Schultz, J. C. (2001). Limitations of Folin assays of foliar phenolics in ecological studies. *Journal of Chemical Ecology*, 27(4), 761-778. https://doi.org/10.1023/a:1010306103643

Aryal, G. M., Kandel, K. P., Bhattarai, R. K., Giri, B., Adhikari, M., Ware, A., & Neupane, B. B. (2022). Material properties of traditional handmade paper samples fabricated from cellulosic fiber of lokta bushes. *ACS Omega*, 7(36), 32717-32726. https://doi.org/10.1021/acsomega.2c04398

Balasubramaniam, S. L., Patel, A. S., & Nayak, B. (2020). Surface modification of cellulose nanofiber film with fatty acids for developing renewable hydrophobic food packaging. *Food Packaging and Shelf Life*, 26, 100587. https://doi.org/10.1016/j.fpsl.2020.100587

Barbash, V. A., Yaschenko, O. V., & Shniruk, O. M. (2017). Preparation and properties of nanocellulose from organosolv straw pulp. *Nanoscale Research Letters*, 12, 1-8. https://doi.org/10.1186/s11671-017-2001-4

Baruah, J., Deka, R. C., & Kalita, E. (2020). Greener production of microcrystalline cellulose (MCC) from Saccharum spontaneum (Kans grass): Statistical optimization. *International Journal of Biological Macromolecules*, 154, 672-682. https://doi.org/10.1016/j.ijbiomac.2020.03.158

Bedane, A. H., Eić, M., Farmahini-Farahani, M., & Xiao, H. (2015). Water vapor transport properties of regenerated cellulose and nanofibrillated cellulose films. *Journal of Membrane Science*, 493, 46-57. https://doi.org/10.1016/j.memsci.2015.06.009

Bian, H., Gao, Y., Luo, J., Jiao, L., Wu, W., Fang, G., & Dai, H. (2019). Lignocellulosic nanofibrils produced using wheat straw and their pulping solid residue: From agricultural waste to cellulose nanomaterials. *Waste Management*, 91, 1-8. https://doi.org/10.1016/j.wasman.2019.04.052

Bian, H., Gao, Y., Yang, Y., Fang, G., & Dai, H. (2018). Improving cellulose nanofibrillation of waste wheat straw using the combined methods of prewashing, p-toluenesulfonic acid hydrolysis, disk grinding, and endoglucanase post-treatment. *Bioresource Technology*, 256, 321-327. https://doi.org/10.1016/j.biortech.2018.02.038

Brunner, G. (2014). Chapter 8. Processing of biomass with hydrothermal and supercritical water. In *Supercritical Fluid Science and Technology* (Vol. 5, pp. 395-509). Elsevier Science. ISBN:9780080931302, 0080931308. https://doi.org/10.1016/B978-0-444-59413-6.00008-X

Budynski, S. (2020). Straw manufacturing in Alberta (pp. 3-15). Alberta Agriculture and Forestry. ISBN 978-1-4601-4685-9

Caballero, B., Finglas, P., & Toldrá, F. (2015). *Encyclopedia of food and health*. Oxford, UK; Academic Press. ISBN 978-0-12-384953-3.

Cachon, R., Girardon, P., & Voilley, A. (Eds.). (2019). Gases in agro-food processes. Cambridge, MA, USA; Academic Press. IBSN: 978-o-12-812465-9

Chen, J., Wang, X., Zhang, B., Yang, Y., Song, Y., Zhang, F., Liu, B., Zhou, Y.m Yi, Y., Shan, Y., & Lü, X. (2021). Integrating enzymatic hydrolysis into subcritical water pretreatment optimization for bioethanol production from wheat straw. *Science of the Total Environment*, 770, 145321. https://doi.org/10.1016/j.scitotenv.2021.145321

Chen, W., Yu, H., Liu, Y., Hai, Y., Zhang, M., & Chen, P. (2011). Isolation and characterization of cellulose nanofibers from four plant cellulose fibers using a chemical-ultrasonic process. *Cellulose*, 18, 433-442. http://dx.doi.org/10.1007/s10570-011-9497-z

Cherubini, F., & Ulgiati, S. (2010). Crop residues as raw materials for biorefinery systems–A LCA case study. *Applied Energy*, 87(1), 47-57. https://doi.org/10.1016/j.apenergy.2009.08.024

Ciftci, D., & Saldaña, M. D. (2015). Hydrolysis of sweet blue lupin hull using subcritical water technology. *Bioresource Technology*, 194, 75-82. https://doi.org/10.1016/j.biortech.2015.06.146

Ciftci, D., Flores, R. A., & Saldaña, M. D. (2018). Cellulose fiber isolation and characterization from sweet blue lupin hull and canola straw. *Journal of Polymers and the Environment*, 26, 2773-2781. https://doi.org/10.1007/s10924-017-1164-5

Ciftci, D., Ubeyitogullari, A., Huerta, R. R., Ciftci, O. N., Flores, R. A., & Saldaña, M. D. (2017). Lupin hull cellulose nanofiber aerogel preparation by supercritical CO2 and freeze drying. *The Journal of Supercritical Fluids*, 127, 137-145. http://dx.doi.org/10.1016/j.supflu.2017.04.002

Clark, M. (Ed.). (2011). Chapter 3. Pe-treatment and preparation of textile materials prior to dyening. In *Handbook of textile and industrial dyeing: principles, processes and types of dyes*. Elsevier. ISBN: 978-1-84569-695-5

Cocero, M. J., Cabeza, A., Abad, N., Adamovic, T., Vaquerizo, L., Martinez, C. M., & Pazo-Cepeda, M. V. (2018). Understanding biomass fractionation in subcritical & supercritical water. *The Journal of Supercritical Fluids*, 133, 550-565. https://doi.org/10.1016/j.supflu.2017.08.012

Collins, S. R., Wellner, N., Martinez Bordonado, I., Harper, A. L., Miller, C. N., Bancroft, I., & Waldron, K. W. (2014). Variation in the chemical composition of wheat straw: the role of tissue ratio and composition. *Biotechnology for Biofuels*, 7, 1-14. http://dx.doi.org/10.1186/s13068-014-0121-y

Czaikoski, A., da Cunha, R. L., & Menegalli, F. C. (2020). Rheological behavior of cellulose nanofibers from cassava peel obtained by combination of chemical and physical processes. *Carbohydrate Polymers*, 248, 116744. https://doi.org/10.1016/j.carbpol.2020.116744

de Oliveira, M. B., dos Santos, M. S., Pogorzelski, E. S., de Souza, V. L., Pfeifenberg, R., Vieira, J., & Tres, M. V. (2022). Potential of canola feedstocks for fermentable sugars production by subcritical water hydrolysis. *Biomass and Bioenergy*, 162, 106505. https://doi.org/10.1016/j.biombioe.2022.106505

Debnath, B., Haldar, D., & Purkait, M. K. (2021). A critical review on the techniques used for the synthesis and applications of crystalline cellulose derived from agricultural wastes and forest residues. *Carbohydrate Polymers*, 273, 118537. https://doi.org/10.1016/j.carbpol.2021.118537

del Río, J. C., Prinsen, P., & Gutiérrez, A. (2013). A comprehensive characterization of lipids in wheat straw. *Journal of Agricultural and Food Chemistry*, 61(8), 1904-1913. https://doi.org/10.1021/jf304252m

Demirbaş, A. (1997). Calculation of higher heating values of biomass fuels. *Fuel*, 76(5), 431-434. https://doi.org/10.1016/S0016-2361(97)85520-2

Deswarte, F. E., Clark, J. H., Hardy, J. J., & Rose, P. M. (2006). The fractionation of valuable wax products from wheat straw using CO_2. *Green Chemistry*, 8(1), 39-42. https://doi.org/10.1039/B514978A

Dubois, M., Gilles, K. A., Hamilton, J. K., Rebers, P. T., & Smith, F. (1956). Colorimetric method for determination of sugars and related substances. *Analytical Chemistry*, 28(3), 350-356. DOI: 10.1021/ac60111a017

Duguid, K. B., Montross, M. D., Radtke, C. W., Crofcheck, C. L., Shearer, S. A., & Hoskinson, R. L. (2007). Screening for sugar and ethanol processing characteristics from anatomical fractions of wheat stover. *Biomass and Bioenergy*, 31(8), 585-592. https://doi.org/10.1016/j.biombioe.2007.03.002

Dumitriu, S. (2004). Polysaccharides: structural diversity and functional versatility. Boca Raton, FL, USA; CRC press. International Standard Book Number-13: 978-1-4200-3082-2

Espinosa, E., Rol, F., Bras, J., & Rodríguez, A. (2019). Production of lignocellulose nanofibers from wheat straw by different fibrillation methods. Comparison of its viability in cardboard recycling process. *Journal of Cleaner Production*, 239, 118083. https://doi.org/10.1016/j.jclepro.2019.118083

Espinosa, E., Tarrés, Q., Delgado-Aguilar, M., González, I., Mutjé, P., & Rodríguez, A. (2016). Suitability of wheat straw semichemical pulp for the fabrication of lignocellulosic nanofibres and their application to papermaking slurries. *Cellulose*, 23, 837-852. https://doi.org/10.1007/s10570-015-0807-8

Ezati, P., Rhim, J. W., Moradi, M., Tajik, H., & Molaei, R. (2020). CMC and CNF-based alizarin incorporated reversible pH-responsive color indicator films. *Carbohydrate Polymers*, 246, 116614. https://doi.org/10.1016/j.carbpol.2020.116614

Fang, J. M., Sun, R. C., Salisbury, D., Fowler, P., & Tomkinson, J. (1999). Comparative study of hemicelluloses from wheat straw by alkali and hydrogen peroxide extractions. *Polymer Degradation and Stability*, 66(3), 423-432. https://doi.org/10.1016/S0141-3910(99)00095-6

FAO. (2021). World Food and Agriculture - Statistical Yearbook 2021. Rome. Accessed on August 17th, 2022 in: https://www.fao.org/documents/card/en/c/cb4477en/

FAOSTAT. (2022). Crops and livestock products. Accessed on August 17th, 2022 in: https://www.fao.org/faostat/en/#data/QCL

FDA. (2023a). Code of Federal Regulations. Accessed on July 21st, 2023, on: https://www.ecfr.gov/current/title-21/chapter-I/subchapter-B/part-184

FDA. (2023b). Code of Federal Regulations. Accessed on July 24th, 2023 on: https://www.ecfr.gov/current/title-21/chapter-I/subchapter-B/part-184

Fu, D., & Mazza, G. (2011). Optimization of processing conditions for the pretreatment of wheat straw using aqueous ionic liquid. *Bioresource Technology*, 102(17), 8003-8010. https://doi.org/10.1016/j.biortech.2011.06.023

García, R., Pizarro, C., Lavín, A. G., & Bueno, J. L. (2014). Spanish biofuels heating value estimation. Part II: Proximate analysis data. *Fuel*, 117, 1139-1147. https://doi.org/10.1016/j.fuel.2013.08.049

Garrido-Romero, M., Aguado, R., Moral, A., Brindley, C., & Ballesteros, M. (2022). From traditional paper to nanocomposite films: Analysis of global research into cellulose for food packaging. *Food Packaging and Shelf Life*, 31, 100788. https://doi.org/10.1016/j.fpsl.2021.100788

Gill, R.A. (1995). Fillers for papermaking. In: Au, C.O., Thorn, I. (eds) *Applications of Wet-End Paper Chemistry*. Springer, Dordrecht. https://doi.org/10.1007/978-94-017-0756-5_4

Government of Canada, (2022). Area, Yield, and Production of Canadian Principal Field Crops Report. Accessed on August 17th 2022 in: https://agriculture.canada.ca/en/market-information-system/rp/index-eng.cfm?action=pR&r=243&pdctc

Government of Canada. (2023). Single-use Plastics Prohibition Regulations – Overview. Accessed on March 27, 2023, on: https://www.canada.ca/en/environment-climate-change/services/managing-reducing-waste/reduce-plastic-waste/single-use-plastic-overview.html

Grandviewresearch (2021). Food Packaging Market Size, Share & Trends Analysis Report By Type (Rigid, Semi-Rigid, Flexible), By Material (Paper, Plastics), By Application (Bakery & Confectionery) By Region, And Segment Forecasts, 2023 – 2030. Accessed on June 21, 2023, on: https://www.grandviewresearch.com/industry-analysis/food-packaging-market

Gu, F., Wang, W., Cai, Z., Xue, F., Jin, Y., & Zhu, J. Y. (2018). Water retention value for characterizing fibrillation degree of cellulosic fibers at micro and nanometer scales. *Cellulose*, 25, 2861-2871. https://doi.org/10.1007/s10570-018-1765-8

Hafez, I., Amini, E., & Tajvidi, M. (2020). The synergy between cellulose nanofibrils and calcium carbonate in a hybrid composite system. *Cellulose*, 27, 3773-3787. https://doi.org/10.1007/s10570-020-03032-w

Hahladakis, J. N., & Iacovidou, E. (2018). Closing the loop on plastic packaging materials: What is quality and how does it affect their circularity? *Science of the Total Environment*, 630, 1394-1400. https://doi.org/10.1016/j.scitotenv.2018.02.330

Hassan, E. A., Hassan, M. L., Abou-Zeid, R. E., & El-Wakil, N. A. (2016). Novel nanofibrillated cellulose/chitosan nanoparticles nanocomposites films and their use for paper coating. *Industrial Crops and Products*, 93, 219-226. https://doi.org/10.1016/j.indcrop.2015.12.006

He, M., Cho, B. U., & Won, J. M. (2016). Effect of precipitated calcium carbonate—cellulose nanofibrils composite filler on paper properties. *Carbohydrate Polymers*, 136, 820-825. https://doi.org/10.1016/j.carbpol.2015.09.069

Hossain, R., Tajvidi, M., Bousfield, D., & Gardner, D. J. (2021). Multi-layer oil-resistant food serving containers made using cellulose nanofiber coated wood flour composites. *Carbohydrate Polymers*, 267, 118221. https://doi.org/10.1016/j.carbpol.2021.118221

Hu, X., Shen, Y., Zhang, H., Xia, J., Kong, F., & Zhang, W. H. (2022). Insight into the effect of calcium carbonate filler on the dewatering performance of simulated pulp & paper mill sludge. *Journal of Environmental Chemical Engineering*, 10(6), 108863. https://doi.org/10.1016/j.jece.2022.108863

Huang, C., Lai, C., Wu, X., Huang, Y., He, J., Huang, C., & Yong, Q. (2017). An integrated process to produce bio-ethanol and xylooligosaccharides rich in xylobiose and xylotriose from high ash content waste wheat straw. *Bioresource Technology*, 241, 228-235. https://doi.org/10.1016/j.biortech.2017.05.109

Huerta, R. R., & Saldaña, M. D. A. (2018a). Biorefining of canola straw using pressurized aqueous ethanol: nanosized cellulose. *Proceedings of Supercritical Fluids,* 8pp, France.

Huerta, R. R., & Saldaña, M. D. (2018b). Pressurized fluid treatment of barley and canola straws to obtain carbohydrates and phenolics. *The Journal of Supercritical Fluids*, 141, 12-20. https://doi.org/10.1016/j.supflu.2017.11.029

Huerta, R. R., & Saldana, M. D. (2019). Sequential treatment with pressurized fluid processing and ultrasonication for biorefinery of canola straw towards lignocellulosic nanofiber production. *Industrial Crops and Products*, 139, 111521. https://doi.org/10.1016/j.indcrop.2019.111521

Huerta, R. R., Silva, E. K., El-Bialy, T., & Saldaña, M. D. (2020a). Clove essential oil emulsion-filled cellulose nanofiber hydrogel produced by high-intensity ultrasound technology for tissue engineering applications. *Ultrasonics Sonochemistry*, 64, 104845. https://doi.org/10.1016/j.ultsonch.2019.104845.

Huerta, R. R., Silva, E. K., Ekaette, I., El-Bialy, T., & Saldana, M. D. (2020b). High-intensity ultrasound-assisted formation of cellulose nanofiber scaffold with low and high lignin content and their cytocompatibility with gingival fibroblast cells. *Ultrasonics Sonochemistry*, 64, 104759. https://doi.org/10.1016/j.ultsonch.2019.104759

Huerta, R. (2020c). Nanofiber production from agricultural straw biomass using pressurized fluids and ultrasound processing for tissue engineering scaffolds. [Doctoral thesis, University of Alberta] https://doi.org/10.7939/r3-tt6y-y033

Jamshidian, M., Tehrany, E. A., Imran, M., Jacquot, M., & Desobry, S. (2010). Poly-Lactic Acid: Production, applications, nanocomposites, and release studies. *Comprehensive Reviews in Food Science and Food Safety*, 9(5), 552–571. https://doi.org/10.1111/j.1541-4337.2010.00126.x

Jiang, Y., Liu, X., Yang, Q., Song, X., Qin, C., Wang, S., & Li, K. (2018). Effects of residual lignin on mechanical defibrillation process of cellulosic fiber for producing lignocellulose nanofibrils. *Cellulose,* 25, 6479-6494. https://doi.org/10.1007/s10570-018-2042-6

Fan, M., & Fu, F. (Eds.). (2016). Advanced high strength natural fibre composites in construction. Cambridge, UK; Woodhead Publishing. ISBN:9780081004302, 0081004303

Kang, X., Zhang, Y., Li, L., Sun, Y., Kong, X., & Yuan, Z. (2020). Enhanced methane production from anaerobic digestion of hybrid Pennisetum by selectively removing lignin with sodium chlorite. *Bioresource Technology*, 295, 122289. https://doi.org/10.1016/j.biortech.2019.122289

Kim, S. Y., Seo, Y. B., & Han, J. S. (2022). Effect of calendering on the properties of paper containing flexible calcium carbonate with a cellulose nanofibril core. *ACS Omega*, 7(39), 35305-35315. https://doi.org/10.1021/acsomega.2c04967

Kruželák, J., Hložeková, K., Kvasničáková, A., Džuganová, M., Chodák, I., & Hudec, I. (2023). Application of plasticizer glycerol in lignosulfonate-filled rubber compounds based on SBR and NBR. *Materials*, 16(2), 635. https://doi.org/10.3390/ma16020635

Kuan, C. Y., Yuen, K. H., Bhat, R., & Liong, M. T. (2011). Physicochemical characterization of alkali-treated fractions from corncob and wheat straw and the production of nanofibres. *Food Research International*, 44(9), 2822-2829. https://doi.org/10.1016/j.foodres.2011.06.023

Kupczak, A., Bratasz, Ł., Kryściak-Czerwenka, J., & Kozłowski, R. (2018). Moisture sorption and diffusion in historical cellulose-based materials. *Cellulose*, 25, 2873-2884. https://doi.org/10.1007/s10570-018-1772-9

Lachos-Perez, D., Martinez-Jimenez, F., Rezende, C. A., Tompsett, G., Timko, M., & Forster-Carneiro, T. (2016). Subcritical water hydrolysis of sugarcane bagasse: An approach on solid residues characterization. *The Journal of Supercritical Fluids*, 108, 69-78. https://doi.org/10.1016/j.supflu.2015.10.019

Le, D. M., Sørensen, H. R., Knudsen, N. O., Schjoerring, J. K., & Meyer, A. S. (2014). Biorefining of wheat straw: accounting for the distribution of mineral elements in pretreated biomass by an extended pretreatment-severity equation. *Biotechnology for Biofuels*, 7(1), 1-13. https://doi.org/10.1186/s13068-014-0141-7

Liu, C. F., Xu, F., Sun, J. X., Ren, J. L., Curling, S., Sun, R. C., & Baird, M. S. (2006). Physicochemical characterization of cellulose from perennial ryegrass leaves (Lolium perenne). *Carbohydrate Research*, 341(16), 2677-2687. https://doi.org/10.1016/j.carres.2006.07.008

Liu, C., & Wyman, C. E. (2003). The effect of flow rate of compressed hot water on xylan, lignin, and total mass removal from corn stover. *Industrial & Engineering Chemistry Research*, 42(21), 5409-5416. https://doi.org/10.1021/ie030458k

Liu, H. M., Feng, B., & Sun, R. C. (2011). Acid–chlorite pretreatment and liquefaction of cornstalk in hot-compressed water for bio-oil production. *Journal of Agricultural and Food Chemistry*, 59(19), 10524-10531. https://doi.org/10.1021/jf2025902

Liu, Q., Lu, Y., Aguedo, M., Jacquet, N., Ouyang, C., He, W., & Richel, A. (2017). Isolation of high-purity cellulose nanofibers from wheat straw through the combined environmentally friendly methods of steam explosion, microwave-assisted hydrolysis, and microfluidization. *ACS Sustainable Chemistry & Engineering*, 5(7), 6183-6191. https://doi.org/10.1021/acssuschemeng.7b01108

Liu, Q., Sun, W., Yuan, T., Liang, S. B., Peng, F., & Yao, C. L. (2021). Green and cost-effective synthesis of flexible, highly conductive cellulose nanofiber/reduced graphene oxide composite film with deep eutectic solvent. *Carbohydrate Polymers*, 272, 118514. https://doi.org/10.1016/j.carbpol.2021.118514

Liu, R., Yu, H., & Huang, Y. (2005). Structure and morphology of cellulose in wheat straw. *Cellulose*, 12, 25–34. https://doi.org/10.1007/s10570-004-0955-8

Liu, Z., Khurshid, K., & Saldana, S. M. D. (2023). Biorefinery of Barley Straw using Pressurized Fluids: Biocompounds and Biopolymers Production. The Journal of Supercritical Fluids, 106078. https://doi.org/10.1016/j.supflu.2023.106078

Lou, R., & Zhang, X. (2022). Evaluation of pretreatment effect on lignin extraction from wheat straw by deep eutectic solvent. *Bioresource Technology*, 344, 126174. https://doi.org/10.1016/j.biortech.2021.126174

Low, Z. L., Low, D. Y. S., Tang, S. Y., Manickam, S., Tan, K. W., & Ban, Z. H. (2022). Ultrasonic cavitation: An effective cleaner and greener intensification technology in the extraction and surface modification of nanocellulose. *Ultrasonics Sonochemistry*, 106176. https://doi.org/10.1016/j.ultsonch.2022.106176

Malik, S., Rana, V., Joshi, G., Gupta, P. K., & Sharma, A. (2020). Valorization of wheat straw for the paper industry: pre-extraction of reducing sugars and its effect on pulping and papermaking properties. *ACS Omega*, 5(47), 30704-30715. https://doi.org/10.1021/acsomega.0c04883

Manzocco, L., Plazzotta, S., Powell, J., de Vries, A., Rousseau, D., & Calligaris, S. (2022). Structural characterization and sorption capability of whey protein aerogels obtained by freeze-drying or supercritical drying. *Food Hydrocolloids*, 122, 107117. https://doi.org/10.1016/j.foodhyd.2021.107117

Markets and markets (2014). Market research report: Food packaging market size by material. Consulted on March 27, 2023: https://www.marketsandmarkets.com/Market-Reports/food-packaging-market-70874880.html

Markets and markets (2018). Market research report: Food Packaging technology and equipment market by technology. Accessed on March 27, 2023: https://www.marketsandmarkets.com/Market-Reports/food-packaging-technology-equipment-market-171847215.html

Markets and markets (2020). Market research report: Fresh food packaging market by material. Accessed on March 27, 2023: https://www.marketsandmarkets.com/Market-Reports/fresh-food-packaging-market-240678791.html

Martín-Diana, A. B., Tomé-Sánchez, I., García-Casas, M. J., Martínez-Villaluenga, C., Frías, J., & Rico, D. (2021). A novel strategy to produce a soluble and bioactive wheat bran ingredient rich in ferulic acid. *Antioxidants*, 10(6), 969. https://doi.org/10.3390/antiox10060969

Mekala, S., Silva, E. K., & Saldaña, M. D. (2022). Mechanism, kinetics, and physicochemical properties of ultrasound-produced emulsions stabilized by lentil protein: A non-dairy alternative in food systems. *European Food Research and Technology*, 248(1), 185-196. https://doi.org/10.1007/s00217-021-03871-2

Mokhena, T. C., Sadiku, E. R., Mochane, M. J., Ray, S. S., John, M. J., & Mtibe, A. (2021). Mechanical properties of cellulose nanofibril papers and their bionanocomposites: A review. *Carbohydrate Polymers*, 273, 118507. https://doi.org/10.1016/j.carbpol.2021.118507

Montero, G., Coronado, M. A., Torres, R., Jaramillo, B. E., García, C., Stoytcheva, M., Vazquez, A. M., Leon, J. A., Lambert, A. A., & Valenzuela, E. (2016). Higher heating value determination of wheat straw from Baja California, Mexico. *Energy*, 109, 612-619. https://doi.org/10.1016/j.energy.2016.05.011

Montoya Sánchez, N., Link, F., Chauhan, G., Halmenschlager, C., El-Sayed, H. E., Sehdev, R., & de Klerk, A. (2022). Conversion of waste to sustainable aviation fuel via Fischer–Tropsch synthesis: Front-end design decisions. *Energy Science & Engineering*, 10(5), 1763-1789. https://doi.org/10.1002/ese3.1072

Moradi, M., Tajik, H., Almasi, H., Forough, M., & Ezati, P. (2019). A novel pH-sensing indicator based on bacterial cellulose nanofibers and black carrot anthocyanins for monitoring fish freshness. *Carbohydrate Polymers*, 222, 115030. https://doi.org/10.1016/j.carbpol.2019.115030

Mujtaba, M., Fernández-Marín, R., Robles, E., Labidi, J., Yilmaz, B. A., & Nefzi, H. (2021). Understanding the effects of copolymerized cellulose nanofibers and diatomite nanocomposite on blend chitosan films. *Carbohydrate Polymers*, 271, 118424. https://doi.org/10.1016/j.carbpol.2021.118424

Nagarajan, K. J., Ramanujam, N. R., Sanjay, M. R., Siengchin, S., Surya Rajan, B., Sathick Basha, K., ... & Raghav, G. R. (2021). A comprehensive review on cellulose nanocrystals and cellulose nanofibers: Pretreatment, preparation, and characterization. *Polymer Composites*, 42(4), 1588-1630. https://doi.org/10.1002/pc.25929

Naik, S., Goud, V. V., Rout, P. K., Jacobson, K., & Dalai, A. K. (2010). Characterization of Canadian biomass for alternative renewable biofuel. *Renewable Energy*, 35(8), 1624-1631. https://doi.org/10.1016/j.renene.2009.08.033

Nan, Y., Jia, L., Yang, M., Xin, D., Qin, Y., & Zhang, J. (2018). Simplified sodium chlorite pretreatment for carbohydrates retention and efficient enzymatic saccharification of silvergrass. *Bioresource Technology*, 261, 223-231. https://doi.org/10.1016/j.biortech.2018.03.106

Nanda, S., Reddy, S. N., Vo, D. V. N., Sahoo, B. N., & Kozinski, J. A. (2018). Catalytic gasification of wheat straw in hot compressed (subcritical and supercritical) water for hydrogen production. *Energy Science & Engineering*, 6(5), 448-459. https://doi.org/10.1002/ese3.219

Okahisa, Y., Matsuoka, K., Yamada, K., & Wataoka, I. (2020). Comparison of polyvinyl alcohol films reinforced with cellulose nanofibers derived from oil palm by impregnating and casting methods. *Carbohydrate Polymers*, 250, 116907. https://doi.org/10.1016/j.carbpol.2020.116907

Pan, G. X., Bolton, J. L., & Leary, G. J. (1998). Determination of ferulic and p-coumaric acids in wheat straw and the amounts released by mild acid and alkaline peroxide treatment. *Journal of Agricultural and Food Chemistry*, 46(12), 5283-5288. https://doi.org/10.1021/jf980608f

Patil, P. T., Armbruster, U., & Martin, A. (2014). Hydrothermal liquefaction of wheat straw in hot compressed water and subcritical water–alcohol mixtures. *The Journal of Supercritical Fluids*, 93, 121-129. https://doi.org/10.1016/j.supflu.2014.01.006

Patil, T. V, Patel, D. K., Deb, S., Ganguly, K., Subhra, T., & Lim, K. (2022). Bioactive Materials Nanocellulose, a versatile platform : From the delivery of active molecules to tissue engineering applications. *Bioactive Materials*, 9, 566–589. https://doi.org/10.1016/j.bioactmat.2021.07.006

Pazo-Cepeda, V., Benito-Román, Ó., Navarrete, A., & Alonso, E. (2020). Valorization of wheat bran: Ferulic acid recovery using pressurized aqueous ethanol solutions. *Waste*

and Biomass Valorization, 11, 4701-4710. https://doi.org/10.1007/s12649-019-00787-7

Perumal, A. B., Nambiar, R. B., Moses, J. A., & Anandharamakrishnan, C. (2022). Nanocellulose: Recent trends and applications in the food industry. *Food Hydrocolloids*, 107484. https://doi.org/10.1016/j.foodhyd.2022.107484

Petersen, M. Ø., Larsen, J., & Thomsen, M. H. (2009). Optimization of hydrothermal pretreatment of wheat straw for production of bioethanol at low water consumption without addition of chemicals. *Biomass and Bioenergy*, 33(5), 834-840. https://doi.org/10.1016/j.biombioe.2009.01.004

Pinjari, D. V., & Pandit, A. B. (2010). Cavitation milling of natural cellulose to nanofibrils. *Ultrasonics Sonochemistry*, 17(5), 845-852. https://doi.org/10.1016/j.ultsonch.2010.03.005

Portugal, I., Dias, V. M., Duarte, R. F., & Evtuguin, D. V. (2010). Hydration of cellulose/silica hybrids assessed by sorption isotherms. *The Journal of Physical Chemistry B*, 114(11), 4047-4055. https://doi.org/10.1021/jp911270y

Pourali, O., Asghari, F. S., & Yoshida, H. (2009a). Simultaneous rice bran oil stabilization and extraction using sub-critical water medium. *Journal of Food Engineering*, 95(3), 510-516. https://doi.org/10.1016/j.jfoodeng.2009.06.014

Pourali, O., Asghari, F. S., & Yoshida, H. (2009b). Sub-critical water treatment of rice bran to produce valuable materials. *Food Chemistry*, 115(1), 1-7. https://doi.org/10.1016/j.foodchem.2008.11.099

Prado, J. M., Follegatti-Romero, L. A., Forster-Carneiro, T., Rostagno, M. A., Maugeri Filho, F., & Meireles, M. A. A. (2014). Hydrolysis of sugarcane bagasse in subcritical water. *Journal of Supercritical Fluids*, 86, 15-22. https://doi.org/10.1016/j.supflu.2013.11.018

Prado, J. M., Lachos-Perez, D., Forster-Carneiro, T., & Rostagno, M. A. (2016). Sub-and supercritical water hydrolysis of agricultural and food industry residues for the production of fermentable sugars: a review. *Food and Bioproducts Processing*, 98, 95-123. https://doi.org/10.1016/j.fbp.2015.11.004

Qin, Q., Li, W., Zhang, X., Gao, B., Han, L., & Liu, X. (2022). Feasibility of bionanocomposite films fabricated using capsicum leaf protein and cellulose nanofibers. *Food Chemistry*, 387, 132769. https://doi.org/10.1016/j.foodchem.2022.132769

Quirijns, E. J., Van Boxtel, A. J., van Loon, W. K., & Van Straten, G. (2005). Sorption isotherms, GAB parameters and isosteric heat of sorption. *Journal of the Science of Food and Agriculture*, 85(11), 1805-1814. https://doi.org/10.1002/jsfa.2140

Rajput, A. A., & Visvanathan, C. (2018). Effect of thermal pretreatment on chemical composition, physical structure and biogas production kinetics of wheat straw. *Journal of Environmental Management*, 221, 45-52. https://doi.org/10.1016/j.jenvman.2018.05.011

Redlinger-Pohn, J. D., Petkovšek, M., Gordeyeva, K., Zupanc, M., Gordeeva, A., Zhang, Q., & Söderberg, L. D. (2022). Cavitation fibrillation of cellulose fiber. *Biomacromolecules*, 23(3), 847-862. https://doi.org/10.1021/acs.biomac.1c01309

Reynolds, W., Singer, H., Schug, S., & Smirnova, I. (2015). Hydrothermal flow-through treatment of wheat-straw: Detailed characterization of fixed-bed properties and axial dispersion. *Chemical Engineering Journal*, 281, 696-703. https://doi.org/10.1016/j.cej.2015.06.117

Rhim, J. W., & Lee, J. H. (2009). Thermodynamic analysis of water vapor sorption isotherms and mechanical properties of selected paper-based food packaging materials. *Journal of Food Science*, 74(9), E502-E511. https://doi.org/10.1111/j.1750-3841.2009.01373.x

Robertson, G. L. (2016). Food packaging: principles and practice. CRC press. https://doi.org/10.1201/9781420056150

Rodríguez-Sanz, A., Fucinos, C., Torrado, A. M., & Rúa, M. L. (2022). Extraction of the wheat straw hemicellulose fraction assisted by commercial endo-xylanases. Role of the accessory enzyme activities. *Industrial Crops and Products*, 179, 114655. https://doi.org/10.1016/j.indcrop.2022.114655

Roy, S., & Rhim, J. W. (2021). Fabrication of cellulose nanofiber-based functional color indicator film incorporated with shikonin extracted from Lithospermum erythrorhizon root. *Food Hydrocolloids*, 114, 106566. https://doi.org/10.1016/j.foodhyd.2020.106566

Ruel, K., Nishiyama, Y., & Joseleau, J. P. (2012). Crystalline and amorphous cellulose in the secondary walls of Arabidopsis. *Plant Science*, 193, 48-61. https://doi.org/10.1016/j.plantsci.2012.05.008

Sáenz Ezquerro, C., Laspalas, M., García Aznar, J. M., & Crespo Miñana, C. (2023). Monitoring interactions through molecular dynamics simulations: effect of calcium carbonate on the mechanical properties of cellulose composites. *Cellulose*, 30(2), 705-726. https://doi.org/10.1007/s10570-022-04902-1

Saini, S., Kardam, S. K., Kadam, A. A., Kumar, V., & Gaikwad, K. K. (2022). Green and energy-efficient extraction of cellulose nano-fibrils from rice straw and its coating to improve functional properties of rice straw paperboard made via refiner mechanical pulping. *Progress in Organic Coatings*, 165, 106747. https://doi.org/10.1016/j.porgcoat.2022.106747

Sánchez Bastardo, N., Cocero Alonso, M. J., & Alonso Sánchez, G. E. (2016). Heterogeneous catalysis for the extraction of arabinoxylans from wheat bran. Presented in the 5th International Congress on Green Process Engineering. Mont Tremblant, Quebec, Canada. http://uvadoc.uva.es/handle/10324/23497

Sarkar, S., Alvarez, V.H. And Saldaña, M.D.A. (2014) Relevance of ions in pressurized fluid extraction of carbohydrates and phenolics from barley hull. *Journal of Supercritical Fluids*, 93, 27-37. https://doi.org/10.1016/j.supflu.2014.04.019

Sasaki, M., Adschiri, T., & Arai, K. (2003a). Production of cellulose II from native cellulose by near-and supercritical water solubilization. *Journal of Agricultural and Food Chemistry*, 51(18), 5376-5381. https://doi.org/10.1021/jf025989i

Sasaki, M., Adschiri, T., & Arai, K. (2003b). Fractionation of sugarcane bagasse by hydrothermal treatment. *Bioresource Technology*, 86(3), 301-304. https://doi.org/10.1016/S0960-8524(02)00173-6

Saskatchewan's Agriculture Knowledge Centre. Harvesting Surplus Cereal Straw. Accessed on August 13th, 2020 on: https://www.saskatchewan.ca/business/agriculture-natural-resources-and-industry/agribusiness-farmers-and-ranchers/crops-and-irrigation/field-crops/cereals-barley-wheat-oats-triticale/harvesting-surplus-cereal-straw#:~:text=Straw to grain ratio%2C and,wheat (grain) harvested).

Sereewatthanawut, I., Prapintip, S., Watchiraruji, K., Goto, M., Sasaki, M., & Shotipruk, A. (2008). Extraction of protein and amino acids from deoiled rice bran by subcritical water hydrolysis. *Bioresource Technology*, 99(3), 555-561. https://doi.org/10.1016/j.biortech.2006.12.030

Shahbazi, P., Behzad, T., & Heidarian, P. (2017). Isolation of cellulose nanofibers from poplar wood and wheat straw: optimization of bleaching step parameters in a chemo-mechanical process by experimental design. *Wood Science and Technology*, 51, 1173-1187. https://doi.org/10.1007/s00226-017-0929-2

Sing, K. S. (1985). Reporting physisorption data for gas/solid systems with special reference to the determination of surface area and porosity (Recommendations 1984). Pure and applied chemistry, 57(4), 603-619. https://doi.org/10.1351/pac198557040603

Silva, G. G. D., Guilbert, S., & Rouau, X. (2011). Successive centrifugal grinding and sieving of wheat straw. *Powder Technology*, 208(2), 266-270. https://doi.org/10.1016/j.powtec.2010.08.015

Sluiter, A., Hames, B., Ruiz, R., Scarlata, C., Sluiter, J., Templeton, D., & Crocker, D. L. A. P. (2008). Determination of structural carbohydrates and lignin in biomass. *National Renewable Energy Laboratory*, 1617(1), 1-16. http://www.nrel.gov/biomass/analytical_procedures.html

Song, S., Qiang, S., Liang, J., Li, L., Shi, Y., Nie, J., ... & Zhang, M. (2022). Cellulose nanofibril/mineral composites induced by H-bond/ionic coordination in co-refining system. *Carbohydrate Polymers*, 289, 119425. https://doi.org/10.1016/j.carbpol.2022.119425

Soni, R., Asoh, T. A., & Uyama, H. (2020). Cellulose nanofiber reinforced starch membrane with high mechanical strength and durability in water. *Carbohydrate polymers*, 238, 116203. https://doi.org/10.1016/j.carbpol.2020.116203

Soto-Salcido, L. A., Anugwom, I., Mänttäri, M., & Kallioinen-Mänttäri, M. (2022). Cellulose nanofibers derived surface coating in enhancing the dye removal with cellulosic ultrafiltration membrane. *Membranes*, 12(11), 1082. https://doi.org/10.3390/membranes12111082

Strieder, M. M., Silva, E. K., Mekala, S., Meireles, M. A. A., & Saldaña, M. D. (2022). Pulsed high-pressure processing of barley-based non-dairy alternative milk: β-carotene retention, protein solubility and antioxidant activity. *Innovative Food Science & Emerging Technologies*, 82, 103212. https://doi.org/10.1016/j.ifset.2022.103212

Sun, R., Tomkinson, J., Wang, S., & Zhu, W. (2000). Characterization of lignins from wheat straw by alkaline peroxide treatment. *Polymer Degradation and Stability*, 67(1), 101-109. https://doi.org/10.1016/S0141-3910(99)00099-3

Templeton, D. W., Wolfrum, E. J., Yen, J. H., & Sharpless, K. E. (2016). Compositional analysis of biomass reference materials: results from an interlaboratory study. *Bioenergy Research*, 9(1), 303-314. https://doi.org/10.1007/s12155-015-9675-1

Thongmeepech, A., Koda, T., & Nishioka, A. (2023). Effect of shear and heat milling of starch on the properties of tapioca starch/cellulose nanofiber composites. *Carbohydrate Polymers*, 306, 120618. https://doi.org/10.1016/j.carbpol.2023.120618

Toor, S. S., Rosendahl, L., & Rudolf, A. (2011). Hydrothermal liquefaction of biomass: A review of subcritical water technologies. *Energy*, 36(5), 2328-2342. https://doi.org/10.1016/j.energy.2011.03.013

UN environment progremme. Plastic pollution. Accessed on March 27, 2023, on: https://www.unep.org/plastic-pollution#:~:text=Plastic%20pollution%20can%20alter%20habitats,t%20exist%20in%20a%20vacuum.

USDA (2022). Crop Production Maps. Accessed on August 17th, 2022 in: https://ipad.fas.usda.gov/rssiws/al/global_cropprod.aspx

Ventura-Cruz, S., & Tecante, A. (2019). Extraction and characterization of cellulose nanofibers from Rose stems (Rosa spp.). *Carbohydrate Polymers*, 220, 53-59. https://doi.org/10.1016/j.carbpol.2019.05.053

Ventura-Cruz, S., Flores-Alamo, N., & Tecante, A. (2020). Preparation of microcrystalline cellulose from residual Rose stems (Rosa spp.) by successive delignification with alkaline hydrogen peroxide. *International Journal of Biological Macromolecules*, 155, 324-329. https://doi.org/10.1016/j.ijbiomac.2020.03.222

Vieira, M. G. A., Da Silva, M. A., Dos Santos, L. O., & Beppu, M. M. (2011). Natural-based plasticizers and biopolymer films: A review. *European Polymer Journal*, 47(3), 254-263. https://doi.org/10.1016/j.eurpolymj.2010.12.011

Vo, H., & Saldaña, M. D. (2023). Hydrolysis of pea protein concentrate in subcritical water media with addition of citrus pectin and citric acid. *The Journal of Supercritical Fluids*, 195, 105866. https://doi.org/10.1016/j.supflu.2023.105866

Wang, Y., Yang, Y., Qu, Y., & Zhang, J. (2021). Selective removal of lignin with sodium chlorite to improve the quality and antioxidant activity of xylo-oligosaccharides from lignocellulosic biomass. *Bioresource Technology*, 337, 125506. https://doi.org/10.1016/j.biortech.2021.125506

Wu, C., McClements, D. J., He, M., Zheng, L., Tian, T., Teng, F., & Li, Y. (2021). Preparation and characterization of okara nanocellulose fabricated using sonication or high-pressure homogenization treatments. *Carbohydrate Polymers*, 255, 117364. https://doi.org/10.1016/j.carbpol.2020.117364

Xu, J., Krietemeyer, E. F., Boddu, V. M., Liu, S. X., & Liu, W. C. (2018). Production and characterization of cellulose nanofibril (CNF) from agricultural waste corn stover. *Carbohydrate Polymers*, 192, 202-207. https://doi.org/10.1016/j.carbpol.2018.03.017

Xu, J., Sagnelli, D., Faisal, M., Perzon, A., Taresco, V., Mais, M., Giosafatto, C.V.L., Hebelstrup, K.H., Ulvskov, P., Jørgensen, B., Chen, L & Blennow, A. (2021).

Amylose/cellulose nanofiber composites for all-natural, fully biodegradable and flexible bioplastics. *Carbohydrate Polymers*, 253, 117277. https://doi.org/10.1016/j.carbpol.2020.117277

Xu, J., Xia, R., Zheng, L., Yuan, T., & Sun, R. (2019). Plasticized hemicelluloses/chitosan-based edible films reinforced by cellulose nanofiber with enhanced mechanical properties. *Carbohydrate Polymers*, 224, 115164. https://doi.org/10.1016/j.carbpol.2019.115164

Yamazaki, J., Minami, E., & Saka, S. (2006). Liquefaction of beech wood in various supercritical alcohols. *Journal of Wood Science*, 52(6), 527-532. https://doi.org/10.1007/s10086-005-0798-4

Yang, J., Zhang, L., Wang, P., & Zhou, J. (2022). Cellulose nanofibers prepared from pulp through ultrasound treatment followed semi-dry esterification and their application for transparent and anti-fingerprint coating. *Progress in Organic Coatings*, 167, 106844. https://doi.org/10.1016/j.porgcoat.2022.106844

Yong, T. L. K., & Matsumura, Y. (2013). Kinetic analysis of lignin hydrothermal conversion in sub-and supercritical water. *Industrial & Engineering Chemistry Research*, 52(16), 5626-5639. https://doi.org/10.1021/ie400600x

Yoshida, C. M., Maciel, V. B. V., Mendonça, M. E. D., & Franco, T. T. (2014). Chitosan biobased and intelligent films: Monitoring pH variations. *LWT-Food Science and Technology*, 55(1), 83-89. https://doi.org/10.1016/j.lwt.2013.09.015

Zhang, L., Larsson, A., Moldin, A., & Edlund, U. (2022). Comparison of lignin distribution, structure, and morphology in wheat straw and wood. *Industrial Crops and Products*, 187, 115432. https://doi.org/10.1016/j.indcrop.2022.115432

Zhang, X., Li, Y., Guo, M., Jin, T. Z., Arabi, S. A., He, Q., & Liu, D. (2021). Antimicrobial and UV blocking properties of composite chitosan films with curcumin grafted cellulose nanofiber. *Food Hydrocolloids*, 112, 106337. https://doi.org/10.1016/j.foodhyd.2020.106337

Zhao, T., Chen, Z., Lin, X., Ren, Z., Li, B., & Zhang, Y. (2018). Preparation and characterization of microcrystalline cellulose (MCC) from tea waste. *Carbohydrate polymers*, 184, 164-170. https://doi.org/10.1016/j.carbpol.2017.12.024

Zhao, Y., & Saldaña, M. D. (2019). Use of potato by-products and gallic acid for development of bioactive film packaging by subcritical water technology. *The Journal of Supercritical Fluids*, 143, 97-106. https://doi.org/10.1016/j.supflu.2018.07.025

Zhao, Y., Lu, W. J., Wang, H. T., & Yang, J. L. (2009). Fermentable hexose production from corn stalks and wheat straw with combined supercritical and subcritical hydrothermal technology. *Bioresource Technology*, 100(23), 5884-5889. https://doi.org/10.1016/j.biortech.2009.06.079

Appendix A: Mass balances of the hydrolysis and the bleaching treatments

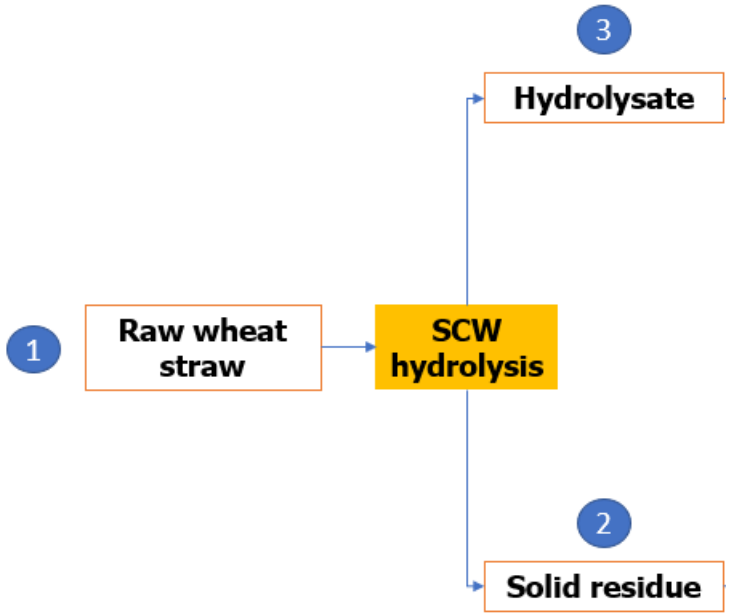

Fig. A.1. Mass balance of the wheat straw SCW hydrolysis treatment with three main streams.

Total mass balance for the SCW hydrolysis process is:

$$m_{Raw\ wheat\ straw} = m_{Hydrolysate} + m_{Solid\ residue} \qquad \text{Eq. A.1}$$

$Raw\ wheat\ straw =$ 3.03 g with a moisture content of 4.87% ∴ $m_{Raw\ wheat\ straw} =$ 2.878 g dw

$Solid\ residue =$ 1.39 g with a moisture content of 3.01% ww ∴ $m_{Solid\ residue} =$ 1.34 g dw

The solid residue was not totally recovered during the separation of the sample and the glass beads. Thus, the dry weight of the hydrolysate was determined using the methodology for moisture content reported in Section 3.2.2.2.1. During the experiments, it was found that:

$$Hydrolyzate = 1.47\ g\ dw$$

A more accurate value for the solid residue would be:

$$m_{Solid\ residue} = m_{Raw\ wheat\ straw} - m_{Hydrolyzate} \qquad \text{Eq. A.2}$$

Substituting:

$$Solid\ residue = 2.88\ g\ dw - 1.47\ g\ dw$$

$$Solid\ residue = \underline{1.40\ g\ dw} \therefore \underline{1.45\ g\ dw}$$

Cellulose, hemicellulose, and lignin contents in the streams 1 and 2 were analyzed as in Section 3.2.2.2.2.

Table A.1. Structural carbohydrate and lignin fractions on the raw wheat straw and solid residue

	X Cellulose	**X Hemicellulose**	**X Lignin**	**X other**	**Total**
Raw (stream 1)	0.37	0.23	0.21	0.16	0.96
Solid residue (stream 2)	0.67	0.09	0.19	0.09	1.05

X: Fraction

The rationale for the calculations of the structural carbohydrates and lignin contents (fractions) in the hydrolyzate was the following:

- Cellulose:

$$(X_{3\ cellulose} \cdot m_{Hydrolyzate}) = (X_{1\ cellulose} \cdot m_{Raw\ wheat\ straw}) - (X_{2\ cellulose} \cdot m_{Solid\ residue}) \quad \text{Eq. A.3}$$

$$X_{3\ cellulose} = \frac{(X_{1\ cellulose} \cdot m_{Raw\ wheat\ straw}) - (X_{2\ cellulose} \cdot m_{Solid\ residue})}{m_{Hydrolyzate}}$$

- Hemicellulose:

$$(X_{3\ hemicellulose} \cdot m_{Hydrolyzate}) = (X_{1\ hemicellulose} \cdot m_{Raw\ wheat\ straw}) - (X_{2\ hemicellulose} \cdot m_{Solid\ residue}) \quad \text{Eq. A.4}$$

$$X_{3\ hemicellulose} = \frac{(X_{1\ hemicellulose} \cdot m_{Raw\ wheat\ straw}) - (X_{2\ hemicellulose} \cdot m_{Solid\ residue})}{m_{Hydrolyzate}}$$

- Lignin

$$(X_{3\ lignin} \cdot m_{Hydrolyzate}) = (X_{1\ lignin} \cdot m_{Raw\ wheat\ straw}) - (X_{2\ lignin} \cdot m_{Solid\ residue}) \quad \text{Eq. A.5}$$

$$X_{3\ lignin} = \frac{(X_{1\ lignin} \cdot m_{Raw\ wheat\ straw}) - (X_{2\ lignin} \cdot m_{Solid\ residue})}{m_{Hydrolyzate}}$$

- Other compounds (ash, proteins, and lipids)

$$(X_{3\ other} \cdot m_{Hydrolyzate}) = (X_{1\ other} \cdot m_{Raw\ wheat\ straw}) - (X_{2\ other} \cdot m_{Solid\ residue}) \quad \text{Eq. A.6}$$

$$X_{3\ other} = \frac{(X_{1\ other} \cdot m_{Raw\ wheat\ straw}) - (X_{2\ other} \cdot m_{Solid\ residue})}{m_{Hydrolyzate}}$$

The rationale to calculate structural carbohydrates and lignin removal from the raw wheat straw was the following:

- Cellulose:

$$m_{Cellulose\ removal} = \frac{(X_{3\ cellulose} \cdot m_{Hydrolyzate})}{(X_{1\ cellulose} \cdot m_{Raw\ wheat\ straw})}\ x\ 100\% \quad \text{Eq. A.7}$$

- Hemicellulose:

$$m_{Hemicellulose\ removal} = \frac{(X_{3\ hemicellulose} \cdot m_{Hydrolyzate})}{(X_{1\ hemicellulose} \cdot m_{Raw\ wheat\ straw})}\ x\ 100\% \quad \text{Eq. A.8}$$

- Lignin

$$m_{Lignin\ removal} = \frac{(X_{3\ lignin} \cdot m_{Hydrolyzate})}{(X_{1\ lignin} \cdot m_{Raw\ wheat\ straw})}\ x\ 100\% \quad \text{Eq. A.9}$$

- Other compounds (ash, proteins, and lipids)

$$m_{Other\ compounds\ removal} = \frac{(X_{3\ other} \cdot m_{Hydrolyzate})}{(X_{1\ other} \cdot m_{Raw\ wheat\ straw})}\ x\ 100\% \quad \text{Eq. A.10}$$

Results:

Table A.2. Hydrolysates (stream 3) composition and structural components removal from stream 1

	X_3	**Removal (%)**
Cellulose	0.05	11.06
Hemicellulose	0.35	80.27
Lignin	0.20	53.92
Other	0.23	72.07

X_3: Fraction of stream 3

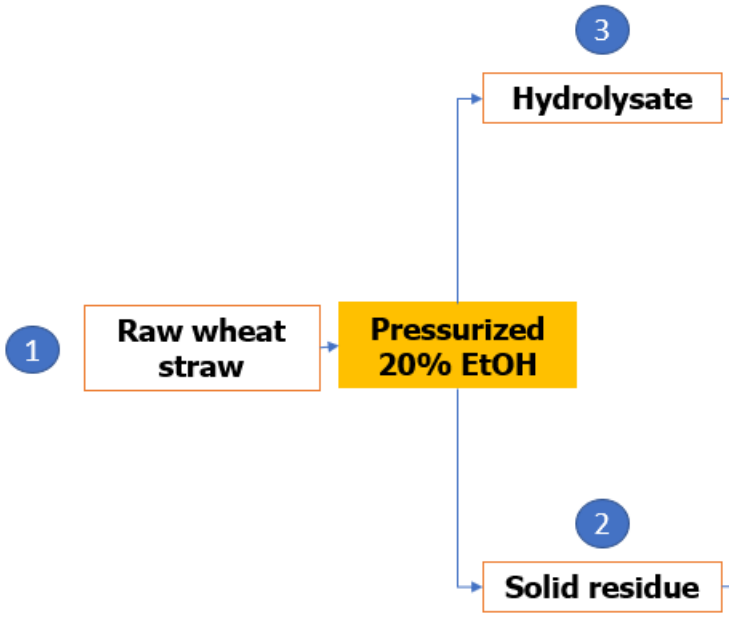

Fig. A.2. Mass balance of the pressurized 20% aqueous ethanol (EtOH) with three main streams.

The total mass balance for the hydrolysis treatment was:

$$m_{Raw\ wheat\ straw} = m_{Hydrolyzate} + m_{Solid\ residue} \qquad \text{Eq. A.11}$$

$Raw\ wheat\ straw =$ 3.06 g with a moisture content of 4.87% ∴ $m_{Raw\ wheat\ straw} =$ 2.91 g dw

$Solid\ residue\ (collected) =$ 1.26 g ww with a moisture content of 3.01%

$Hydrolyzate =$ 1.59 g dry basis

$Solid\ residue\ (corrected) =$ 1.32 g db ∴ 1.36 g ww

Table A.3 Structural carbohydrate and lignin fractions on the raw wheat straw and solid residue

	$X_{Cellulose}$	$X_{Hemicellulose}$	X_{Lignin}	X_{other}	Total
Raw (stream 1)	0.37	0.23	0.21	0.165	0.95
Solid residue (stream 2)	0.69	0.09	0.14	0.075	1.00

X: Fraction

The rationale for the calculations of structural carbohydrates and lignin contents (fractions) in the hydrolysate was the same as in the SCW hydrolysis.

Table A.4. Hydrolysates (stream 3) composition and structural components removal from stream 1.

	X_3	Removal (%)
Cellulose	0.08	12.47
Hemicellulose	0.34	81.09
Lignin	0.34	0.41
Other	0.24	79.44

X3: Fraction of stream 3

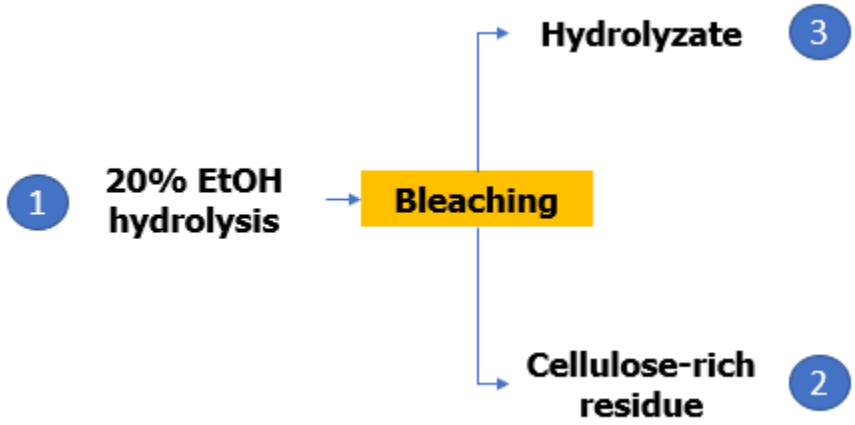

Fig. A.3. Mass balance of beaching treatments (ASC for 2h and AHP for 1, 2, and 2.5 h) with three main streams considered per treatment.

The total mass balance for the bleaching treatment was:

$$m_{20\%\ EtOH\ treated\ residue} = m_{Hydrolyzate} + m_{Cellulose-rich\ residue} \quad \text{Eq. A.12}$$

Table A.5. Weights of the feed and cellulose-rich residues after bleaching treatments

Treatment	20% EtOH treated residue (g ww)	Cellulose rich residue (g ww)	Moisture content (%)	20% EtOH treated residue (g dw)	Cellulose rich residue (g dw)
ASC 2h	8.90	7.60	8.49	8.63	6.95
AHP 2.5h	8.00	6.16	4.99	7.76	5.86
AHP 2h	8.00	7.19	9.62	7.76	6.50
AHP 1h	8.00	7.14	10.62	7.76	6.38

ASC: acidified sodium chlorite, AHP: alkaline hydrogen peroxide, EtOH: ethanol

*Weights in wet basis (ww) represent the weight of the sample collected after bleaching and drying. Weights in dry basis (dw) were determined using the methodology for moisture content removed in Section 3.2.2.2.1.

Table A.6. Structural carbohydrate and lignin fractions on the raw wheat straw and solid residue

Treatment	$X_{Cellulose}$	$X_{Hemicellulose}$	X_{Lignin}	X_{other}	Total
20% EtOH treated	0.69	0.09	0.14	0.075	1.00
ASC 2h	0.86	0.09	0.04	0.052	1.04
AHP 2.5h	0.85	0.11	0.04	0.044	1.04
AHP 2h	0.83	0.10	0.07	0.068	1.06
AHP 1h	0.81	0.09	0.08	0.059	1.04

ASC: acidified sodium chlorite, AHP: alkaline hydrogen peroxide, EtOH: ethanol, X: fraction

The rationale for the calculations of structural carbohydrates and lignin removal are the same as in the SCW hydrolysis.

Table A.7. structural components removal from stream 1.

Treatment	Cellulose removal (%)	Hemicellulose removal (%)	Lignin removal (%)
ASC 2h	-0.76	22.59	77.57
AHP 2.5h	6.73	12.06	80.02
AHP 2h	-1.29	13.97	59.08
AHP 1h	2.62	17.93	53.71

ASC: acidified sodium chlorite, AHP: alkaline hydrogen peroxide

Table A.8. Proximate composition of hydrolyzed and bleached wheat straw.

Treatment	Ash (% dw)	Protein (% dw)	Fat (% dw)	Carbohydrate (% dw)
20% EtOH	6.62 ± 0.12^{a}	0.21 ± 0.02^{a}	0.65 ± 0.04^{a}	92.53 ± 0.14^{d}
AHP 2.5	3.91 ± 0.48^{c}	0.06 ± 0.03^{bc}	0.43 ± 0.10^{a}	95.60 ± 0.60^{ab}
AHP 2	6.01 ± 0.67^{ab}	0.09 ± 0.01^{bc}	0.65 ± 0.31^{a}	93.26 ± 0.37^{bc}
AHP 1	5.26 ± 0.04^{abc}	$0.11\pm.00^{b}$	0.57 ± 0.01^{a}	94.02 ± 0.05^{cd}
ASC 2	4.57 ± 0.09^{bc}	0.03 ± 0.01^{c}	0.56 ± 0.14^{a}	94.85 ± 0.24^{a}

ASC: acidified sodium chlorite, AHP: alkaline hydrogen peroxide, EtOH: ethanol

Appendix B: Wheat straw hydrolysis using pressurized mixtures of water + ethanol: Behavior of structural compounds.

Table B.1. Effect of ethanol concentration on the structural sugars and lignin contents of wheat straw using SCW and pressurized water + ethanol (EtOH) at 180°C, 50 bar, and 5 mL/min.

Sample	Cellulose (% dw)	Hemicellulose (% dw)	Lignin (% dw)
Raw	36.77±0.14^{c}	22.63±0.05^{a}	20.55±0.44^{a}
SCW	66.92±1.73^{a}	9.14±2.12^{b}	19.38±0.93^{a}
20% EtOH	68.79±4.14^{a}	9.43±1.57^{b}	14.01±0.19^{b}
60% EtOH	57.06±2.32^{b}	22.38±0.51^{a}	11.41±0.69^{c}
100% EtOH	41.76±0.04^{c}	26.17±0.29^{a}	16.50±0.40^{b}

SCW: subcritical water, EtOH: ethanol. $^{A-B}$ Values in the same column represent significant differences at $p < 0.05$.

Table B.2. Analysis of hydrolysates obtained from wheat straw hydrolysis using SCW and pressurized water + ethanol (EtOH) at 180°C, 50 bar, and 5 mL/min.

Hydrolysis treatment	Total phenolics (mg GAE/ g wheat straw)	Total carbohydrates (mg GE/g wheat straw)	Brown color	pH
SCW	38.28±2.98^{a}	259.46±33.82^{a}	0.78±0.03^{b}	4.584±0.01^{a}
20 % EtOH	35.43±4.77^{ab}	227.56±0.57^{a}	1.18±0.10^{a}	4.767±0.04^{a}
60 % EtOH	40.18±1.97^{a}	82.44±0.13^{b}	1.39±0.10^{a}	5.671±0.03^{b}
100 % EtOH	24.54±2.73^{b}	26.00±0.86^{b}	0.82±0.50^{b}	5.793±0.11^{b}

SCW: subcritical water, EtOH: ethanol, GAE: gallic acid equivalents, GE: glucose equivalents. $^{A-B}$ Values in the same column represent significant differences at $p < 0.05$.

Appendix C: Sustainable cellulose-based micro/nanopaper development

Table C.1. Bleached residues composition.

Sample	Cellulose	Hemicellulose	Lignin
Untreated	35.62±0.14[c]	22.60±0.05[a]	20.52±0.44[a]
20% EtOH	68.79±4.14[b]	9.43±1.57[b]	14.01±0.19[b]
AHP 1 h	80.52±1.87[a]	9.31±0.31[b]	7.80±0.57[c]
AHP 2 h	83.14±0.17[a]	9.68±0.12[b]	6.84±0.57[c]
AHP 2.5 h	85.48±0.65[a]	9.77±0.30[b]	3.71±0.25[d]
*ASC 2 h	87.34±2.43[a]	8.99±0.60[b]	3.90±0.07[d]

SCW: subcritical water, EtOH: ethanol, ASC: acidified sodium chlorite, AHP: alkaline hydrogen peroxide. [A-B] Values in the same column represent significant differences at $p < 0.05$. *ASC bleaching results obtained from two samples obtained from one experiment.

Table C.2. Size distribution of solid residue bleached with AHP for 2.5 h, dispersed in water at a concentration of 1%, and defibrillated with HIUS at 1200 W for 6 min, 13 min, and 20 min; and solid residue bleached with AHP for 2.5 h, dispersed in water at concentration of 2%, and defibrillated with HIUS at 1200 W for 13 min.

Treatment	***Class***	***Frequency***	***Accumulation (%)***
AHP 2.5; 1%; 1200 W/ 6 min	< 10	4	4
	10 to 20	31	35
	20 to 30	26	61
	30 to 40	25	86
	40 to 50	4	90
	50 <	10	100
AHP 2.5; 1%; 1200 W/ 13 min	< 10	3	2.7
	10 to 20	44	42.34
	20 to 30	35	73.87
	30 to 40	15	87.39
	40 to 50	6	92.79
	50 <	8	100
AHP 2.5; 1%; 1200 W/ 20 min	< 10	8	7.92
	10 to 20	54	61.39
	20 to 30	22	83.17
	30 to 40	10	93.07
	40 to 50	3	96.04
	50 <	4	100
AHP 2.5; 2%; 1200 W/ 13 min	< 10	4	4
	10 to 20	22	26
	20 to 30	23	49
	30 to 40	13	62
	40 to 50	7	69
	50 <	31	100

Table C.3 Analysis of HIUS treated dispersions of bleached (AHP for 2.5 h) solid residue at concentrations of 1% and 2%.

HIUS treatment at 1200 W	**Fibrillation yield (%)**		**WRV_w (g/g)**	
Time (min)	1%	2%	1%	2%
6	18.09±1.12[a]	13.17±5.46[a]	29.04±0.91[b]	27.21±0.43[b]
13	18.72±0.22[a]	17.84±4.18[a]	30.53±1.11[ab]	28.08±0.26[b]
20	16.96±0.18[a]	16.96±3.92[a]	34.88±1.23[a]	27.40±1.70[a]

WRVw: water retention value of the wet dispersion

Table C.4. WRV_d of solid residues bleached with AHP for 2.5 h dispersed in water at concentrations of 1% and 2% and fibrillated with HIUS at 1200 W for 6, 13, and 20 min and 720 W 20 min. Effect of the fibrillated cellulose concentration on the WRV_d.

	1200 W; 6 min		**1200 W; 13 min**		**1200 W; 20 min**		**720 W; 20 min**	
Time (min)	**2%**	**1%**	**2%**	**1%**	**2%**	**1%**	**2%**	**1%**
0.0	0.00	0.00	0.00	0.00	0.00	0.00	0.00	0.00
0.5	186.73±50.09^{a}	137.76±9.55^{a}	101.97±24.59^{a}	103.53±17.03^{a}	49.92±20.90^{a}	118.53±4.49^{a}	208.61±35.58^{a}	97.96±3.64^{b}
1.0	195.07±52.44^{a}	144.89±12.84^{a}	133.48±6.29^{a}	127.36±7.38^{a}	118.61±14.09^{a}	133.95±2.31^{a}	215.89±36.81^{a}	104.62±17.04^{b}
3.0	208.37±52.53^{a}	156.39±3.47^{a}	140.11±3.98^{a}	142.66±2.82^{a}	130.20±17.79^{a}	132.97±5.21^{a}	227.41±30.21^{a}	126.68±16.15^{b}
5.0	202.49±59.53^{a}	160.08±13.33^{a}	144.67±0.69^{a}	137.17±9.05^{a}	130.77±17.52^{a}	144.28±9.34^{a}	231.17±42.82^{a}	124.92±7.41^{b}
7.0	212.83±49.40^{a}	153.70±3.39^{a}	139.97±13.45^{a}	125.50±11.70^{a}	138.44±1.92^{a}	136.10±2.74^{a}	226.54±36.02^{a}	137.25±10.93^{b}
9.0	216.14±54.23^{a}	157.39±5.51^{a}	144.50±17.68^{a}	129.79±21.29^{a}	141.18±5.65^{a}	135.19±15.67^{a}	235.06±29.45^{a}	120.76±6.93^{b}
11.0	212.85±59.80^{a}	169.45±5.27^{a}	151.19±7.80^{a}	127.60±16.15^{a}	144.80±14.59^{a}	143.12±10.48^{a}	238.78±19.62^{a}	130.46±2.19^{b}
13.0	214.72±52.54^{a}	171.75±7.61^{a}	149.36±15.97^{a}	137.19±9.76^{a}	146.26±8.09^{a}	134.85±1.47^{a}	243.79±43.81^{a}	132.57±15.67^{b}
15.0	211.50±54.18^{a}	160.70±12.04^{a}	150.48±8.80^{a}	143.33±0.54^{a}	139.45±16.35a	127.65±13.43^{a}	239.49±34.71^{a}	136.63±6.93^{b}

WRV_d: Water Retention Value of the dried materials. $^{a-b}$ Values at the same WRV_d time but different concentration represent significant differences at $p < 0.05$.

Table C.5. WRV_d of solid residues bleached with AHP for 2.5 h dispersed in water at concentrations of 1% and 2% and fibrillated with HIUS at 1200 W for 6, 13, and 20 min and 720 W 20 min. Effect of the fibrillation time on the WRV_d.

WRV_d	**6 vs 13**		**6 vs 20**		**13 vs 20**	
Time (min)	**6 min**	**13 min**	**6 min**	**20 min**	**13 min**	**20 min**
0.0	0.00	0.00	0.00	0.00	0.00	0.00
0.5	137.76±9.55[a]	103.53±17.03[a]	137.76±9.55[a]	118.53±4.49[a]	103.53±17.03[a]	118.53±4.49[a]
1.0	144.89±12.84[a]	127.36±7.38[a]	144.89±12.84[a]	133.95±2.31[a]	127.36±7.38[a]	133.95±2.31[a]
3.0	156.39±3.47[a]	142.66±2.82[b]	156.39±3.47[a]	132.97±5.21[b]	142.66±2.82[a]	132.97±5.21[a]
5.0	160.08±13.33[a]	137.17±9.05[a]	160.08±13.33[a]	144.28±9.34[a]	137.17±9.05[a]	144.28±9.34[a]
7.0	153.70±3.39[a]	125.50±11.70[a]	153.70±3.39[a]	136.10±2.74[a]	125.50±11.70[a]	136.10±2.74[a]
9.0	157.39±5.51[a]	129.79±21.29[a]	157.39±5.51[a]	135.19±15.67[a]	129.79±21.29[a]	135.19±15.67[a]
11.0	169.45±5.27[a]	127.60±16.15[a]	169.45±5.27[a]	143.12±10.48[a]	127.60±16.15[a]	143.12±10.48[a]
13.0	171.75±7.61[a]	137.19±9.76[a]	171.75±7.61[a]	134.85±1.47[b]	137.19±9.76[a]	134.85±1.47[a]
15.0	160.70±12.04[a]	143.33±0.54[a]	160.70±12.04[a]	127.65±13.43[a]	143.33±0.54[a]	127.65±13.43[a]

WRV_d: Water Retention Value of the dried materials. [a-b] Values at the same WRV_d time but different HIUS treatment times represent significant differences at $p < 0.05$.

Table C.6. Sorption isotherms data for nanomaterials prepared with(out) glycerol and/or calcium carbonate at 22°C.

	1:0 CC			1:0.1 CC			1:2 CC		
Aw	**1:0 G**	**1:0.1 G**	**1:0.2 G**	**1:0 G**	**1:0.1 G**	**1:0.2 G**	**1:0 G**	**1:0.1 G**	**1:0.2 G**
0.985	16.34±0.89^{a}	17.33±0.06^{a}	17.98±0.53^{a}	15.77±1.08^{a}	15.54±0.29^{a}	16.02±0.53^{a}	15.04±0.31^{a}	14.42±0.75^{a}	14.48±0.28^{a}
0.76	10.47±0.07^{a}	9.56±0.29^{ab}	8.55±0.57^{ab}	9.21±0.05^{a}	8.96±0.27^{a}	8.46±0.63^{a}	8.27±0.08^{a}	8.96±1.05^{a}	8.51±0.29^{a}
0.5	7.21±1.18^{a}	6.96±0.83^{a}	7.14 ±0.67^{a}	5.86±1.08^{a}	6.53±0.89^{a}	6.25±1.04^{a}	5.06±0.14^{a}	5.05±0.73^{a}	5.10±0.61^{a}
0.26	4.52±0.64^{a}	5.09±0.40^{a}	4.03±0.03^{a}	4.15±0.50^{a}	3.75±1.30^{a}	4.28±0.49^{a}	3.53±0.40^{a}	3.45±0.17^{a}	3.48±0.76^{a}

Aw: water activity, G: glycerol, CC: calcium carbonate. $^{A-B}$Values in the same column and equal CC ration represent significant differences at $p < 0.05$.

Table C.7. Sorption isotherms data for nanomaterials prepared without glycerol and calcium carbonate at different ratios at 22°C.

	1:0 G		
Aw	**1:0 CC**	**1:0.1 CC**	**1:0.2 CC**
0.985	16.34±0.89[a]	15.77±1.08[a]	15.04±0.31[a]
0.76	10.47±0.07[a]	9.21±0.05[b]	8.27±0.08[c]
0.5	7.21±1.18[a]	5.86±1.08[a]	5.06±0.14[a]
0.26	4.52±0.64[a]	4.15±0.50[a]	3.53±0.40[a]

Aw: water activity, G: glycerol, CC: calcium carbonate. [a-b]Values in the same column and equal G ration represent significant differences at $p<0.05$.

Table C.78. Data points for the GAB model fitting of nanomaterials prepared with calcium carbonate at different concentrations.

Aw	0% CC	10 % CC	20 % CC
0.26	4.53	4.15	3.52
0.5	7.12	5.86	5.14
0.76	10.62	9.21	8.12
0.985	16.28	15.77	15.10

Aw: water activity, CC: calcium carbonate